Hybridization alters the shape of the genotypic fitness landscape, increasing access to novel fitness peaks during adaptive radiation

Austin H. Patton[1,2], Emilie J. Richards[1,2], Katelyn J. Gould[3], Logan K. Buie[3], Christopher H. Martin[1,2]

[1]*Department of Integrative Biology, University of California, Berkeley, CA*

[2]*Museum of Vertebrate Zoology, University of California, Berkeley, CA*

[3]*Department of Biology, University of North Carolina, Chapel Hill, NC*

Keywords: fitness landscape; genotypic fitness network; adaptive radiation; introgression; standing genetic variation; *de novo* mutation

Correspondence: austinhpatton@berkeley.edu, chmartin@berkeley.edu

Abstract

Estimating the complex relationship between fitness and genotype or phenotype (i.e. the adaptive landscape) is one of the central goals of evolutionary biology. However, adaptive walks connecting genotypes to organismal fitness, speciation, and novel ecological niches are still poorly understood and processes for surmounting fitness valleys remain controversial. One outstanding system for addressing these connections is a recent adaptive radiation of ecologically and morphologically novel pupfishes (a generalist, molluscivore, and scale-eater) endemic to San Salvador Island, Bahamas. We leveraged whole-genome sequencing of 139 hybrids from two independent field fitness experiments to identify the genomic basis of fitness, estimate genotypic fitness networks, and measure the accessibility of adaptive walks on the fitness landscape. We identified 132 SNPs that were significantly associated with fitness in field enclosures. Six out of the 13 regions most strongly associated with fitness contained differentially expressed genes and fixed SNPs between trophic specialists; one gene (*mettl21e*) was also misexpressed in lab-reared hybrids, suggesting a potential intrinsic genetic incompatibility. We then constructed genotypic fitness networks from adaptive alleles and show that scale-eating specialists are the most isolated of the three species on these networks. Intriguingly, introgressed and *de novo* variants reduced fitness landscape ruggedness as compared to standing variation, increasing the accessibility of genotypic fitness paths from generalist to specialists. Our results suggest that adaptive introgression and *de novo* mutations alter the shape of the fitness landscape, providing key connections in adaptive walks circumventing fitness valleys and triggering the evolution of novelty during adaptive radiation.

Introduction

First conceptualized by Sewell Wright in 1932, the adaptive landscape describes the complex relationship between genotype or phenotype and fitness (1). The landscape is a concept, a metaphor, and an empirical measurement that exerts substantial influence over all evolutionary dynamics (2–6). Fitness landscapes were originally depicted as high-dimensional networks spanning genotypic space in which each genotype is associated with fitness (1). Simpson (7) later described phenotypic evolution of populations through time on a rugged landscape, in which isolated clusters of fitness peaks represent 'adaptive zones' relative to adjacent regions of low fitness (8). Lande and Arnold formalized the analysis of selection and estimation of phenotypic fitness landscapes (9–11), leading to empirical studies of fitness landscapes in numerous systems (12–18). Fitness surfaces are also central components of speciation models and theory (19–21).

A central focus of fitness landscape theory is the characterization of the shape of the fitness landscape. Theoretical and empirical studies frequently attempt to describe its topography, such as quantifying the number of fitness peaks, one component of landscape ruggedness that affects the predictability of evolution (5, 22–24). Importantly, the existence of multiple peaks and valleys on the fitness landscape implies epistasis for fitness, or non-additive effects on fitness resulting from genotypic interactions (23, 25–28). Fitness epistasis reduces the predictability of evolution because the resultant increase in the number of peaks increases the number of viable evolutionary outcomes (8, 29). Increasing fitness epistasis also increases landscape ruggedness, thus reducing the probability of converging on any one fitness peak and ultimately diversifying potential evolutionary outcomes (8, 30).

This leads to a fundamental concept in fitness landscape theory: Not all genotypic pathways are evolutionarily accessible (5, 26, 31–36). In large populations, paths through genotype space that monotonically increase in fitness at each mutational step are favored over alternatives with neutral or deleterious steps (37). These accessible genotypic paths can be considered adaptive walks under Fisher's geometric model, by which adaptation proceeds towards a phenotypic optimum via additive mutations of small phenotypic effect (37, 38). On rugged landscapes as originally envisioned by Wright (23), greater numbers of peaks (i.e. the ruggedness) increase the mean length of potential adaptive walks to any one fitness optimum, while decreasing the length of accessible paths to the nearest peak. Ultimately, this leads to a decrease in the probability that any one fitness optimum is reached. Simultaneously, increasing landscape ruggedness decreases the length of adaptive walks to the nearest local optimum, owing to the corresponding increase in peak density.

There are a growing number of experimental studies of adaptive walks in nature, including the evolution of toxin resistance in monarch butterflies (39), alcohol tolerance in Drosophila (40, 41), and host-shift in aphids (42). Likewise, the accessibility of genotypic fitness networks has now been explored in numerous microbial systems, including the evolution of antibiotic resistance (31), metabolism (43), citrate exploitation (44), and glucose limitation in *E. coli* (45), and adaptation to salinity in yeast via evolution of heat shock protein *Hsp90* (22). However, these studies are still limited to the investigation of specific coding substitutions and their effects on fitness in laboratory environments. Nosil et al. (46) estimated genotypic fitness networks for *Timema* stick insects based on a field experiment. Similarly, this study focused on a single large-effect locus underlying dimorphic coloration between ecotypes. These studies represent significant advances, but extension of fitness landscape theory to empirical systems

including multiple species remains an underexplored area of future research at the intersection of micro- and macroevolution. Such studies can provide insight into the topography of fitness landscapes in natural systems, the accessibility of interspecific adaptive walks, and ultimately the predictability of evolution.

One promising system for estimating fitness landscapes is a recent adaptive radiation of *Cyprinodon* pupfishes endemic to San Salvador Island, Bahamas (17, 18, 47, 48). This radiation is comprised of two trophic specialists, a molluscivore (durophage: *Cyprinodon brontotheroides*) and a scale-eater (lepidophage: *C. desquamator*), derived from a Caribbean-wide generalist (*C. variegatus*) which also coexists in the same habitats. These three species all occur in sympatry in the hypersaline lakes of San Salvador Island, Bahamas (Fig 1a). Found in the benthic littoral zone of each lake, all three species forage within the same benthic microhabitat; indeed, no habitat segregation has been observed in 14 years of field studies. Originating less than 10,000 years ago (based on geological age estimates for the lakes: (49)), the functional and trophic novelty harbored within this radiation is the product of exceptional rates of craniofacial morphological evolution (50–53). Furthermore, species boundaries persist across multiple lake populations, despite persistent admixture among species (54, 55). We previously estimated fitness landscapes in these hypersaline lakes from two independent field experiments measuring the growth and survival of hybrids placed in field enclosures (Figure 1b). Selection analyses revealed a multi-peaked phenotypic fitness landscape that is stable across lake populations, year of study, and manipulation of the frequency of rare hybrid phenotypes (17, 18, 48)). One of the strongest and most persistent trends across studies and treatments was that hybrid phenotypes resembling the scale-eater were isolated in the lowest fitness region for both growth and survival relative to the other two species (17, 18). In contrast, hybrids resembling the generalist occupied

a fitness peak and were separated by a smaller fitness valley from hybrids resembling the molluscivore, which occurred on a second peak of higher fitness.

Evolutionary trajectories through regions of low fitness should be inaccessible to natural selection. How then did an ancestral generalist population cross these phenotypic fitness valleys to reach new fitness peaks and adapt to novel ecological niches? A growing theoretical and empirical literature on fitness landscapes has demonstrated the limited conditions for crossing fitness valleys (56–59). Fitness peaks and valleys in morphospace may result only from the reduction of the adaptive landscape to two phenotypic dimensions (60). Additional phenotypic and genotypic dimensions may reveal fitness ridges that entirely circumvent fitness valleys (48, 61, 62). Indeed, owing to nonlinearity in the association between phenotype and fitness (63, 64), even a single-peaked phenotypic fitness landscape may be underlaid by a multi-peaked genotypic fitness landscape (65, 66). In this respect, investigating the high-dimensional genotypic fitness landscape is key to understanding the origins of novelty in this system, particularly given the rare evolution of lepidophagy (scale-eating), a niche occupied by less than 0.3% of all fishes (67).

Furthermore, the relative contributions of standing genetic variation, *de novo* mutations, and adaptive introgression to the tempo and mode of evolution are now of central interest to the field of speciation genomics (68–72). The three-dimensional adaptive landscape metaphor is often invoked to explain how the genetic, phenotypic, and ecological diversity introduced to populations by hybridization facilitates the colonization of neighboring fitness peaks that are unoccupied by either hybridizing species (73–75). However, extension of these ideas to more high-dimensional genotypic fitness landscapes remains underexplored. For instance, we have yet to learn how the appearance of novel adaptive genetic variation through introgressive hybridization or *de novo* mutation alters the realized epistatic interactions among loci, thus

potentially altering the shape of the fitness landscape and the accessibility of interspecific adaptive walks.

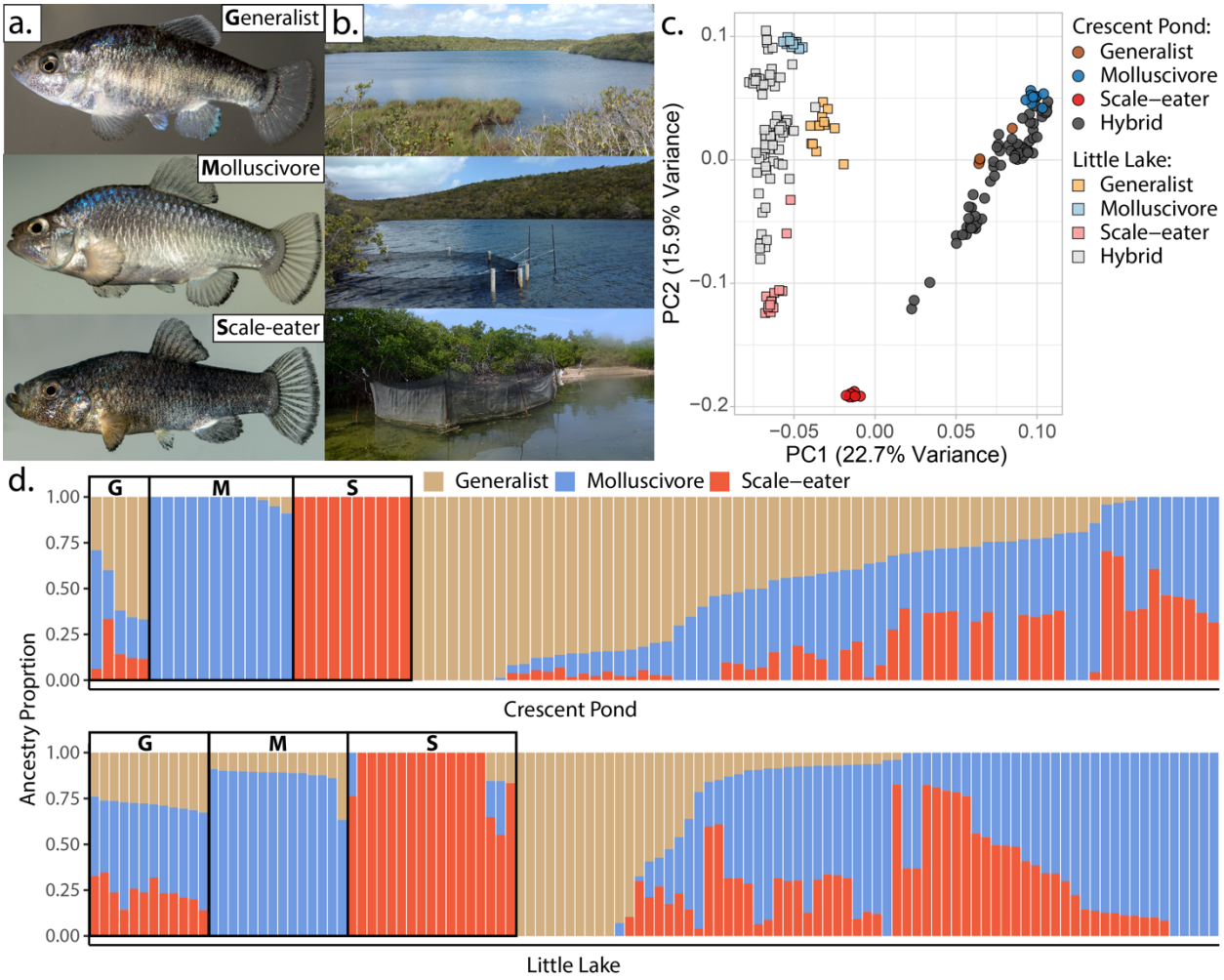

Figure 1. San Salvador Island pupfishes and their hybrids. a. From top to bottom: the generalist, *Cyprinodon variegatus*, the molluscivore *C. brontotheroides*, and the scale-eater *C. desquamator*. **b.** Representative images of experimental field enclosures. **c.** Principal component analysis of 1,129,771 LD-pruned SNPs genotyped in hybrids and the three parental species. **d.** Unsupervised ADMIXTURE analyses for Crescent Pond (top) and Little Lake (bottom). G, M and S indicate individual samples of Generalists (G), Molluscivores (M), and Scale-eaters (S), respectively, followed by all resequenced hybrid individuals from field experiments. Colors indicate ancestry proportions in each population (K = 3).

The adaptive radiation of San Salvador Island pupfishes, like many others (76–80), appears to have originated from a complex interplay of abundant standing genetic variation, adaptive introgression from neighboring islands, and several *de novo* single-nucleotide mutations and deletions found only in the scale-eater (55, 81). Notably, both specialists harbor numerous

142 introgressed SNPs showing evidence of hard selective sweeps in the regulatory regions of known
143 craniofacial genes (55, 81). In contrast, hard selective sweeps of *de novo* mutations only appear
144 in the scale-eating species, *C. desquamator*. Here, we leverage whole genome sequencing of 139
145 hybrids measured in field experiments to identify the genomic basis of fitness differences, infer
146 genotypic fitness networks, summarize their topography, and quantify the accessibility of novel
147 fitness peaks and the influence of each source of genetic variation on interspecific adaptive
148 walks.
149
150 **Results**
151 *Sample collection and genomic resequencing*
152 We resequenced 139 hybrids (86 survivors, 56 deaths (Appendix 1—table 1)) from two
153 independent field experiments across a total of six field enclosures and two lake populations
154 (2011: two high-density 3 m diameter enclosures exposed for three months: Crescent Pond n =
155 796; Little Lake n = 875 F2 hybrids (17); 2014/2015: four high-density 4 m diameter enclosures
156 exposed for three months in Crescent Pond, n = 923 F4/F5 hybrids and eleven months in Little
157 Lake, n = 842 F4/F5 hybrids (18)). We then characterized patterns of genetic variation among
158 parental species in each lake and their lab-reared hybrids used in field experiments. We
159 genotyped 1,129,771 SNPs with an average coverage of 9.79x per individual.
160
161 *Population structure and ancestry associations with fitness*
162 Principal components analysis (PCA) of genetic variation strongly differentiated pupfishes
163 sampled from Little Lake/Osprey Lake and Crescent Pond (PC1: 22.7% variance explained) and
164 among species within each lake (PC2: 15.9% variance explained: Figure 1d; Figure 1—figure
165 supplement 1-2). These results were supported by ADMIXTURE analyses (82, 83) (Figure 1e).

166 However, some hybrids were genotypically transgressive, falling outside the genotypic
167 distributions of the three parental species (Figure 1—figure supplement 2), leading
168 ADMIXTURE to assign the third cluster to these hybrids, rather than generalists which often
169 contain segregating variation found in trophic specialists (67). This pattern persisted in a
170 supervised ADMIXTURE analysis, in which we assigned individuals from the three parental
171 species *a priori* to their own population and estimated admixture proportions for the remaining
172 hybrids (Figure 1—figure supplement 3). Pairwise genetic distances did not predict pairwise
173 morphological distances (Figure 1—figure supplement 4).

174 We analyzed three measures of fitness (growth, survival, and their composite: see
175 Methods and Supplement for details), but focus herein on composite fitness, which is equal to
176 growth for survivors and zero for non-survivors. Growth could not be measured for tagged
177 hybrids that died in field enclosures and thus were not recovered. Because reproductive success
178 was not possible to quantify in field experiments (due to continuous egg-laying and very small,
179 newly hatched fry), composite fitness included only measurements of growth and survival.

180 Interestingly, in no case were genome-wide patterns of parental ancestry in hybrids
181 (estimated from unsupervised ADMIXTURE analyses) associated with hybrid composite fitness
182 (generalist $P = 0.385$; scale-eater $P = 0.439$; molluscivore $P = 0.195$), growth (generalist $P =$
183 0.119; scale-eater $P = 0.283$; molluscivore $P = 0.328$), or survival probability (generalist $P =$
184 0.440; scale-eater $P = 0.804$; molluscivore $P = 0.313$) while controlling for effects of lake and
185 experiment (Figure 1—figure supplement 5; Appendix 1—table 2). Similar results were obtained
186 when repeating these analyses using admixture proportions estimated from a supervised
187 ADMIXTURE analysis (Appendix 1—table 3), using only samples from the second field
188 experiment (Appendix 1—table 4), or using principal component axes estimated from genome-

wide SNPs (Appendix 1—table 5: See Supplementary Results). Therefore, in contrast to previous studies (84–86), in this system genome-wide ancestry is not consistently associated with fitness, highlighting the complex nonlinear relationship between genotype, phenotype, and fitness within this nascent adaptive radiation. We must look to local ancestry to understand fitness relationships (e.g. (87)).

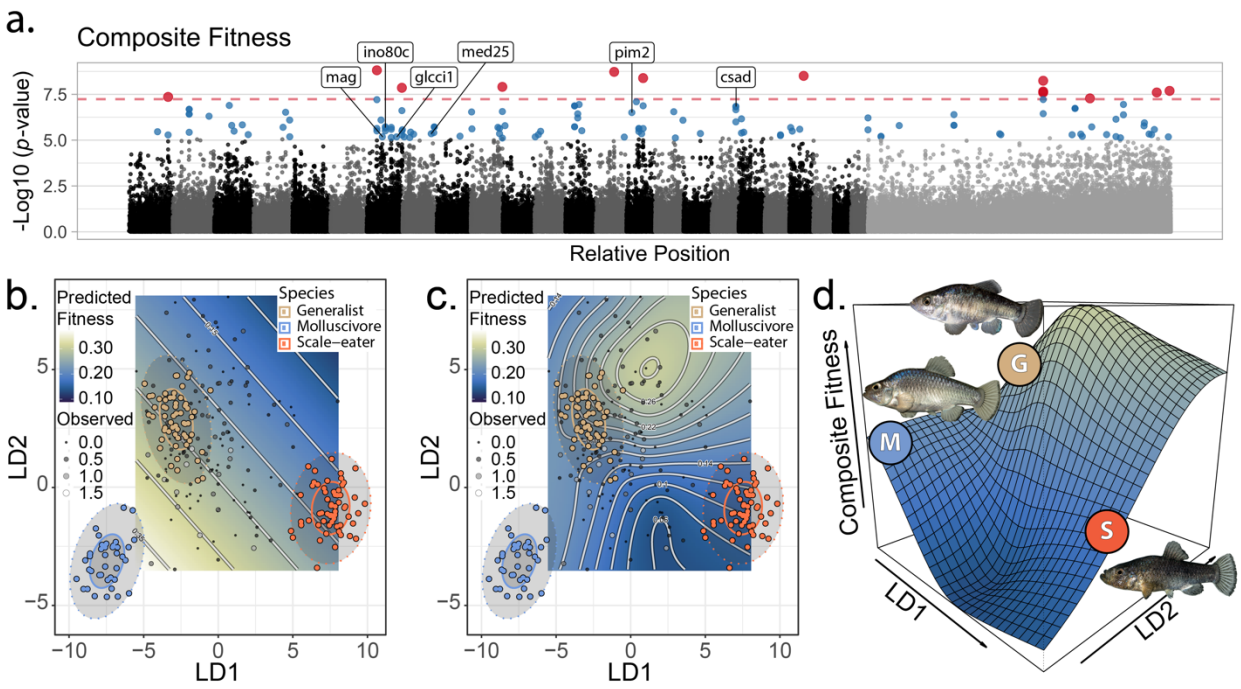

Figure 2. The genetic basis of fitness variation and improved inference of adaptive landscapes. a) Per-SNP log10 *p*-values from a genome-wide association test with GEMMA for composite fitness (survival x growth). Lake and experiment were included as covariates in the linear mixed model. SNPs that were significant at FDR < 0.05 are indicated in blue; red SNPs above dashed red line cross the threshold for Bonferroni significance at $\alpha = 0.05$. The first twenty-four scaffolds are sorted from largest to smallest and remaining scaffolds were pooled. The six genes associated with composite fitness which were both strongly differentiated ($F_{ST} > 0.95$) and differentially expressed between specialists (88) are annotated. **b-c)** Best-fit adaptive landscape for composite fitness using either morphology alone (**b:** flat surface with only directional selection) or morphology in combination with fitness-associated SNPs (**c:** highly nonlinear surface). Best-fit model in **c** was a generalized additive model (GAM) including a thin-plate spline for both LD axes, fixed effects of experiment and lake, and fixed effects of the seven (see supplementary methods) SNPs most strongly associated with fitness shown in red in panel **a**. **d)** Three-dimensional view of **c** with relative positions of the three parental phenotypes indicated.

208 *Genome-wide association mapping of fitness*

209 From our LD-pruned dataset we used a linear mixed model in GEMMA to identify 132 SNPs in
210 regions that were strongly associated with composite fitness, including 13 which remained
211 significant at the conservative Bonferroni-corrected threshold (Figure 2a, Appendix 1—table 6-
212 7; see supplement for results for survival and growth alone [Appendix 1—table 8-9; Figure 2—
213 figure supplement 1]). Gene ontologies for these 132 fitness-associated regions were
214 significantly enriched for synaptic signaling and chemical synaptic transmission [False discovery
215 rate (FDR) rate < 0.01; Figure 2—figure supplement 2; Appendix 1—table 7]. Ontologies
216 enriched at an FDR rate < 0.05 were related to signaling and regulation of cell communication
217 (for growth, see Figure 2—figure supplement 3). We did not identify any enrichment for
218 ontologies related to craniofacial development which have previously been identified to play a
219 significant role in the adaptive divergence of these fishes (55, 81, 88). This suggests that fitness-
220 associated regions in our field experiments captured additional components of fitness beyond the
221 external morphological phenotypes measured in previous studies.

222 We characterized whether genes in or near fitness-associated regions were implicated in
223 adaptive divergence of the specialists. Surprisingly, no fitness-associated regions overlapped
224 with regions showing significant evidence of a hard selective sweep (55). However, six fitness-
225 associated genes were previously shown to contain either fixed divergent SNPs (*csad, glcci1,*
226 *ino80c, mag, pim2, mettl21e*), or a fixed deletion between specialists (*med25*) (88). *Med25*
227 (Mediator Complex Subunit 25) is a craniofacial transcription factor associated with cleft palate
228 in humans and zebrafish (89, 90); a precursor of *mag* (Myelin Associated Glycoprotein) was also
229 associated with the parallel evolution of the thick-lipped phenotype in Midas cichlids based on
230 differential expression among morphs (91). Three of the six remaining fitness-associated genes

231 containing divergent SNPs (88) were associated with growth and/or body size measurements in
232 other fishes. First, *csad* plays an important role in synthesizing taurine which is a rate-limiting
233 enzyme affecting growth rate in parrotfishes (92), rainbow trout (93), and Japanese flounder
234 (94). Second, *glcci1* is associated with the body depth/length ratio in yellow croaker (95). Third,
235 *ino80c* is associated with measures of body size in Nile tilapia (96). Finally, *mettl21e* was
236 differentially expressed among specialists and also misexpressed in F1 hybrids between scale-
237 eaters and molluscivores at eight days post-fertilization and thus is a putative genetic
238 incompatibility in this system that may impact their fitness in field enclosures (88, 97). Although
239 it has not been associated with growth or body size in fishes, *mettl21e* is associated with
240 intramuscular fat deposition in cattle (98). Taken together, these findings support the
241 interpretation that fitness-associated regions are associated with unmeasured traits, particularly
242 physiological growth rate, or craniofacial shape in the case of the deletion in *med25*, that affect
243 fitness in our hybrid field experiments. However, the fitness associated loci we identified appear
244 not to have the subject of selective sweeps in either specialist.
245
246 *Fitness-associated SNPs improve inference of the adaptive landscape*
247 Fitness landscapes in past studies were estimated using slightly different sets of morphological
248 traits; thus, to enable inclusion of all hybrids on a single fitness landscape, a single observer
249 (AHP) remeasured all sequenced hybrids for 31 morphological trats (Figure 2—figure
250 supplement 4; Appendix 1—table 10). We used linear discriminant axes and generalized additive
251 modelling (GAM) to estimate phenotypic fitness landscapes for the sequenced hybrids on a two-
252 dimensional morphospace indicating similarity to each of the three parental populations
253 following previous studies (17, 18)(Figure 2—figure supplements 5; Appendix 1—table 11-13).

We then tested whether the inclusion of the 13 genomic regions most strongly associated with fitness (red: Figure 2a) in GAM models improved our inference of the underlying adaptive landscape. Models including fitness-associated SNPs were invariably favored over models with external morphology alone (ΔAICc > 8.6: Appendix 1—table 14-15). Morphology-only models predicted a flat fitness surface (Figure 2b, Figure 2—figure supplement 6; predictions restricted to observed hybrid morphospace). In contrast, models including fitness-associated SNPs predicted a complex and nonlinear fitness landscape, despite our limited dataset of 139 sequenced hybrids relative to samples in previous morphology-only studies of around 800 hybrids per enclosure.

To reduce complexity of the full model estimated from 31 morphological traits including all 13 fitness-associated SNPs, we fit an additional model including only the seven most significant fitness-associated SNPs in the full model. This reduced model was the best-fit; the inferred adaptive landscape was complex and characterized by a fitness peak near hybrids resembling the generalist phenotype separated by a small fitness valley from a second region of high fitness for hybrids resembling the molluscivore phenotype. Hybrids resembling the scale-eater phenotype again occurred in a large fitness valley (Figure 2b-2d: For results pertaining to growth or survival see Appendix 1: Figure 2—figure supplement 6, Appendix 1—table 11-15). Each of these fitness peaks and valleys were frequently recovered across 10,000 bootstrap replicates; landscapes inferred from bootstrap replicates were often more complex with increased curvature relative to inferences from our observed dataset (Figure 2—figure supplement 7). Thus, the fitness landscape estimated from our observed dataset appears robust to sampling uncertainty.

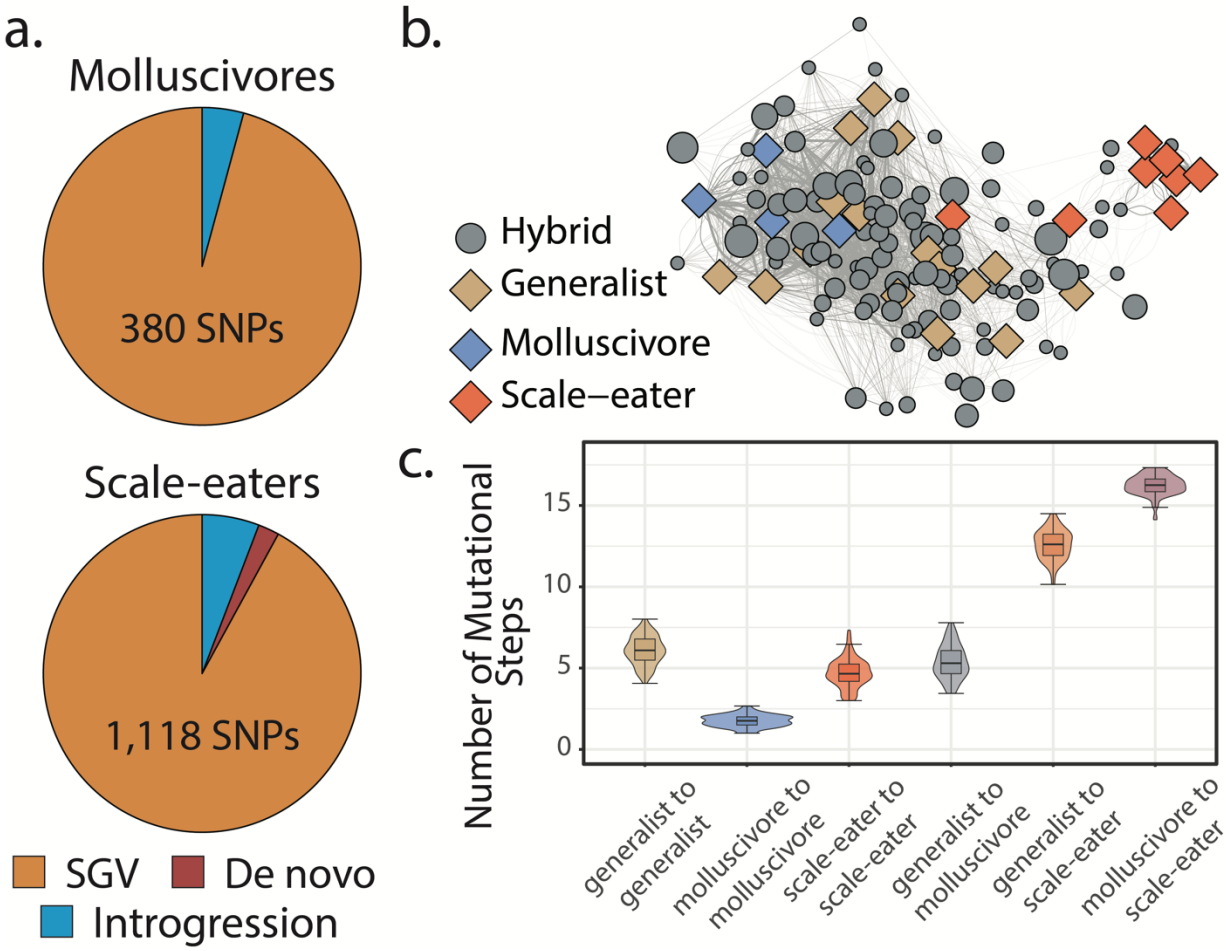

Figure 3. Scale-eaters are isolated on the fitness landscape. a. Most nearly fixed or fixed variants (F_{ST} ≥ 0.95) experiencing hard selective sweeps (hereafter 'adaptive alleles') originated as standing genetic variation (SGV: molluscivores = 96%, scale-eaters = 92%), followed by introgression (molluscivores = 4%, scale-eaters = 6%), and *de novo* mutation (scale-eaters = 2%)(55). Pie charts show adaptive alleles retained in our study for each species; networks are constructed from either set of adaptive alleles. **b.** Genotypic network constructed from a random sample of ten SNPs, sampled from all SNPs shown in **a**. Each edge between nodes is up five mutational steps away; edge width is proportional to mutational distance: wider edges connect closer haplotypes; hybrid node size is proportional to fitness (larger nodes are of greater fitness value). **c.** Median number of mutational steps within or between species (e.g. Figure 4a). All pairwise comparisons using Tukey's HSD test (after FDR correction) were significant.

Compared to previous studies, the highest fitness optimum was shifted from the molluscivore to the generalist phenotype. This suggests that fitness-associated SNPs increased the fitness of hybrids resembling generalists beyond expectations based on their morphology alone, consistent with the hypothesis that fitness-associated SNPs are associated with unmeasured non-morphological traits affecting fitness. Indeed, visualization of observed haplotypes in hybrids across the fitness landscape supported this interpretation; one of the most

293 common haplotypes was most frequent in hybrids resembling generalists near the peak of high
294 fitness and rare in hybrids resembling either trophic specialist (Figure 2—figure supplement 8).
295 Regardless, this two-dimensional phenotypic fitness landscape did not reveal fitness ridges
296 connecting generalists to specialists, further emphasizing the need to investigate the genotypic
297 fitness landscape.
298
299 *Trophic novelty is associated with isolation on the genotypic fitness network*
300 The adaptive radiation of pupfishes on San Salvador island originated within the last 10,000
301 years through a combination of selection on standing genetic variation, adaptive introgression,
302 and *de novo* mutations (55). However, it is unclear how each source of genetic variation aided in
303 the traversal of fitness paths or contributed to the colonization of novel fitness peaks. To address
304 this knowledge gap, we first sought to visualize genotypic fitness networks and gain insight into
305 how isolated the three species are in genotypic space. Understanding the relative isolation of
306 each specialist from the generalist can reveal the relative accessibility of their respective adaptive
307 walks on the genotypic fitness landscape.
308 To accomplish this, we reconstructed genotypic fitness networks from 1,498 candidate
309 adaptive alleles previously identified in this system (e.g. Figure 3a (55)). These regions displayed
310 significant evidence of a hard selective sweep using both site frequency spectrum and LD-based
311 methods, SweeD (99) and OmegaPlus (100), and contained fixed or nearly fixed SNPs (F_{ST} >
312 0.95) differentiating trophic specialists across lakes (55). Adaptive alleles were classified as
313 standing variation, introgressed, or *de novo* mutations based on extensive sampling of focal and
314 related *Cyprinodon* pupfish species across San Salvador Island and neighboring Caribbean
315 islands, as well as North and South American outgroups (55). We note, however, that adaptive

316 alleles designated as *de novo* on San Salvador Island may be segregating at low frequencies in
317 other sampled populations or present in unsampled populations.

318 These fitness networks depict both hybrids and parental species in genotypic space, with
319 nodes representing SNP haplotypes and edges connecting mutational neighbors (Figure 3b).
320 Genotypic space is immense; using SNPs coded as homozygous reference, heterozygote, or
321 homozygous alternate, the number of potential haplotypes is equal to $3^{\#\ SNPs\ in\ network}$. For
322 instance, to construct a reduced network of 100 SNPs, there are a total of $3^{100} = 5.17\ X\ 10^{57}$
323 possible nodes. Thus, unlike experimental studies of individual proteins in haploid *E. coli* (31,
324 45) or yeast (22), it is not possible for us to investigate the full breadth of genotypic space.

325 Instead, to understand the distribution of parental species and their hybrids in genotypic
326 space, we began by using a random sample of ten SNPs drawn from our set of candidate adaptive
327 alleles in this system. Here, we plotted edges between nodes up to five mutational steps away
328 (e.g. Figure 3b) and found that generalists and molluscivores are closer on the genotypic fitness
329 network than either is to scale-eaters (Figure 3c), as expected based on their genetic distance.
330 Most scale-eaters appear quite isolated in genotypic space, separated from the generalist cluster
331 of nodes by 12.6 ± 0.091 (mean ± SE: $P < 0.001$) mutational steps and from molluscivores by
332 16.3 ± 0.060 steps ($P < 0.001$). In contrast, molluscivores were separated from generalists by
333 5.37 ± 0.103 steps ($P < 0.001$). Generalists show the greatest intrapopulation distances, separated
334 from each other by 6.08 ± 0.088 steps ($P < 0.001$). In contrast, molluscivores exhibited the
335 smallest intrapopulation distances, separated by 1.75 ± 0.021 steps ($P < 0.001$). Scale-eater
336 intrapopulation distances were intermediate (4.71 ± 0.088 steps: $P < 0.001$).

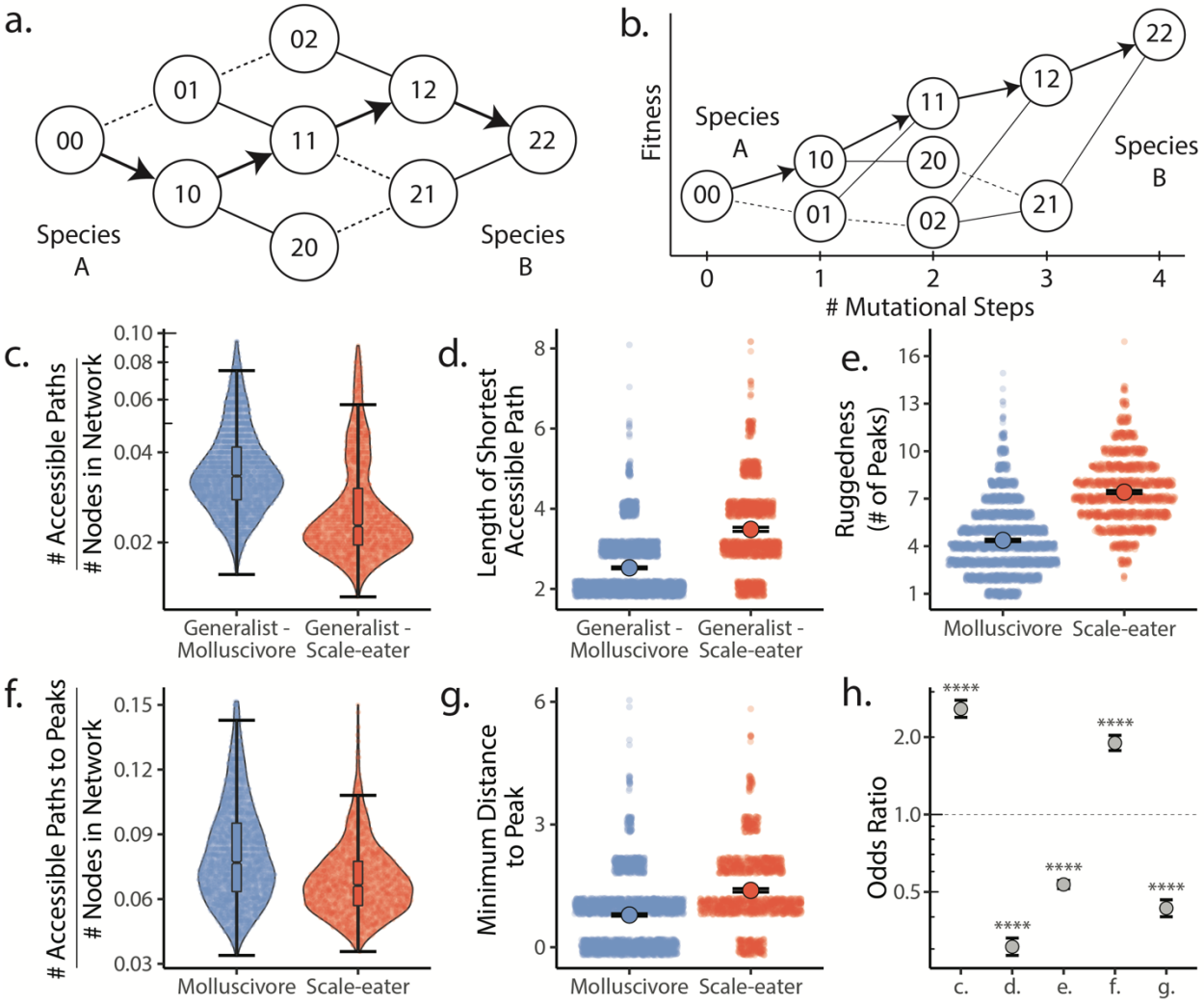

Figure 4. Molluscivore genotypes were more accessible to generalists on the genotypic fitness landscape than scale-eater genotypes. a. Diagram illustrating genotypic fitness networks and adaptive walks between species for a hypothetical two-SNP genotypic fitness landscape. Species A & B are separated by four mutational steps. Dashed lines indicate inaccessible paths that decrease in fitness leaving a single possible accessible evolutionary trajectory between species A and B (indicated by bold arrows). Each node in our study is associated with an empirical measure of hybrid fitness from field experiments (17, 18). Edges are always drawn as directed from low to high fitness. **b.** The same network as in (**a.**), with fitness plotted on the Y-axis and number of mutational steps from species A to B on the X-axis. The only accessible path between species A and B is indicated by solid arrows. **c.** Number of accessible paths between generalists and either specialist, scaled by network size. **d.** Length (# of nodes) of the shortest accessible paths. Means (large points) ± 2 standard errors are plotted. **e.** Ruggedness, as measured by the number of peaks (genotypes with no fitter neighbors within a single mutational step (32)). **f.** Number of accessible paths to peaks, scaled by network size. **g.** Length of the shortest accessible path to the nearest peak. **h.** Odds ratios (OR: ML estimate and 95% CI) for each measure of accessibility (x-axis corresponds to panel letters); molluscivore networks have significantly greater summary statistics when OR > 1. Molluscivore genotypes are more accessible to generalists than scale-eater genotypes due to a significantly greater number of accessible paths separating them (**c.**) that are significantly shorter (**d.**). Molluscivore genotypic networks were also less rugged, i.e. they contained significantly fewer peaks (**e.**), each of which were in turn more accessible from the generalist genotypes (**f.**, **g.**).

357 *Molluscivore genotypes are more accessible to generalists than scale-eater genotypes on the*
358 *genotypic fitness landscape*

359 The most accessible paths through genotypic fitness networks are characterized by
360 monotonically increasing fitness at each mutational step and the smallest possible number of
361 steps between two states (5, 31, 33) (Figure 4a-b). Furthermore, as described earlier, the
362 accessibility of individual fitness peaks is predicted to be reduced on increasingly rugged fitness
363 landscapes that are characterized by a greater number of fitness peaks (8, 30, 33, 101). This
364 provides three useful metrics of evolutionary accessibility for genotypic trajectories: 1) the total
365 number of accessible paths relative to network size (Figure 4—figure supplement 1; Appendix
366 1—table 16), 2) the length of the shortest accessible paths, and 3) the number of fitness peaks
367 (ruggedness). Here, we define peaks as genotypes with no fitter neighbors and within a single
368 mutational step (32). With these three metrics, we can quantify the accessibility of interspecific
369 genotypic pathways.

370 We used these measures of accessibility to ask: 1) whether molluscivore or scale-eater
371 genotypes were more accessible to generalists on the fitness landscape (Figure 4c-d), and 2)
372 whether molluscivore and scale-eater genotypic fitness networks differed in their ruggedness,
373 characterized by peak number (Figure 4e-g). These measures provide insight into the
374 predictability of evolution and the role that epistasis plays in their evolution (8, 23, 29, 102).

375 We constructed 5,000 genotypic fitness networks from a random sample of five species-
376 specific candidate adaptive SNPs (Figure 3a) for either molluscivores or scale-eaters, requiring
377 that at least one SNP of each source of genetic variation be present in the sample. We used odds
378 ratios to compare the relative accessibility and ruggedness of molluscivore fitness networks

379 compared to scale-eater networks (Figure 4h). Thus, odds ratios (OR) greater than 1 imply
380 summary statistics are greater for molluscivores than for scale-eaters.

381 We found that molluscivore genotypes were significantly more accessible to generalists
382 on the fitness landscape than scale-eaters (Appendix 1—table 17); molluscivore networks had
383 significantly more accessible paths [OR: (95% CI)= 2.095: (1.934, 2.274)] that were
384 significantly shorter [OR and 95% CI = 0.253: (0.231, 0.277)]. Not only were molluscivore
385 genotypes more accessible to generalists, but molluscivore fitness networks were significantly
386 less rugged than scale-eater networks, comprised of fewer peaks [OR and 95% CI = 0.604:
387 (0.575, 0.634)], and connected by significantly more accessible paths [OR and 95% CI = 1.514:
388 (1.404, 1.635)], that contained fewer mutational steps [OR and 95% CI = 0.539: (0.500, 0.579)].
389

390 *Adaptive introgression and* de novo *mutations increase accessibility of novel fitness peaks*
391 We further used our two metrics of accessibility and landscape ruggedness to ask how different
392 sources of adaptive genetic variation may influence the topography of the fitness landscape, the
393 traversal of fitness paths separating generalists from specialists, and ultimately colonization of
394 novel fitness peaks. We constructed genotypic fitness networks limited to only one of the three
395 main sources of adaptive genetic variation: standing genetic variation, introgression from one of
396 four focal Caribbean generalist populations, or *de novo* mutations unique to San Salvador Island.
397 We also examined all combinations of these three sources to better reflect the actual process of
398 adaptive divergence originating from only standing genetic variation, then adaptive introgression
399 plus standing genetic variation, and finally the refinement stage of de novo mutations (55).

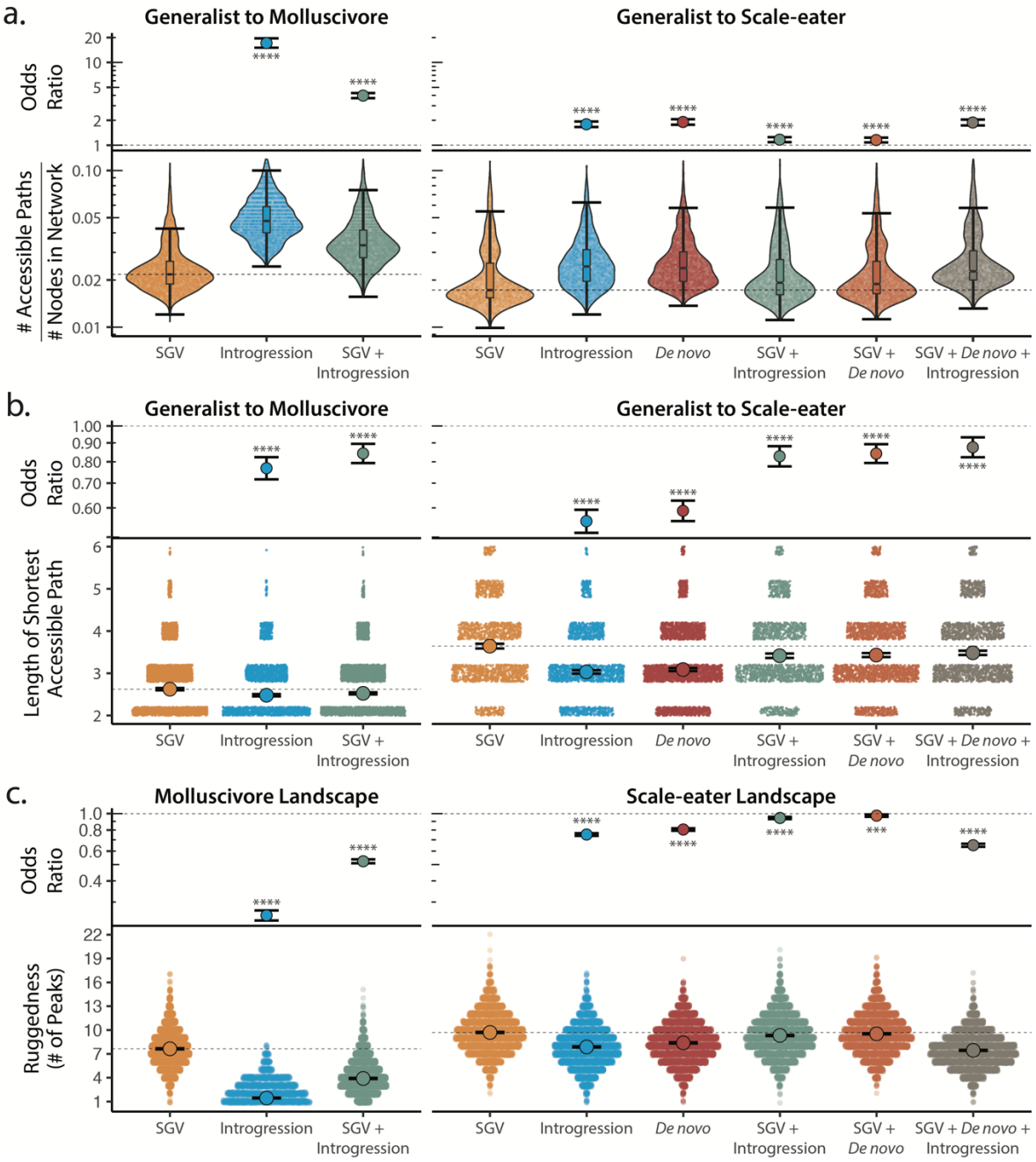

Figure 5. Adaptive introgression and *de novo* mutations increase access to specialist fitness peaks. Odds ratios (maximum likelihood estimate and 95% CI) indicate the effect of each source of variation on accessibility compared to networks estimated from standing variation alone. Asterisks denote significance ($p < 0.0001$ = ****, < 0.001 = ***). **a.** The number of accessible (i.e. monotonically increasing in fitness) paths per network, scaled by the size of the network (# of nodes in network). Significance was assessed using a likelihood ratio test, corrected for the false discovery rate (reported in Appendix 1—table 18). Dashed lines correspond to the median estimate for standing genetic variation to aid comparison to other sources of adaptive variation. **b.** Number of mutational steps in the shortest accessible path. Means are plotted as large circles, with two standard errors shown; dashed horizontal lines correspond to the mean for standing genetic variation. **c.** Ruggedness of molluscivore and scale-eater genotypic fitness networks constructed from each source of genetic variation measured by the number of peaks (genotypes with no fitter neighbors).

We compared sets of 5,000 random 5-SNP genotypic networks drawn from different sources of adaptive variation (Figure 4a) and compared the effect of each source of variation on measures of accessibility and landscape ruggedness relative to standing genetic variation. We treated standing variation as our basis for comparison because this is the source of genetic variation first available to natural selection (103).

We discovered that genotypic trajectories between generalists and either trophic specialist in genotypic fitness networks constructed from introgressed or *de novo* adaptive mutations were significantly more accessible than networks constructed from standing genetic variation (Figure 5). Specifically, random networks that included alternate sources of adaptive variation contained significantly more accessible fitness paths from generalist to specialists than networks constructed from standing genetic variation alone, while controlling for differences in overall network size (Figure 5a; Appendix 1—table 18). Furthermore, accessible paths between generalists and specialists in networks constructed from introgressed or *de novo* adaptive loci were significantly shorter in length (Figure 5b). We recovered the same pattern whether constructing fitness networks from these sources of variation alone or in combination. These results held across all measures of fitness and for analyses repeated using only hybrids sampled from the second field experiment (Figure 5—figure supplement 1-2, Appendix 1—table 18-19).

Our finding of increased accessibility of interspecific genotypic trajectories suggests that fitness landscapes constructed from adaptive standing genetic variation alone are more rugged than networks including adaptive loci originating from either introgression or *de novo* mutation. Quantification of landscape ruggedness supported this hypothesis in all cases (Figure 5c; Appendix 1—table 18-19). Additionally, increasing landscape ruggedness significantly

435 decreased the length of accessible paths to the nearest local peak [glm(Min. Path Length ~ # of
436 Peaks, family = "poisson"): $P < 0.0001$, $\beta = -0.088$, 95% CI = -0.095 – 0.081].

437 Scale-eater fitness genotypic fitness landscapes constructed from a combination of
438 adaptive loci sourced from standing variation, introgression, and *de novo* mutations had
439 significantly more accessible paths (scaled by network size) separating generalists from scale-
440 eaters [OR and 95% CI = 1.879: (1.743, 2.041); LRT $P < 0.0001$; Figure 5a] and these paths
441 were significantly shorter in length compared to networks constructed from standing variation
442 alone [OR and 95% CI = 0.876: (0.823, 0.932); LRT $P < 0.0001$; Figure 5b]. The only exception
443 to this pattern across all three fitness measures was for growth rate in genotypic fitness networks
444 constructed for molluscivore adaptive loci; no significant difference was observed in the length
445 of the shortest accessible path between networks constructed using standing variation alone or
446 those constructed using introgressed alleles [OR and 95% CI = 0.994: (0.915, 1.079); LRT $P =$
447 0.8826; Appendix 1—table 18]. Interestingly, however, for networks constructed from standing
448 variation and introgressed alleles, we again observed a significant reduction in length of the
449 shortest accessible paths [OR and 95% CI = 0.897: (0.835, 0.962); LRT $P = 0.0050$; Appendix
450 1—table 18].
451

452 **Discussion**

453 We developed a new approach for estimating genotypic fitness landscapes for diploid organisms
454 and applied it to a system in which phenotypic fitness landscapes have been extensively
455 investigated. We were able to address long-standing questions posed by fitness landscape theory
456 in an empirical system and assess the extent to which the shape of the fitness landscape and
457 accessibility of adaptive walks are contingent upon the source of adaptive genetic variation. We

show that not only are scale-eaters more isolated than molluscivores from generalists on the fitness landscape, but that the scale-eater fitness landscape is more rugged than molluscivores. This indicates that epistasis is more pervasive on the scale-eater fitness landscape, leading to less predictable evolutionary outcomes and fewer accessible trajectories from generalist to scale-eater genotypes. Overall, we found that most genotypic trajectories were inaccessible and included one or more mutational steps that decreased in fitness from generalist to specialist. This finding is consistent with the patterns observed by Weinreich et al. (31), who constructed combinatorially complete fitness networks for five mutations contributing to antibiotic resistance in *E. coli* and found that only 18 of 120 possible genotypic trajectories were evolutionarily accessible. In contrast, Khan et al. (45) estimated that over half of all trajectories were accessible on a complete fitness landscape constructed using the first five adaptive mutations to fix in an experimental population of *E. coli*.

We also show that fitness landscapes are most rugged, and therefore epistasis is most pervasive, when constructed from standing genetic variation alone, ultimately leading to a reduction in the accessibility of fitness peaks on these landscapes (Figure 5). This finding has significant implications for the predictability of evolution in the earliest stages of the speciation process. Adaptation from standing genetic variation is thought to initially be more rapid due to its initial availability and potentially reduced genetic load within a population (103–105). In contrast, we consistently found that networks constructed from a combination of adaptive standing variation, introgression, and *de novo* mutations reduced the ruggedness of fitness landscapes and thus increased accessibility of interspecific evolutionary trajectories (Figure 5). This would suggest that adaptive introgression or *de novo* mutations reduce the impacts of epistasis, resulting in a smoother fitness landscape with a greater number of accessible adaptive

walks, facilitating the colonization of new adaptive zones. Future studies testing the generality of these findings will be invaluable for our understanding of the speciation process.

Furthermore, our results shed light on the classic problem of crossing fitness valleys on three-dimensional phenotypic fitness landscapes. We show that phenotypic fitness valleys may be circumvented by rare accessible paths on the genotypic fitness landscape. These results are consistent with increasing recognition that three-dimensional depictions of the fitness landscape may lead to incorrect intuitions about how populations evolve (3, 5, 106).

Our study represents a significant contribution to the growing body of work applying fitness landscape theory to empirical systems (39, 46, 107–109). Unlike previous studies that experimentally generated combinatorically complete fitness landscapes (22, 31, 45), we subsampled loci across the genome, enabling us to quantify aspects of the genotypic fitness landscape, despite the limitations imposed by large genome sizes and non-model vertebrates. One limitation of this approach is that subsampled fitness networks may not directly correspond to the full landscape (5, 110). For instance, a given subsampled fitness landscape may be present on multiple global, fully sampled fitness landscapes (110). Secondly, nodes (here, SNP haplotypes) can appear disconnected in a subsampled fitness landscape, but may be connected in the full fitness landscape (5). Nevertheless, given that there are more possible genotypes for a gene of 1,000 base-pairs than particles in the known universe (1, 111), nearly all empirical fitness landscapes must necessarily be subsampled at some scale.

Although inferences from subsampled fitness networks have their limitations, so too do those obtained from combinatorically complete fitness landscapes, which may themselves be misleading (102). By including mutations that are not segregating in natural populations, the shape of the "complete" fitness landscape and thus accessibility of fitness peaks may be quite

different from what occurs in nature. The shape of fitness landscapes in nature is dictated by the "realized" epistasis that occurs among naturally segregating loci (102). Changes to "realized" epistasis induced by introgression or *de novo* mutations appears to be the mechanism altering the shape of the fitness landscape and thus accessibility of fitness peaks. Our findings that adaptive introgression and *de novo* mutations make fitness peaks more accessible points towards a pervasive role of epistasis in determining the predictability of evolution and the speciation process (5, 8, 22–24, 30).

In the present study we have taken snapshots of the fitness landscape from loci that have already undergone hard selective sweeps. Consequently, we cannot directly assess the influence of each adaptive allele on the fitness landscape through time as it increases in frequency. However, so far we have failed to detect evidence of frequency-dependent selection in this system after experimental manipulations, at least for morphological traits (18). Future experimental or simulation studies may track how novel adaptive alleles affect fitness landscape topography as they increase in frequency.

Conclusion

Our findings are consistent with a growing body of evidence that *de novo* and introgressed adaptive variation may contribute to rapid speciation and evolution towards novel fitness peaks (44, 70, 78, 112–116). We demonstrate that adaptive introgression smooths the fitness landscape and increases the accessibility of fitness peaks. This provides an alternative mechanism to explain why hybridization appears to play such a pervasive role in adaptive radiation and speciation. There are many examples of hybridization promoting or inducing rapid speciation and adaptive radiation. Whether in Galapagos finches (117), African cichlids (77, 78, 113, 118,

119), or *Heliconius* butterflies (75, 120), hybridization has been shown to play a generative role in adaptive radiation and the evolution of novelty. One mechanism is the increased genotypic, phenotypic, and ecological diversity generated by hybridization in the form of transgressive phenotypes (74, 121–124). This diversity in turn facilitates the colonization of novel fitness peaks and ecological niches, particularly after colonization of a new environment rich in ecological opportunity (73, 74, 125). However, this model often assumes that the fitness landscape remains static after adaptive introgression. Here we show that adaptive introgression directly alters the shape of the fitness landscape, making novel fitness peaks more accessible to natural selection. Thus, hybridization not only generates genetic diversity, but this diversity can alter the shape of the fitness landscape, changing which genotypic combinations are favored by natural selection along with the adaptive walks that lead to them.

Acknowledgements:

We thank Michelle St. John, David Tian, Jacqueline Galvez, and Maria Fernanda Palominos for insightful discussion of the results; the Gerace Research Centre and Troy Day for logistical support; the BEST Commission and the government of the Bahamas for permission to collect, import, and export samples; the Vincent J. Coates Genomics Sequencing Center and Functional Genomics Laboratory at UC Berkeley for performing whole genome library preparation and sequencing (supported by NIH S10 OD018174 Instrumentation Grant), and the University of California, Berkeley and University of North Carolina at Chapel Hill for computational resources. This work was funded by the National Science Foundation DEB CAREER grant #1749764, National Institutes of Health grant 5R01DE027052-02, the University of North Carolina at Chapel Hill, and the University of California, Berkeley to CHM, graduate research

550 funding from the Museum of Vertebrate Zoology to EJR, and an NSF Postdoctoral Research
551 Fellowship in Biology under Grant No. 2109838 to AHP.

552

553 **Data availability:**

554 Genomic data are archived at the National Center for Biotechnology Information BioProject
555 Database (Accessions: PRJNA690558; PRJNA394148, PRJNA391309). Sample metadata
556 including morphological measurements and admixture proportions have been uploaded to Dryad:
557 https://doi.org/10.5061/dryad.0vt4b8h0m.

558

559 **Methods:**

560 ***Sampling***

561 Our final genomic dataset was comprised of 139 hybrid samples used in two separate field
562 experiments (17, 18) on San Salvador Island. Experiments were conducted in two lakes: Little
563 Lake (N = 71) and Crescent Pond (N = 68). Hybrids used in the first field experiment (17) were
564 comprised of F2 and backcrossed outbred juveniles resulting from crosses between all three
565 species. Juveniles were raised for 2 months in the lab, individually tagged by injecting a stainless
566 steel sequential coded wire tag (Northwest Marine Technologies, Inc.) into their left dorsal
567 musculature, and photographed pre-release for morphometric analyses. Experimental field
568 enclosures consisted of high- and low-density treatments; density was varied by the number of
569 tagged juveniles released into each enclosure. Hybrids in the second field experiment (18) were
570 comprised of F4-F5 outbred juveniles resulting from crosses between all three species.
571 Individuals were spawned, raised, tagged, and photographed in the same way prior to release.
572 The second field experiment consisted of high- and low-frequency treatments of approximately

equal densities. The frequency of rare transgressive hybrid phenotypes was manipulated between treatments in each lake, such that the high- and low-frequency treatments harbored an artificially increased and decreased frequency of transgressive phenotypes, respectively (18).

All hybrids were measured for 32 external morphological traits (see below). Additionally, we sequenced parental species of the generalist (N = 17), molluscivores (N = 27), and scale-eaters (N = 25) sampled from these two lakes and previously included in Richards et al. (55). Note that we treated samples from Little Lake and Osprey Lake as the same population because these two lakes are connected through a sand bar and fish from these populations are genetically undifferentiated (54, 55). For morphological analyses, we additionally measured samples of 60 generalists, 38 molluscivores, and 60 scale-eaters raised in the same laboratory common garden environment as the hybrids used in field experiments. A full list of samples is included in the supplement (Appendix 1—table 1).

Sequencing, genotyping, and filtering

Raw reads from a combined set of 396 samples (see supplement) were first mapped to the *C. brontotheroides* reference genome (genome size = 1.16 Gb; scaffold N50 = 32 Mb) (55) using bwa-mem (v. 0.7.2). Duplicate reads were identified using MarkDuplicates and BAM indices were subsequently generated using the Picard software package (126). Samples were genotyped following Richards et al. (55) according to GATK best practices (127). Specifically, Single Nucleotide Polymorphisms (SNPs) were called and filtered using hard-filtering criteria in HaplotypeCaller. We used the following criteria in our filtering approach: QD < 2.0; QUAL < 20; FS < 60; MQRankSum < -12.5; ReadPosRankSum < -8 (127–129).

595 Following initial genotyping with GATK, we subsequently filtered our data further using
596 VCFtools (130). Specifically, we filtered using the following flags: --maf 0.05; --min-alleles 2; --
597 max-alleles 2; --min-meanDP 7; --max-meanDP 100; --max-missing 0.85. Indels were removed.
598 To reduce non-independence among sites in our final dataset, we conservatively removed sites in
599 strong linkage disequilibrium using plink v1.9 (--indep-pairwise 10['kb'] 50 0.5: (131)). This
600 resulted in the retention of 1,129,771 SNPs across 139 hybrid samples and the 69 wild-caught
601 samples from Richards et al (55). Unless otherwise specified, these SNPs were used for all
602 downstream analyses.
603
604 ***Hybrid fitness measures***
605 We used three proxies for fitness: survival, growth, or a composite measure of the two. Survival
606 was a binary trait indicating whether a fish survived (i.e. a tagged fish was recovered) or not
607 during its exposure period in field enclosures. Growth was a continuous measure, defined as the
608 proportional increase in Standard Length $\left(\frac{Final\ SL - Starting\ SL}{Starting\ SL}\right)$. Lastly, we defined composite
609 fitness as survival * growth, similar to the metric used in (132), and analogous to composite
610 fitness in Hereford (133) who used fecundity as their second fitness measure, rather than growth.
611 Composite fitness is equal to growth for survivors and equals zero for non-survivors because
612 growth could not be assessed for non-surviving individuals. Because composite fitness represents
613 the most information-rich metric of fitness, we report composite fitness results in the main text;
614 results for growth and survival are included in the supplement.

615 ***Population genetic variation***

616 To visualize genetic variation present in hybrids and across lakes (Crescent Pond and Little
617 Lake), we first used a Principal Components Analysis (PCA) of genetic variation using plink
618 v1.90 ((131), Figure 1), plotting the first two principal component axes using R (version 3.6.3 (R
619 Core team 2020). We then estimated admixture proportions in hybrids using ADMIXTURE
620 v1.3.0 (82). Populations of each species were substantially differentiated between Crescent Pond
621 and Little Lake (54, 55); thus, independent ADMIXTURE analyses were conducted for each
622 lake. Because we were primarily interested in admixture proportions of hybrids, we set K = 3 in
623 these analyses, corresponding to the three parental species used in hybrid crosses. Using
624 admixture proportions of hybrid individuals, we tested the hypothesis that ancestry predicts
625 hybrid composite fitness in experimental field enclosures by fitting a generalized additive model
626 including either 1) scale-eater ancestry or 2) molluscivore ancestry with fixed effects for
627 experiment and lake. This was repeated for survival and growth separately. Composite fitness
628 was analyzed using a tobit (zero-censored) model to account for zero-inflation using the censReg
629 R package (134), survival was analyzed using a binomial model, and growth was analyzed using
630 a gaussian model. We conducted additional ADMIXTURE analyses that either 1) were
631 supervised, with generalist, molluscivore, and scale-eater parentals *a priori* assigned to one of
632 three populations, with only hybrid ancestry proportions being estimated by admixture, or 2)
633 using only samples from the second field experiment. The same linear models described above
634 were subsequently repeated using these alternative admixture proportions.

635 ***Genome-wide association tests***

636 To identify SNPs that were most strongly associated with fitness (survival, growth, or
637 composite), we implemented the linear mixed model (LMM) approach in GEMMA (v. 0.98.1:
638 (135)). This analysis was repeated using each fitness measure as the response variable. To
639 account for relatedness among samples we estimated the kinship matrix among all 139 hybrid
640 samples, which in turn were used in downstream LMMs. To account for the potentially
641 confounding effect of year/experiment and lake on estimated fitness measures, we included each
642 as covariates in the LMMs. To ensure rare variants were not included in these analyses, we only
643 included sites that had a minor allele frequency greater than 5% across all hybrids. A total of
644 933,520 SNPs were analyzed; 196,251 SNPS were excluded due to allele frequency change
645 following removal of parental species. SNPs strongly associated with fitness were identified with
646 1) a False Discovery Rate (FDR: Benjamini and Hochberg 1995) less than 0.05, or a 2) *P*-value
647 < 0.05 following Bonferroni correction. We focused primarily on the sites identified by the
648 conservative Bonferroni correction, however.
649
650 ***Gene ontology enrichment***
651 We annotated sites that were significantly associated with fitness using snpEff (136) and the
652 annotated *C. brontotheroides* reference genome (55). We constructed a custom database within
653 snpEff using the functional annotations originally produced by Richards et al. (55), and
654 subsequently extracted information on the annotations and putative functional consequences of
655 each variant.
656 Using genes identified for each SNP that was significantly associated with one of the
657 fitness measures, we performed Gene Ontology (GO) enrichment analyses using ShinyGO v0.61

(137). For genes identified as being intergenic, we included both flanking genes. As in Richards et al. (2021), the gene symbol (abbreviation) database that had the greatest overlap with ours was that of the human database; thus, we tested for enrichment of biological process ontologies curated for human gene functions, based on annotations from Ensembl. Results are reported for biological processes that were significantly enriched with FDR < 0.05. We then compared this list of candidate loci to those identified in past studies of San Salvador Island pupfishes (55, 88, 138).

Morphometrics

We measured 31 external morphological traits for all 139 hybrids and 69 parental individuals from Crescent Pond (30 generalists, 19 molluscivores, and 30 scale-eaters) and 85 from Little Lake (30 generalists, 25 molluscivores, and 30 scale-eaters). We digitally landmarked dorsal and lateral photographs (both sides) of each lab-reared hybrid (pre-release) or parent using DLTdv8 (139). Measurements included 27 linear distances and three angles. For nearly all individuals, lateral measurements were collected from both lateral photographs and averaged. Morphological variables were size-corrected using the residuals of a log10(trait) ~ log10(standard length) regression standardized for selection analyses as outlined in the supplement. We used these 31 morphological traits to estimate two linear discriminant (LD) axes that best distinguished the generalist, molluscivore, and scale-eater using the LDA function in the mass package in R. We then used the resultant LD model to predict LD-scores for the 139 sequenced hybrids for later use in generalized additive models.

680 ***Estimation of adaptive landscapes***

681 We fit generalized additive models (GAMs) using the mgcv package v. 1.8.28 (140) in R to
682 estimate fitness landscapes for the two discriminant axes (LD1-2) and fitness. All models
683 included a thin-plate spline fit to the two linear discriminant axes and we included both lake and
684 experiment in all models as fixed effects. Lake by experiment interaction terms were also
685 included in some models. Models were ranked using the corrected Akaike Information Criterion
686 for small sample sizes (AICc) and were considered to be a substantially worse fit to the data if
687 ΔAICc > 4 from the best-fit model (141). The best-fit model from the above approach was in
688 turn used to visualize fitness landscapes, plotting predicted values of fitness measures on the two
689 discriminant axes in R (Figure 2).

690 Using these results, we tested whether inclusion of SNPs that were strongly associated
691 with fitness (i.e., those that surpassed the 0.05 Bonferroni threshold) improved estimation of
692 fitness landscapes. We first extracted genotypes for the highly significant SNPs identified by
693 GEMMA (13 for composite fitness, four for only growth: see section *Fitness-genotype*
694 *association test*), and coded these as either reference, single, or double mutants using VCFtools
695 (130). We then used the best-fit models identified above and fit a range of models that included
696 one or all SNPs. Individual fitness-associated SNPs were treated as ordered factors (i.e. transition
697 from homozygous reference to heterozygote to homozygous alternate) and modeled using a
698 factor-smooth in the generalized additive models. Note that factor "smooths" are effectively
699 modeled as step-functions.

700 To quantify whether the local features of the complete fitness landscape constructed
701 using all morphological variables and the most strongly fitness-associated SNPs were robust to
702 sampling uncertainty, we conducted a bootstrapping procedure for this model. Specifically, we

resampled hybrids with replacement 10,000 times and refit the full model. We then calculated the mean predicted composite fitness for each linear discriminant (LD) axis in slices across the fitness landscape, both for our observed dataset, and for each bootstrap replicate. Slices divided the fitness landscape into thirds for each LD axis. We then quantified the mean and standard deviation of the predicted composite fitness for each position along the other LD axis.

We quantified uncertainty (mean ± SD) around local features of the bootstrapped fitness landscapes as compared to the observed values of predicted fitness for the same 'slice' of the fitness landscape. We predicted values at the same 30 points along each LD axis. We then plotted the locations of parents along the x-axis (LD1 or LD2) to enable relation of features on the fitness landscape to parental phenotypic distributions.

Estimation of genotypic fitness networks

We first estimated genotypic networks using sites previously shown to be highly divergent (F_{ST} > 0.95) and showing significant evidence of a hard selective sweep in one of the trophic specialists (based on evidence from both SweeD and OmegaPlus: (55, 99, 100)). We identified the SNPs in our unpruned full dataset overlapping with sites inferred to have undergone selective sweeps (55), resulting in 380 SNPs for molluscivores and 1,118 SNPs for scale-eaters. We subsequently constructed genotypic fitness networks in igraph v. 1.2.4.1 (142) following the procedure outlined in the supplement.

To visualize the high-dimensional genotypic fitness network, we randomly sampled ten adaptive loci 100 times and plotted haplotypes connected by edges if they were within five mutational steps of one another (Figure 3C). Then we calculated the mean distance between all

725 species pairs (in number of mutational steps). We used pairwise Tukey's HSD tests to test whether
726 inter-species distances differed.
727
728 ***Estimation of evolutionary accessibility***
729 We tested whether the evolutionary accessibility of genotypic fitness trajectories through
730 observed hybrid genotypes from generalist to each specialist species differed based on the source
731 of genetic variation. We restricted our investigation to networks composed of adaptive loci as
732 previously described (Figure 3A: Richards et al. 2021). This included a total of 380 SNPs in the
733 molluscivores, and 1,118 in the scale-eaters. The reduced number of adaptive SNPs sites in our
734 dataset as compared to that of (55) is due primarily to the increased stringency of our filtering.
735 We further partitioned these SNPs by their respective sources: standing genetic variation
736 (molluscivore N = 364; scale-eater N = 1,029), *de novo* mutation (scale-eater N = 24), or
737 introgression (molluscivore N = 16; scale-eater N = 65), again using the assignments from
738 Richards et al. (55). For analyses of trajectories between generalists and molluscivores, we
739 included only SNPs found to be sweeping in molluscivores; likewise, we included only SNPs
740 sweeping in scale-eaters for analysis of trajectories between generalists and scale-eaters.
741 The full procedure for constructing genotypic fitness networks, identifying accessible
742 paths, and quantifying accessibility is outlined in the supplement. Briefly, we randomly
743 generated 5,000 datasets of five SNPs comprised of either 1) standing genetic variation, 2)
744 adaptive introgression, 3) *de novo* mutation (scale-eaters only), 4) standing genetic variation +
745 adaptive introgression, 5) standing genetic variation + *de novo* mutation, or 6) standing genetic
746 variation + adaptive introgression + *de novo* mutation (scale-eaters only). We additionally
747 repeated this procedure using both classes of SNPs for molluscivores to determine whether

748 genotypic trajectories separating generalists to molluscivores are more accessible than those
749 between generalists and scale-eaters. Because different sets of sites are sweeping in each
750 specialist, we conducted these analyses separately for each species. We then constructed
751 genotypic networks, in which nodes are haplotypes of SNPs encoded in 012 format (0 =
752 homozygous reference, 1 = heterozygote, 2 = homozygous alternate), and edges link mutational
753 neighbors. When determining whether a path was accessible or not, we only included paths for
754 which each mutational step (i.e. each intervening haplotype) between generalist to specialist was
755 observed in at least one hybrid sample.

756 With these networks, we sought to ask 1) whether molluscivores or scale-eaters are more
757 accessible to generalists on their respective genotypic fitness landscapes, 2) whether the
758 ruggedness of the genotypic fitness landscape varied among specialists, and 3) whether
759 accessibility is contingent upon the source of genetic variation available to natural selection. For
760 each random network sampled and for each measure of fitness we calculated 1) the minimum
761 length of accessible paths between a random generalist and specialist sampled from our
762 sequenced individuals, 2) the number of accessible paths between the same generalist and
763 specialist pair, 3) the number of nodes, 4) the number of edges in the network, 5) the number of
764 peaks on the landscape (genotypes with no fitter neighbors (32)), 6) the distance of parental
765 nodes to these peaks, and 7) the number of accessible paths separating them. Larger networks
766 often have a greater number of potential paths, including both accessible and inaccessible paths
767 (Figure 4—figure supplement 1), and we were interested in the relative availability of accessible
768 adaptive pathways. Consequently, we divided the number of accessible paths in each random
769 network sampled by the number of nodes. Using our six summary statistics, we tested whether
770 accessibility and landscape ruggedness differed between networks constructed from

SGV/Introgression/*De novo* mutations (for scale-eaters) or SGV/Introgression (for molluscivores). To do so, we calculated the mean and standard error of each summary statistic across all 5,000 replicates. We then modeled the association between each summary statistic and species using a logistic regression, whereby species was modeled as a binary response variable (i.e. scale-eater networks = 0, molluscivore networks = 1), with each measure of accessibility as the predictor. We arbitrarily treated scale-eater networks as the control, and using the estimated coefficients obtained an odds ratio (OR) that corresponds to the extent to which molluscivore networks either have increased (OR > 1) or decreased (OR < 1) accessibility measures relative to scale-eater networks. Significance was similarly assessed using a likelihood ratio test. Additional details on this procedure may be found in the supplement. Using the fitted logistic model, we conducted a likelihood ratio test to quantify significance. To explicitly test the hypothesis that increasing landscape ruggedness reduced the length of accessible paths to the nearest fitness peak, we fit a Poisson regression model in R in which the number of fitness peaks predicts the length of the shortest accessible path between any generalist or specialist node and any fitness peak on that landscape: glm(Min. Distance to Peak ~ Number of Peaks, family = "poisson").

A similar procedure was used to assess whether measures of accessibility (scaled number of accessible paths, length of the shortest accessible path) and landscape ruggedness (number of peaks) differed within species among networks constructed from different sources of genetic variation. Here, networks constructed from SGV were treated as the control, to which all other networks were compared. For example, to test whether accessibility of the generalist-to-scale-eater paths are greater in networks constructed from *de novo* mutations than those from SGV, a logistic model was fitted wherein the response variable for SGV networks was assigned to be 0, and 1 for *de novo* networks. As before, significance was similarly assessed using a likelihood

ratio test, but here *P*-values were corrected for multiple testing using the false discovery rate (143). We assessed whether differences in these measures among the two alternate generalist to specialist trajectories in networks constructed from all three sources of variation were significant using an ANOVA in R (144). Due to the highly skewed nature of these distributions, post-hoc pairwise significance was assessed using a nonparametric Kruskal-Wallis one-way analysis of variance in the agricolae package (145) in R.

Literature Cited

1. S. Wright, The roles of mutation, inbreeding, crossbreeding and selection in evolution. *Sixth Int. Congr. Genet.*, 356–366 (1932).
2. S. Gavrilets, Evolution and speciation on holey adaptive landscapes. *Trends Ecol. Evol.* **12**, 307–312 (1997).
3. S. Gavrilets, "High-dimensional fitness landscapes and speciation" in *Evolution—the Extended Synthesis*, M. Pigliucci, G. B. Müller, Eds. (MIT Press, 2010), pp. 51–64.
4. E. Svensson, R. Calsbeek, *The adaptive landscape in evolutionary biology*, E. Svensson, R. Calsbeek, Eds. (Oxford University Press, 2012).
5. I. Fragata, A. Blanckaert, M. A. Dias Louro, D. A. Liberles, C. Bank, Evolution in the light of fitness landscape theory. *Trends Ecol. Evol.* **34**, 69–82 (2019).
6. K. K. Fear, T. Price, The adaptive surface in ecology. *Oikos* **82**, 440–448 (1998).
7. G. G. Simpson, *Tempo and mode in evolution* (Columbia University Press, 1944).
8. S. Kauffman, S. Levin, Towards a general theory of adaptive walks on rugged landscapes. *J. Theor. Biol.* **128**, 11–45 (1987).
9. R. Lande, S. J. Arnold, The measurement of selection on correlated characters. *Evolution* **37**, 1226 (1983).
10. S. J. Arnold, M. E. Pfrender, A. G. Jones, "The adaptive landscape as a conceptual bridge between micro- and macroevolution" in *Microevolution Rate, Pattern, Process*, (Springer, Dordrecht, 2001), pp. 9–32.
11. S. J. Arnold, Performance surfaces and adaptive landscapes. *Integr. Comp. Biol.* **43**, 367–375 (2003).
12. D. Schluter, P. R. Grant, Determinants of morphological patterns in communities of Darwin's finches. *Am. Nat.* **123**, 175–196 (1984).
13. D. Schluter, Estimating the form of natural selection on a quantitative trait. *Evolution* **42**, 849–861 (1988).
14. A. P. Hendry, S. K. Huber, L. F. De León, A. Herrel, J. Podos, Disruptive selection in a bimodal population of Darwin's finches. *Proc. R. Soc. B Biol. Sci.* **276**, 753–759 (2009).
15. M. O. Beausoleil, *et al.*, Temporally varying disruptive selection in the medium ground finch (Geospiza fortis). *Proc. R. Soc. B Biol. Sci.* **286** (2019).
16. C. W. Benkman, Divergent selection drives the adaptive radiation of crossbills. *Evolution* **57**, 1176–1181 (2003).
17. C. H. Martin, P. C. Wainwright, Multiple fitness peaks on the adaptive landscape drive adaptive radiation in the wild. *Science* **339**, 208–211 (2013).
18. C. H. Martin, K. J. Gould, Surprising spatiotemporal stability of a multi-peak fitness landscape revealed by independent field experiments measuring hybrid fitness. *Evol. Lett.* **4**, 530–544 (2020).
19. S. Gavrilets, *Fitness landscapes and the origin of species* (Princeton University Press, 2004).
20. M. Turelli, N. H. Barton, J. A. Coyne, Theory and speciation. *Trends Ecol. Evol.* **16**, 330–343 (2001).
21. M. R. Servedio, J. W. Boughman, The role of sexual selection in local adaptation and speciation. *Annu. Rev. Ecol. Evol. Syst.* **48**, 85–109 (2017).
22. C. Bank, S. Matuszewski, R. T. Hietpas, J. D. Jensen, On the (un)predictability of a large intragenic fitness landscape. *Proc. Natl. Acad. Sci. U. S. A.* **113**, 14085–14090 (2016).
23. S. Wright, Evolution in Mendelian Populations. *Genetics* **16**, 97–159 (1931).

24. T. Aita, M. Iwakura, Y. Husimi, A cross-section of the fitness landscape of dihydrofolate reductase. *Protein Eng. Des. Sel.* **14**, 633–638 (2001).
25. M. C. Whitlock, P. C. Phillips, F. B. G. Moore, S. J. Tonsor, Multiple fitness peaks and epistasis. *https://doi.org/10.1146/annurev.es.26.110195.003125* **26**, 601–629 (1995).
26. F. J. Poelwijk, D. J. Kiviet, D. M. Weinreich, S. J. Tans, Empirical fitness landscapes reveal accessible evolutionary paths. *Nature* **445**, 383–386 (2007).
27. F. J. Poelwijk, S. Tănase-Nicola, D. J. Kiviet, S. J. Tans, Reciprocal sign epistasis is a necessary condition for multi-peaked fitness landscapes. *J. Theor. Biol.* **272**, 141–144 (2011).
28. F. J. Poelwijk, S. Tănase-Nicola, D. J. Kiviet, S. J. Tans, Reciprocal sign epistasis is a necessary condition for multi-peaked fitness landscapes. *J. Theor. Biol.* **272**, 141–144 (2011).
29. J. Neidhart, I. G. Szendro, J. Krug, Adaptation in tunably rugged fitness landscapes: The Rough Mount Fuji model. *Genetics* **198**, 699–721 (2014).
30. J. Neidhart, I. G. Szendro, J. Krug, Adaptation in tunably rugged fitness landscapes: The Rough Mount Fuji model. *Genetics* **198**, 699–721 (2014).
31. D. M. Weinreich, N. F. Delaney, M. A. DePristo, D. L. Hartl, Darwinian evolution can follow only very few mutational paths to fitter proteins. *Science* **312**, 111–114 (2006).
32. L. Ferretti, D. Weinreich, F. Tajima, G. Achaz, Evolutionary constraints in fitness landscapes. *Heredity (Edinb).* **121**, 466–481 (2018).
33. J. Franke, A. Klözer, J. A. G. M. de Visser, J. Krug, Evolutionary accessibility of mutational pathways. *PLoS Comput. Biol.* **7**, 1002134 (2011).
34. J. A. G. M. De Visser, J. Krug, Empirical fitness landscapes and the predictability of evolution. *Nat. Rev. Genet. 2014 157* **15**, 480–490 (2014).
35. J. Maynard Smith, Natural selection and the concept of a protein space. *Nat. 1970 2255232* **225**, 563–564 (1970).
36. C. Brandon Ogbunugafor, A reflection on 50 years of John Maynard Smith's "Protein Space." *Genetics* **214**, 749–754 (2020).
37. R. A. Fisher, *The genetical theory of natural selection* (Oxford University Press, 1930).
38. H. A. Orr, The genetic theory of adaptation: A brief history. *Nat. Rev. Genet.* **6**, 119–127 (2005).
39. M. Karageorgi, *et al.*, Genome editing retraces the evolution of toxin resistance in the monarch butterfly. *Nature* **574**, 409–412 (2019).
40. M. A. Siddiq, D. W. Loehlin, K. L. Montooth, J. W. Thornton, Experimental test and refutation of a classic case of molecular adaptation in Drosophila melanogaster. *Nat. Ecol. Evol.* **1**, 25 (2017).
41. M. A. Siddiq, J. W. Thornton, Fitness effects but no temperature-mediated balancing selection at the polymorphic Adh gene of Drosophila melanogaster. *Proc. Natl. Acad. Sci. U. S. A.* **116**, 21634–21640 (2019).
42. K. S. Singh, *et al.*, The genetic architecture of a host shift: An adaptive walk protected an aphid and its endosymbiont from plant chemical defenses. *Sci. Adv.* **6**, eaba1070 (2020).
43. F. Peng, *et al.*, Effects of beneficial mutations in pykF gene vary over time and across replicate populations in a long-term experiment with bacteria. *Mol. Biol. Evol.* **35**, 202–210 (2018).
44. Z. D. Blount, C. Z. Borland, R. E. Lenski, Historical contingency and the evolution of a key innovation in an experimental population of Escherichia coli. *Proc. Natl. Acad. Sci.*

U. S. A. **105**, 7899–7906 (2008).
45. A. I. Khan, D. M. Dinh, D. Schneider, R. E. Lenski, T. F. Cooper, Negative epistasis between beneficial mutations in an evolving bacterial population. *Science* **332**, 1193–1196 (2011).
46. P. Nosil, *et al.*, Ecology shapes epistasis in a genotype–phenotype–fitness map for stick insect colour. *Nat. Ecol. Evol.* **4**, 1673–1684 (2020).
47. C. H. Martin, P. C. Wainwright, A remarkable species flock of Cyprinodon pupfishes endemic to San Salvador Island, Bahamas. *Bull. Peabody Museum Nat. Hist.* **54**, 231–241 (2013).
48. C. H. Martin, Context dependence in complex adaptive landscapes: frequency and trait-dependent selection surfaces within an adaptive radiation of Caribbean pupfishes. *Evolution* **70**, 1265–1282 (2016).
49. B. J. Turner, D. D. Duvernell, T. M. Bunt, M. G. Barton, Reproductive isolation among endemic pupfishes (Cyprinodon) on San Salvador Island, Bahamas: Microsatellite evidence. *Biol. J. Linn. Soc.* **95**, 566–582 (2008).
50. C. H. Martin, P. C. Wainwright, Trophic novelty is linked to exceptional rates of morphological diversification in two adaptive radiations of cyprinodon pupfish. *Evolution* **65**, 2197–2212 (2011).
51. M. E. St. John, K. E. Dixon, C. H. Martin, Oral shelling within an adaptive radiation of pupfishes: Testing the adaptive function of a novel nasal protrusion and behavioural preference. *J. Fish Biol.* **97**, 163–171 (2020).
52. C. H. Martin, J. A. McGirr, E. J. Richards, M. E. St. John, How to investigate the origins of novelty: Insights gained from genetic, behavioral, and fitness perspectives. *Integr. Org. Biol.* **1** (2019).
53. M. E. St. John, R. Holzman, C. H. Martin, Rapid adaptive evolution of scale-eating kinematics to a novel ecological niche. *J. Exp. Biol.* **223** (2020).
54. C. H. Martin, L. C. Feinstein, Novel trophic niches drive variable progress towards ecological speciation within an adaptive radiation of pupfishes. *Mol. Ecol.* **23**, 1846–1862 (2014).
55. E. J. Richards, *et al.*, A vertebrate adaptive radiation is assembled from an ancient and disjunct spatiotemporal landscape. *Proc. Natl. Acad. Sci.* **118**, e2011811118 (2021).
56. D. B. Weissman, M. W. Feldman, D. S. Fisher, The rate of fitness-valley crossing in sexual populations. *Genetics* **186**, 1389–1410 (2010).
57. D. B. Weissman, M. M. Desai, D. S. Fisher, M. W. Feldman, The rate at which asexual populations cross fitness valleys. *Theor. Popul. Biol.* **75**, 286–300 (2009).
58. Y. Iwasa, F. Michor, M. A. Nowak, Stochastic tunnels in evolutionary dynamics. *Genetics* **166**, 1571–1579 (2004).
59. A. F. Bitbol, D. J. Schwab, Quantifying the role of population subdivision in evolution on rugged fitness landscapes. *PLoS Comput. Biol.* **10**, e1003778 (2014).
60. A. Wagner, "High-dimensional adaptive landscapes facilitate evolutionary innovation" in *The Adaptive Landscape in Evolutionary Biology*, E. I. Svensson, R. Calsbeek, Eds. (Oxford University Press, 2012), pp. 271–282.
61. M. Conrad, The geometry of evolution. *Biosystems* **24**, 61–81 (1990).
62. A. C. Whibley, *et al.*, Evolutionary paths underlying flower color variation in Antirrhinum. *Science* **313**, 963–966 (2006).
63. G. Martin, S. F. Elena, T. Lenormand, Distributions of epistasis in microbes fit predictions

from a fitness landscape model. *Nat. Genet. 2007 394* **39**, 555–560 (2007).
64. P. A. Gros, H. Le Nagard, O. Tenaillon, The evolution of epistasis and its links with genetic robustness, complexity and drift in a phenotypic model of adaptation. *Genetics* **182**, 277–293 (2009).
65. S. Hwang, S. C. Park, J. Krug, Genotypic complexity of Fisher's Geometric Model. *Genetics* **206**, 1049–1079 (2017).
66. S. C. Park, S. Hwang, J. Krug, Distribution of the number of fitness maxima in Fisher's geometric model. *J. Phys. A Math. Theor.* **53**, 385601 (2020).
67. R. Froese, D. Pauldy, FishBase. *FishBase* (2021).
68. O. Seehausen, others, Genomics and the origin of species. *Nat. Rev. Genet.* **15**, 176–192 (2014).
69. S. H. Martin, C. D. Jiggins, Interpreting the genomic landscape of introgression. *Curr. Opin. Genet. Dev.* **47**, 69–74 (2017).
70. D. A. Marques, J. I. Meier, O. Seehausen, A Combinatorial View on Speciation and Adaptive Radiation. *Trends Ecol. Evol.* **34**, 531–544 (2019).
71. T. C. Nelson, W. A. Cresko, Ancient genomic variation underlies repeated ecological adaptation in young stickleback populations. *Evol. Lett.* **2**, 9–21 (2018).
72. K. A. Thompson, M. M. Osmond, D. Schluter, Parallel genetic evolution and speciation from standing variation. *Evol. Lett.* **3**, 129–141 (2019).
73. J. Mallet, Hybrid speciation. *Nature* **446**, 279–83 (2007).
74. O. Seehausen, Hybridization and adaptive radiation. *Trends Ecol. Evol.* **19**, 198–207 (2004).
75. C. Pardo-Diaz, *et al.*, Adaptive introgression across species boundaries in Heliconius butterflies. *PLoS Genet.* **8**, e1002752 (2012).
76. J. B. Pease, D. C. Haak, M. W. Hahn, L. C. Moyle, Phylogenomics reveals three sources of adaptive variation during a rapid radiation. *PLoS Biol.* **14**, e1002379 (2016).
77. E. J. Richards, J. W. Poelstra, C. H. Martin, Don't throw out the sympatric speciation with the crater lake water: fine-scale investigation of introgression provides equivocal support for causal role of secondary gene flow in one of the clearest examples of sympatric speciation. *Evol. Lett.* **2**, 524–540 (2018).
78. J. I. Meier, *et al.*, Ancient hybridization fuels rapid cichlid fish adaptive radiations. *Nat. Commun.* **8**, 14363 (2017).
79. M. D. McGee, *et al.*, The ecological and genomic basis of explosive adaptive radiation. *Nature* **586**, 75–79 (2020).
80. I. Irisarri, *et al.*, Phylogenomics uncovers early hybridization and adaptive loci shaping the radiation of Lake Tanganyika cichlid fishes. *Nat. Commun.* **9**, 1–12 (2018).
81. E. J. Richards, C. H. Martin, Adaptive introgression from distant Caribbean islands contributed to the diversification of a microendemic adaptive radiation of trophic specialist pupfishes. *PLoS Genet.* **13**, e1006919 (2017).
82. D. H. Alexander, J. Novembre, K. Lange, Fast model-based estimation of ancestry in unrelated individuals. *Genome Res.* **19**, 1655–1664 (2009).
83. D. H. Alexander, K. Lange, Enhancements to the ADMIXTURE algorithm for individual ancestry estimation. *BMC Bioinformatics* **12**, 1–6 (2011).
84. M. E. Arnegard, *et al.*, Genetics of ecological divergence during speciation. *Nature* **511**, 307–311 (2014).
85. S. Wang, J. J. Hard, F. Utter, Genetic variation and fitness in salmonids. *Conserv. Genet.*

3, 321–333 (2002).
86. R. Leimu, P. Mutikainen, J. Koricheva, M. Fischer, How general are positive relationships between plant population size, fitness and genetic variation? *J. Ecol.* **94**, 942–952 (2006).
87. D. Schluter, *et al.*, Fitness maps to a large-effect locus in introduced stickleback populations. *Proc. Natl. Acad. Sci. U. S. A.* **118**, 1914889118 (2021).
88. J. A. McGirr, C. H. Martin, Ecological divergence in sympatry causes gene misexpression in hybrids. *Mol. Ecol.* **29**, 2707–2721 (2020).
89. Y. Nakamura, *et al.*, Wwp2 is essential for palatogenesis mediated by the interaction between Sox9 and mediator subunit 25. *Nat. Commun.* **2**, 1–10 (2011).
90. L. Mork, G. Crump, "Zebrafish craniofacial development: A Window into early patterning" in *Current Topics in Developmental Biology*, Y. Chai, Ed. (Academic Press Inc., 2015), pp. 235–269.
91. T. Manousaki, *et al.*, Parsing parallel evolution: ecological divergence and differential gene expression in the adaptive radiations of thick-lipped Midas cichlid fishes from Nicaragua. *Mol. Ecol.* **22**, 650–669 (2013).
92. S. J. Lim, *et al.*, Taurine is an essential nutrient for juvenile parrot fish Oplegnathus fasciatus. *Aquaculture* **414**–**415**, 274–279 (2013).
93. T. G. Gaylord, A. M. Teague, F. T. Barrows, Taurine supplementation of all-plant protein diets for rainbow trout (Oncorhynchus mykiss). *J. World Aquac. Soc.* **37**, 509–517 (2006).
94. M. Yokoyama, T. Takeuchi, G. S. Park, J. Nakazoe, Hepatic cysteinesulphinate decarboxylase activity in fish. *Aquac. Res.* **32**, 216–220 (2001).
95. Z. Zhou, *et al.*, Genome-wide association study of growth and body-shape related traits in large yellow croaker (Larimichthys crocea) using ddRAD sequencing. *Mar. Biotechnol.* **21**, 655–670 (2019).
96. G. M. Yoshida, J. M. Yáñez, Multi-trait GWAS using imputed high-density genotypes from whole-genome sequencing identifies genes associated with body traits in Nile tilapia. *BMC Genomics* **22**, 1–13 (2021).
97. J. Kulmuni, A. M. Westram, Intrinsic incompatibilities evolving as a by-product of divergent ecological selection: Considering them in empirical studies on divergence with gene flow. *Mol. Ecol.* **26**, 3093–3103 (2017).
98. L. F. S. Fonseca, *et al.*, Gene expression profiling and identification of hub genes in Nellore cattle with different marbling score levels. *Genomics* **112**, 873–879 (2020).
99. P. Pavlidis, D. Živković, A. Stamatakis, N. Alachiotis, SweeD: Likelihood-based detection of selective sweeps in thousands of genomes. *Mol. Biol. Evol.* **30**, 2224–2234 (2013).
100. N. Alachiotis, A. Stamatakis, P. Pavlidis, OmegaPlus: A scalable tool for rapid detection of selective sweeps in whole-genome datasets. *Bioinformatics* **28**, 2274–2275 (2012).
101. J. A. G. M. De Visser, J. Krug, Empirical fitness landscapes and the predictability of evolution. *Nat. Rev. Genet. 2014 157* **15**, 480–490 (2014).
102. M. C. Whitlock, P. C. Phillips, F. B. G. Moore, S. J. Tonsor, Multiple fitness peaks and epistasis. *https://doi.org/10.1146/annurev.es.26.110195.003125* **26**, 601–629 (1995).
103. R. D. H. Barrett, D. Schluter, Adaptation from standing genetic variation. *Trends Ecol. Evol.* **23**, 38–44 (2008).
104. J. Hermisson, P. S. Pennings, Soft sweeps and beyond: understanding the patterns and probabilities of selection footprints under rapid adaptation. *Methods Ecol. Evol.* **8**, 700–716 (2017).

105. P. W. Hedrick, Adaptive introgression in animals: examples and comparison to new mutation and standing variation as sources of adaptive variation. *Mol. Ecol.* **22**, 4606–4618 (2013).
106. J. Kaplan, The end of the adaptive landscape metaphor? *Biol. Philos. 2008 235* **23**, 625–638 (2008).
107. V. O. Pokusaeva, *et al.*, An experimental assay of the interactions of amino acids from orthologous sequences shaping a complex fitness landscape. *PLOS Genet.* **15**, e1008079 (2019).
108. L. I. Gong, M. A. Suchard, J. D. Bloom, Stability-mediated epistasis constrains the evolution of an influenza protein. *Elife* **2013** (2013).
109. L. I. Gong, J. D. Bloom, Epistatically interacting substitutions are enriched during adaptive protein evolution. *PLOS Genet.* **10**, e1004328 (2014).
110. F. Blanquart, T. Bataillon, Epistasis and the structure of fitness landscapes: Are experimental fitness landscapes compatible with fisher's geometric model? *Genetics* **203**, 847–862 (2016).
111. I. G. Szendro, M. F. Schenk, J. Franke, J. Krug, J. A. G. M. De Visser, Quantitative analyses of empirical fitness landscapes. *J. Stat. Mech. Theory Exp.*, P01005 (2013).
112. T. C. Nelson, *et al.*, Ancient and recent introgression shape the evolutionary history of pollinator adaptation and speciation in a model monkeyflower radiation (Mimulus section Erythranthe). *PLoS Genet.* **17**, e1009095 (2021).
113. H. Svardal, *et al.*, Ancestral hybridization facilitated species diversification in the lake malawi cichlid fish adaptive radiation. *Mol. Biol. Evol.* **37**, 1100–1113 (2020).
114. S. Lamichhaney, *et al.*, Rapid hybrid speciation in Darwin's Finches. *Science* **359**, 224–228 (2018).
115. P. R. Grant, B. R. Grant, Hybridization increases population variation during adaptive radiation. *Proc. Natl. Acad. Sci. U. S. A.* **116**, 23216–23224 (2019).
116. N. B. Edelman, J. Mallet, Prevalence and adaptive impact of introgression. *Annu. Rev. Genet.* **55**, 265–283 (2021).
117. P. R. Grant, B. R. Grant, Hybridization increases population variation during adaptive radiation. *Proc. Natl. Acad. Sci. U. S. A.* **116**, 23216–23224 (2019).
118. J. I. Meier, *et al.*, The coincidence of ecological opportunity with hybridization explains rapid adaptive radiation in Lake Mweru cichlid fishes. *Nat. Commun.* **10** (2019).
119. J. W. Poelstra, E. J. Richards, C. H. Martin, Speciation in sympatry with ongoing secondary gene flow and a potential olfactory trigger in a radiation of Cameroon cichlids. *Mol. Ecol.* **27**, 4270–4288 (2018).
120. M. Moest, *et al.*, Selective sweeps on novel and introgressed variation shape mimicry loci in a butterfly adaptive radiation. *PLoS Biol.* **18**, e3000597 (2020).
121. R. C. Lewontin, L. C. Birch, Hybridization as a Source of Variation for Adaptation to New Environments. *Evolution* **20**, 315–336 (1966).
122. L. H. Rieseberg, M. A. Archer, R. K. Wayne, Transgressive segregation, adaptation and speciation. *Heredity (Edinb).* **83**, 363 (1999).
123. K. Kagawa, G. Takimoto, Hybridization can promote adaptive radiation by means of transgressive segregation. *Ecol. Lett.* **21**, 264–274 (2018).
124. R. Abbott, *et al.*, Hybridization and speciation. *J. Evol. Biol.* **26**, 229–46 (2013).
125. N. B. Edelman, J. Mallet, Prevalence and adaptive impact of introgression. *Annu. Rev. Genet.* **55**, 265–283 (2021).

126. Broad Institute, Picard Toolkit (2018).
127. M. A. Depristo, *et al.*, A framework for variation discovery and genotyping using next-generation DNA sequencing data. *Nat. Genet.* **43**, 491–501 (2011).
128. R. Poplin, *et al.*, Scaling accurate genetic variant discovery to tens of thousands of samples. *bioRxiv*, 201178 (2017).
129. C. D. Marsden, *et al.*, Diversity, differentiation, and linkage disequilibrium: Prospects for association mapping in the malaria vector anopheles arabiensis. *G3 Genes, Genomes, Genet.* **4**, 121–131 (2014).
130. P. Danecek, *et al.*, The variant call format and VCFtools. *Bioinformatics* **27**, 2156–2158 (2011).
131. S. Purcell, *et al.*, PLINK: A tool set for whole-genome association and population-based linkage analyses. *Am. J. Hum. Genet.* **81**, 559–575 (2007).
132. C. T. DiVittorio, *et al.*, Natural selection maintains species despite frequent hybridization in the desert shrub Encelia. *Proc. Natl. Acad. Sci. U. S. A.* **117**, 33373–33383 (2021).
133. J. Hereford, A quantitative survey of local adaptation and fitness trade-offs. *Am. Nat.* **173**, 579–588 (2009).
134. A. Henningsen, censReg: Censored regression (Tobit) models. (2020).
135. X. Zhou, M. Stephens, Genome-wide efficient mixed-model analysis for association studies. *Nat. Genet.* **44**, 821–824 (2012).
136. P. Cingolani, *et al.*, Using Drosophila melanogaster as a model for genotoxic chemical mutational studies with a new program, SnpSift. *Front. Genet.* **3** (2012).
137. S. X. Ge, D. Jung, D. Jung, R. Yao, ShinyGO: A graphical gene-set enrichment tool for animals and plants. *Bioinformatics* **36**, 2628–2629 (2020).
138. J. A. McGirr, C. H. Martin, Few fixed variants between trophic specialist pupfish species reveal candidate cis-regulatory alleles underlying rapid craniofacial divergence. *Mol. Biol. Evol.* **38**, 405–423 (2021).
139. T. L. Hedrick, Software techniques for two- and three-dimensional kinematic measurements of biological and biomimetic systems. *Bioinspiration and Biomimetics* **3**, 034001 (2008).
140. S. N. Wood, Fast stable restricted maximum likelihood and marginal likelihood estimation of semiparametric generalized linear models. *J. R. Stat. Soc. Ser. B (Statistical Methodol.* **73**, 3–36 (2011).
141. K. P. Burnham, D. R. Anderson, *Model Selection and Multimodel Inference* (Springer New York, 2002).
142. G. Csardi, T. Nepusz, The igraph software package for complex network research. *InterJournal Complex Syst.* **1695**, 1–9 (2006).
143. Y. Benjamini, Y. Hochberg, Controlling the false discovery rate: a practical and powerful approach to multiple testing. *J. R. Stat. Soc. Ser. B*, 289–300 (1995).
144. R. C. Team, R: A language and environment for statistical computing. (2019).
145. F. de Mendiburu, agricolae: Statistical procedures for agricultural research (2020).
146. T. Guillerme, dispRity: A modular R package for measuring disparity. *Methods Ecol. Evol.* **9**, 1755–1763 (2018).
147. B. J. Knaus, N. J. Grünwald, VCFR: a package to manipulate and visualize variant call format data in R. *Mol. Ecol. Resour.* **17**, 44–53 (2017).
148. S. Der Yang, T. S. Lin, F. G. Liu, C. H. Liou, Influence of dietary phosphorus levels on growth, metabolic response and body composition of juvenile silver perch (Bidyanus

bidyanus). *Aquaculture* **253**, 592–601 (2006).

149. J. M. Costa, *et al.*, Inadequate dietary phosphorus levels cause skeletal anomalies and alter osteocalcin gene expression in Zebrafish. *Int. J. Mol. Sci.* **19**, 364 (2018).

150. H. Yu, *et al.*, Effects of stocking density and dietary phosphorus levels on the growth performance, antioxidant capacity, and nitrogen and phosphorus emissions of juvenile blunt snout bream (Megalobrama amblycephala). *Aquac. Nutr.* **27**, 581–591 (2021).

Appendix 1:

Supplementary Methods

Sampling of hybrid individuals

Samples of hybrid *Cyprinodon* pupfish included herein were first collected following two separate fitness experiments, conducted on San Salvador Island in 2011 (17) and 2016 (18) respectively. Experiments were carried out in two lakes: Little Lake (LL), and Crescent Pond (CP). Following their initial collection at the conclusion of their respective experiments (see (17) and (18) for protocols), samples were stored in ethanol. In late 2018, 149 hybrid samples were selected for use in this experiment. Of these, 27 are from the experiment conducted in 2011 (14 from LL, 13 from CP), and the remaining 122 are from the 2016 experiment (58 from LL, 64 from CP). Due to reduced sample size for some species within Little Lake, we include fish obtained from Osprey Lake for downstream analyses comparing hybrids to Little Lake, as the two comprise a single, interconnected body of water.

Genomic Library Prep

DNA was extracted from the muscle tissue of hybrids using DNeasy Blood and Tissue kits (Qiagen, Inc.); these extractions were then quantified using a Qubit 3.0 fluorometer (Thermo Scientific, Inc). Genomic libraries were prepared by the Vincent J. Coates Genomic Sequencing Center (QB3) on the automated Apollo 324 system (WaterGen Biosystems, Inc.). Samples were fragmented using a Covaris sonicator, and barcoded with Illumina indices. Samples were quality checked using a Fragment Analyzer (Advanced Analyical Technologies, Inc.). All samples were sequenced to approximately 10x raw coverage on an Illumina NovaSeq.

Genotyping and filtering

Because we are interested in genomic variants found not only within our hybrid samples but across San Salvador island and the Caribbean, we conducted genotyping including all 247 samples from Richards et al. (55). These samples include members of the three species (*C. variegatus*, *C. brontotheroides*, *C. desquamator*) found on San Salvador Island, as well as individuals of *C. variegatus* found throughout the Caribbean, and numerous outgroups (*C. laciniatus*, *C. higuey*, *C. dearborni*, *Megupsilon aporus*, and *Cualac tesselatus*). We then excluded *M. aporus* and *C. tesselatus* along with 18 additional samples for which necessary data for downstream analyses were missing (e.g. quality photographs for the collection of morphological data). This approach led to the retention of a total of 4,206,786 total SNPs and 139 hybrid individuals.

Morphometrics

Because the morphological measurements used in the 2013 and 2016 experiments differ slightly, we remeasured all sequenced hybrid individuals and up to 30 individuals of each parent species for the 30 morphological characters described in Martin & Gould (18), as well as for standard length (SL).

For each photograph, unit-scale was obtained by additionally landmarking points on a regular grid included in each photograph using DLTdv8a (139). Landmark data (x-y coordinates in units of pixels) were subsequently uploaded into R and converted to millimeters (in the case of linear measurements) or degrees (for angular measurements) using a custom script.

We then assessed, for each trait, the need for size-correction. That is, we sought to avoid an outsized role of body size in downstream interpretation. Thus, if a trait was colinear with SL,

we regressed the two (treating SL as the predictor) and took the residuals. In each case, both SL and the response were Log-10 transformed. Subsequently, residuals were scaled such that their distribution had a mean of 0, and a standard deviation of 1. Traits that did not need size correction were also Log-transformed and unit-scaled.

We used these morphological measurements to estimate two linear discriminant (LD) axes that distinguish the generalist, molluscivore, and scale-eater using the LDA function in R. That is, we used morphological data from the 165 parental fish to estimate LD scores for each individual. Doing so, we were able to correctly assign individual fish to their corresponding species with 99.4% accuracy (Figure 2—figure supplement 4-5). Attempting to predict species assignment by lake did not improve this prediction accuracy (instead reducing prediction accuracy to 98.7%); consequently, we proceeded with the LD axes estimated without accounting for lake.

We additionally asked whether 1) specialists were more morphologically constrained than generalists and 2) if hybrids were less constrained than the three parental species. To do so, we calculated morphological disparity per group using the dispRity.per.group function implemented in the R package dispRity v1.3.3 (146). Specifically, this function calculates the median distance between each row (sample) and the centroid of the matrix per group. By bootstrapping the data 100 times, we tested the hypothesis that each of the three parental species differed significantly in their morphological disparity, first using an ANOVA, followed by a post-hoc pairwise t-test to assess pairwise significance in R. We corrected for multiple tests using an FDR correction.

To test whether genetic distance predicts morphological distance, we calculated two distance matrices. First, we calculated pairwise Euclidean distances between all hybrids using all morphological variables. Then, we calculated pairwise genetic distances between all hybrids using the final set of SNPs described above with the genet.dist function implemented in vcfR (147). We then fit a simple linear model, regressing genetic distance on morphological distance.

Estimation of Adaptive Landscapes

We sought to characterize the extent to which the three measures of fitness are predicted by morphology alone and to, in turn, visualize fitness landscapes for our sequenced hybrids. To do so, we fitted six generalized additive models (GAMs) using the mgcv package v. 1.8.28 (140) in R. All models included a thin-plate spline fitted for the two linear discriminant axes. Because we have strong *a priori* knowledge that fitness outcomes will be contingent to some extent on experiment year and on the lake in which hybrids were placed, we include experiment and lake in all fitted models, modeled either as fixed effects, or as an interaction term between the two. Additionally, we fitted models that included individual splines for each linear discriminant axis, either with or without experiment or lake as a factor smooth. The full list of models and their respective fits are included in the supplement (Appendix 1—table 11-13).

For composite fitness, we excluded three SNPs that were within close proximity (i.e. < 1000bp) to a SNP that was more significantly associated. Because of the reduced number of significantly associated SNPs identified for growth (four) as compared to composite fitness (ten), we were able to fit and compare all combinations of significantly associated SNPs for the former. The best-fit model for composite fitness was also the most complex, including all fitness associated SNPs. Thus, to reduce model complexity, we fit one additional model, excluding any of the three SNP (fixed effect) that was not significant in the full model. The full range of models

and their associated fits are reported in Appendix 1—table 14-15. As before, predicted fitness values across LD space were extracted from the best-fit model and plotted using R.

Genotypic Fitness Networks

Recent work has shown that the adaptive radiation of the pupfish of San Salvador island involved selection on standing genetic variation, adaptive introgression, and *de novo* mutation (55). Furthermore, the specialists on San Salvador Island received approximately twice as much adaptive introgression as did generalists on neighboring islands. These findings imply that each source of genetic variation may exert a unique influence on the fitness landscape, in turn facilitating the radiation. We sought to explore this possibility and so estimated genotypic fitness networks using sites previously shown to have undergone hard selective sweeps in specialists. To do so, we identified the SNPs in our un-thinned dataset overlapping with sites inferred to have undergone selective sweeps (55) to produce two datasets (one for each specialist). We then constructed networks using the following procedure:

1) Target SNPs were extracted from the vcf file of all sequenced hybrids and parental species from Crescent Pond and Little Lake in 0/1/2 format using VCFtools. That is, individuals genotyped as homozygote reference were coded as 0, heterozygotes as 1, and homozygote alternatives as 2. Note again that the reference genome used was that of the molluscivore, *C. brontotheroides*.
2) These SNPs were subsequently loaded into R, and concatenated into haplotypes, such that each sequenced individual has a haplotype. These per-sample haplotypes were subsequently associated with metadata, namely the observed binary survival, growth, assignment as hybrid or one of the three parental species, and lake of origin.
3) Each haplotype was subsequently collapsed and summarized, such that mean survival, growth, and composite fitness are retained for each unique haplotype. Additionally, the number of hybrids, generalists, molluscivores and scale-eaters that have the haplotype were recorded.
4) The distance, in number of mutational steps was then calculated for each pairwise combination of haplotypes. For example, the distance between haplotype 000 and 001 is a single mutational step, whereas haplotypes 000 and 002 are two steps away.
5) Lastly, we constructed networks using the R package igraph v. 1.2.4.1 (142). Specifically, nodes represent haplotypes, and edges are drawn between haplotypes that are mutational neighbors (i.e. are a single mutational step away). Nodes present in hybrids were colored and sized proportional to their respective mean fitness. Nodes present only in parental species were colored according to the species in which that haplotype is unique to.

Estimation of evolutionary accessibility

The large number of SNPs in our dataset above raises numerous challenges in the visualization and summarization of fitness networks. Perhaps most significant, is that as the number of sites assessed increases, the sequence space increases vastly; the number of potential haplotypes is defined by 3 to the power of the number of SNPs, and the number of potential edges is defined by the number of haplotypes choose 2. Consequently, networks constructed from a larger number of focal SNPs are comprised of haplotypes that are separated on average by more mutational steps than those constructed from fewer SNPs. Because we can only interpret the fitness consequences of evolutionary trajectories for which we have data along each mutational

step, we restricted analysis to haplotypes that are mutational neighbors (i.e., separated by a single mutational step).

To do so, we developed a permutation approach to construct fitness networks from SNPs that were sourced from the three sources of genetic variation defined above as well as all possible combinations including standing variation (i.e. standing genetic variation + adaptive introgression and/or de novo mutation). Specifically, from each set we sampled five SNPs up to 5000 times. For networks constructed from combinations of sources (e.g. SGV + introgression), we ensured that at least one of each source was present. To do so, we generated 1000 random sets of SNPs for all possible combinations (e.g. 1 SGV - 4 introgression, 2 SGV – 3 introgression, etc). Then, we sampled up to 5000 of these combinations; these samples comprise our permutations. Then, from each permutation, we constructed fitness networks using the five steps defined above; these networks served as the subsequent assessment of evolutionary accessibility of genotypic trajectories separating the generalists from either specialist. Edges were only drawn such that the network is directed; that is, edges were drawn from low to higher or equal fitness nodes.

We constructed networks using both parental species and hybrids. For each trajectory under consideration (generalist → molluscivore & generalist → scale-eater), we first identified all generalist to specialist trajectories that are connected by accessible (monotonically increasing) paths. From these connected generalist-specialist node pairs, we randomly sampled a single pair. We then identified the number and length of accessible paths separating the generalist node from the specialist node and recorded these values using the "all_simple_paths" function in igraph and excluded any paths that traversed through haplotypes not found in any hybrid (i.e., exclusive to parental species) and thus had no information on fitness.

Specifically, two node paths (a single mutational step from generalist to specialist) were allowed only if both parental nodes (SNP haplotypes) were also observed in hybrids, with fitness data. Three-node paths were allowed if hybrid fitness data was present for at least one of the parental nodes and the intervening node between the two parental nodes. Paths that were four nodes or longer were allowed only if all intervening nodes between parental nodes had associated hybrid fitness data.

We additionally calculated the number of peaks on the genotypic fitness landscape, as well as the number of accessible paths between parental nodes and these peaks, and the minimum distance from parental nodes to a peak on the landscape. We define 'peaks' on the genotypic fitness landscape as genotypes (SNP haplotypes) with no-fitter neighboring genotype, follow the definition of Ferretti et al. (32). This definition is inclusive of nodes/genotypes that are equal in fitness to their neighbors, which may be fitter than all other neighboring nodes. We conservatively excluded nodes that shared only a single neighbor.

Supplementary Results

Population ancestry associations with fitness

When repeating our test for an association between fitness measures and ancestry proportions as estimated from a supervised ADMIXTURE analyses, we recovered similar results with one exception; generalist ancestry was significantly associated with growth rate (generalist: $P = 0.021$). Admixture proportions estimated from an unsupervised analysis did not significantly predict any measure of fitness when only using hybrids from the second field experiment (Appendix 1—table 4) (18). Genome-wide PC1 was associated with composite fitness ($P = 0.004$) and survival ($P < 0.001$), whereas PC2 was not (Appendix 1—table 5). However, PC1

largely explains differences among lakes (Figure 1c); thus, the positive correlation between PC1 and fitness is likely explained by the previously described overall differences in survival observed between the two lakes in past experiments (17, 18).

Genomic associations recovered for composite fitness and growth, not survival

Whereas we identified 132 SNPs that were associated with composite fitness, only 58 were associated with growth and none were associated with survival. Of the SNPs associated with growth, only four remained significant using the conservative Bonferroni threshold. Across all significant sites (either via FDR or Bonferroni correction) a total of 11 were shared across analyses. The only gene proximate to a growth associated SNP was *csad.* Lastly, we found a single gene shared between our study and the 125 ecological DMIs (putative genetic incompatibilities that are differentially expressed among specialists and misexpressed in F1 hybrids) presented in McGirr & Martin (88). This gene, associated with growth (but not composite fitness) in our study, is *mettl21e*.

When considering SNPs found to be associated with growth, we did not identify any gene ontologies that were significantly enriched at a False Discovery Rate < 0.01. However, looking at those enriched at an FDR < 0.05, we do observe a number of ontologies related to biosynthetic processes, and regulation of metabolic processes (Figure 2—figure supplement 3). Specifically, the greatest (and most significant) enrichment was for that of phosphorus and phosphate containing compound metabolic processes and their regulation. Phosphorous deficiencies have previously been associated with poor growth in silver perch (*Bidyanus bidyanus*: (148)) and skeletal deformaties (including vertebral compression and craniofacial deformaties) in zebrafish (*Danio rerio*: (149)). Similarly, blunt snout bream (*Megalobrama amblycephala*) exhibited greater growth rates with increasing phosphorous levels in their diets (150). In short, enrichment of growth-associated SNPs for ontologies pertaining to phosphorous metabolism is consistent with the substantial literature documenting that phosphorous availability and metabolism is a determinant of growth in fishes.

Morphological variation within sampled hybrids

As in the previous two experiments, there is a relative paucity of hybrids exhibiting the morphologies that characterize either specialist. Rather, most hybrids fall near the generalists, with a number exhibiting transgressive morphologies (Figure 2—figure supplement 5a). As expected, both specialists exhibit reduced morphological disparity as compared to generalists, and hybrids show the greatest (Figure 2—figure supplement 5b. That is, the specialists appear more morphologically constrained than generalists, falling on average closer to the group centroid. Interestingly molluscivores exhibit the least disparity, even less so than scale-eaters.

Fitness-associated SNPs influence shape of the adaptive landscape

Using morphology alone, the best fit generalized additive model for survival, growth, and composite fitness were simpler than the model for composite fitness using both morphology and fitness-associated SNPs (Appendix 1—table 11-13). For survival and composite fitness (Figure 2—figure supplement 6a-6b), this model included a thin-plate spline for LD1 & LD2, with experiment and lake included as fixed effects. The resultant landscape was also similar for these two analyses, supporting an interpretation of directional selection, favoring molluscivores. For growth, the best-fit model had the thin-plate spline for LD1 & LD2, but included an interaction term between experiment and lake (Figure 2—figure supplement 6c; Appendix 1—table 12). In

contrast to the previous two models, the landscape predicted using growth as our proxy of fitness supported an interpretation of directional selection in favor or hybrids most similar to generalists, and to a lesser extent, scale-eaters.

Notably, model selection using AICc invariably supported the inclusion of fitness associated SNPs for growth and composite fitness (Appendix 1—table 14-15). For growth, the best-fit model including genotypes was an improvement of 22.99 AICc over the model including morphology alone, whereas for composite fitness, the improvement was 94.527 AICc. Interestingly, the best-fit models and growth including associated SNPs was similar to that of the landscape without fitness-associated SNPs, but largely supported an interpretation of directional selection in favor of scale-eaters, and to a lesser extent generalists.

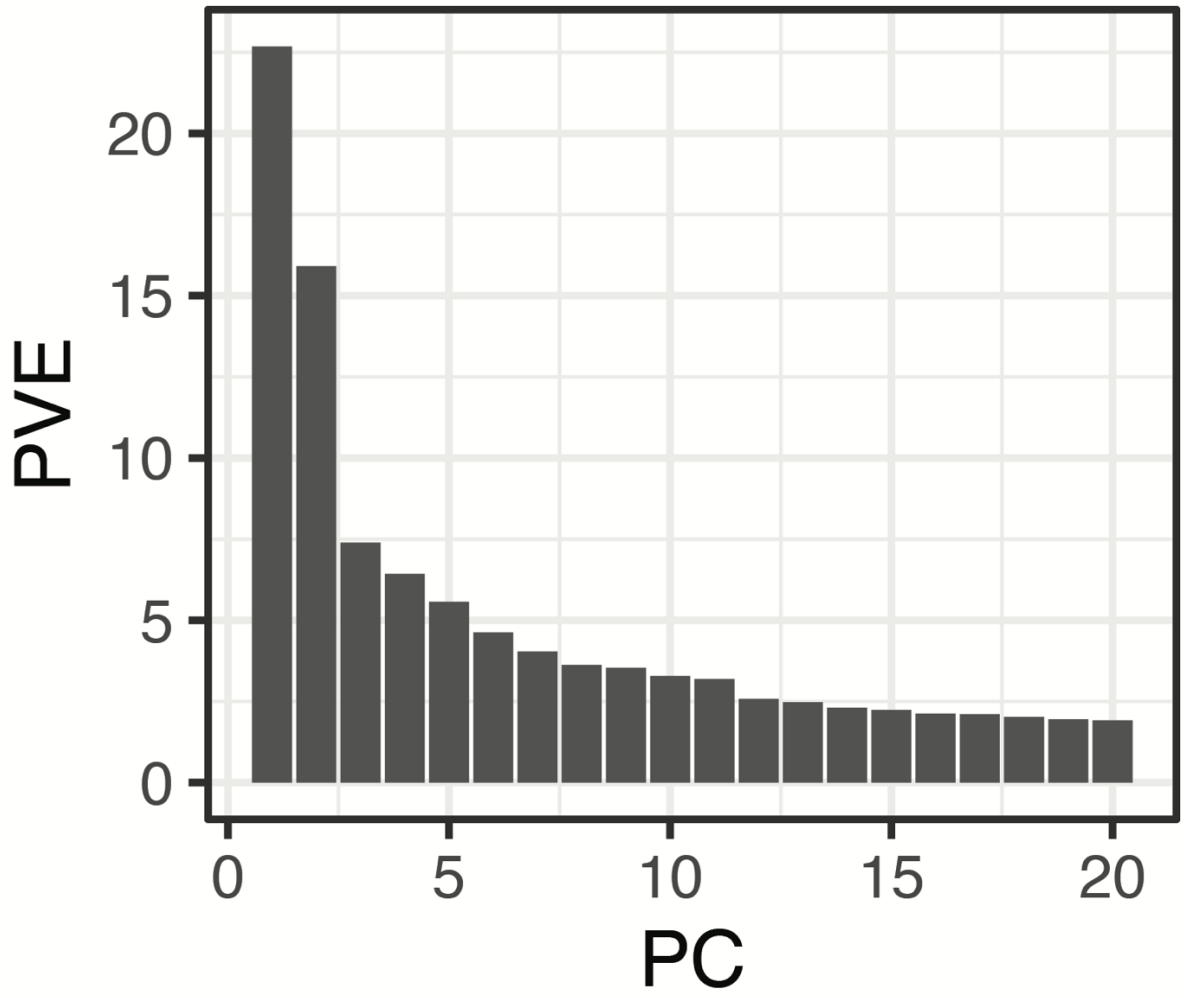

Figure 1—figure supplement 1. Proportion (%) genetic variance explained by the first 20 Principal Components obtained using all SNPs and individuals from Crescent Pond, Little Lake, and Osprey Lake, as well as experimental hybrids. The first two principal component axes are plotted in Figure 1.

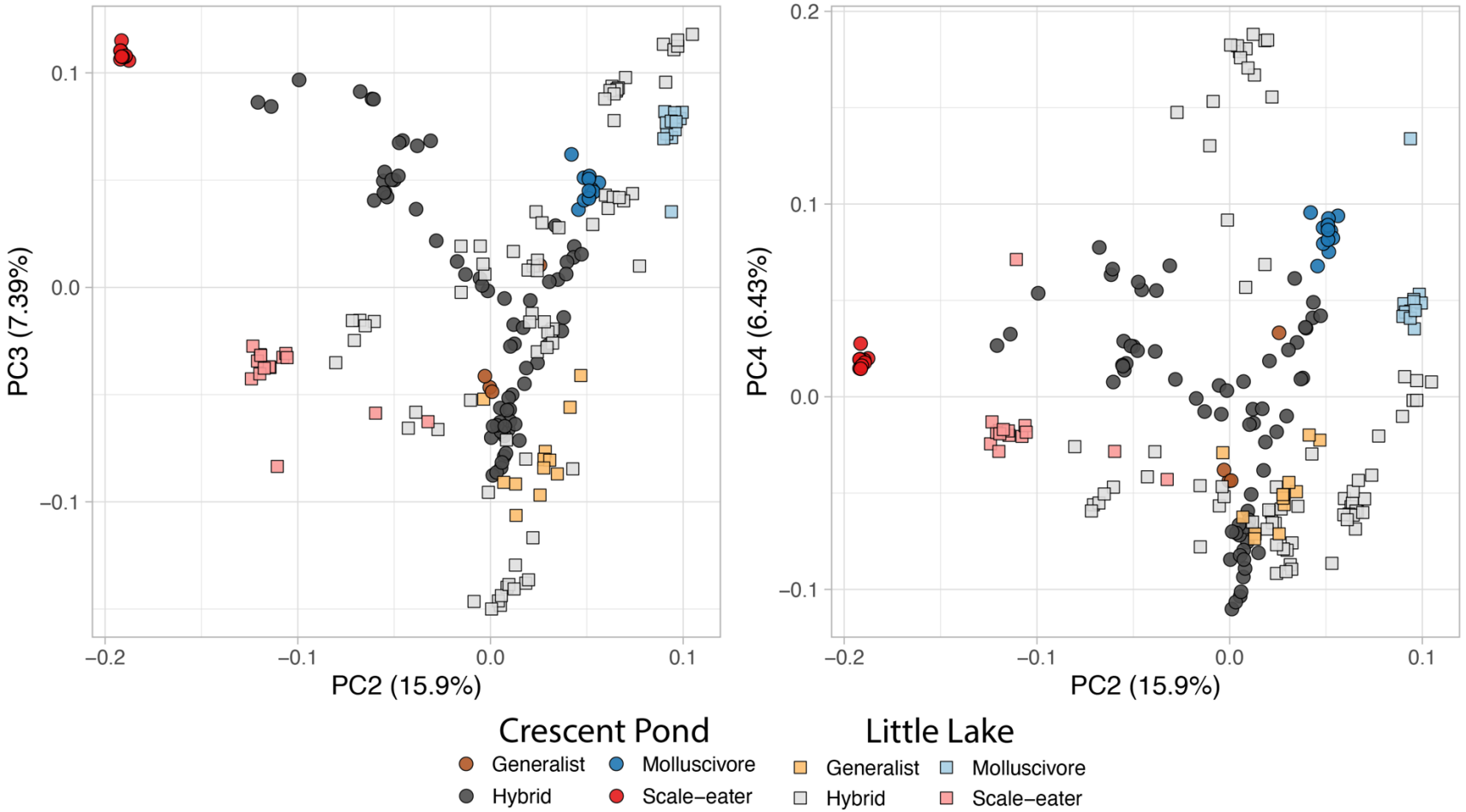

Figure 1—figure supplement 2. Principal components two, three, and four.

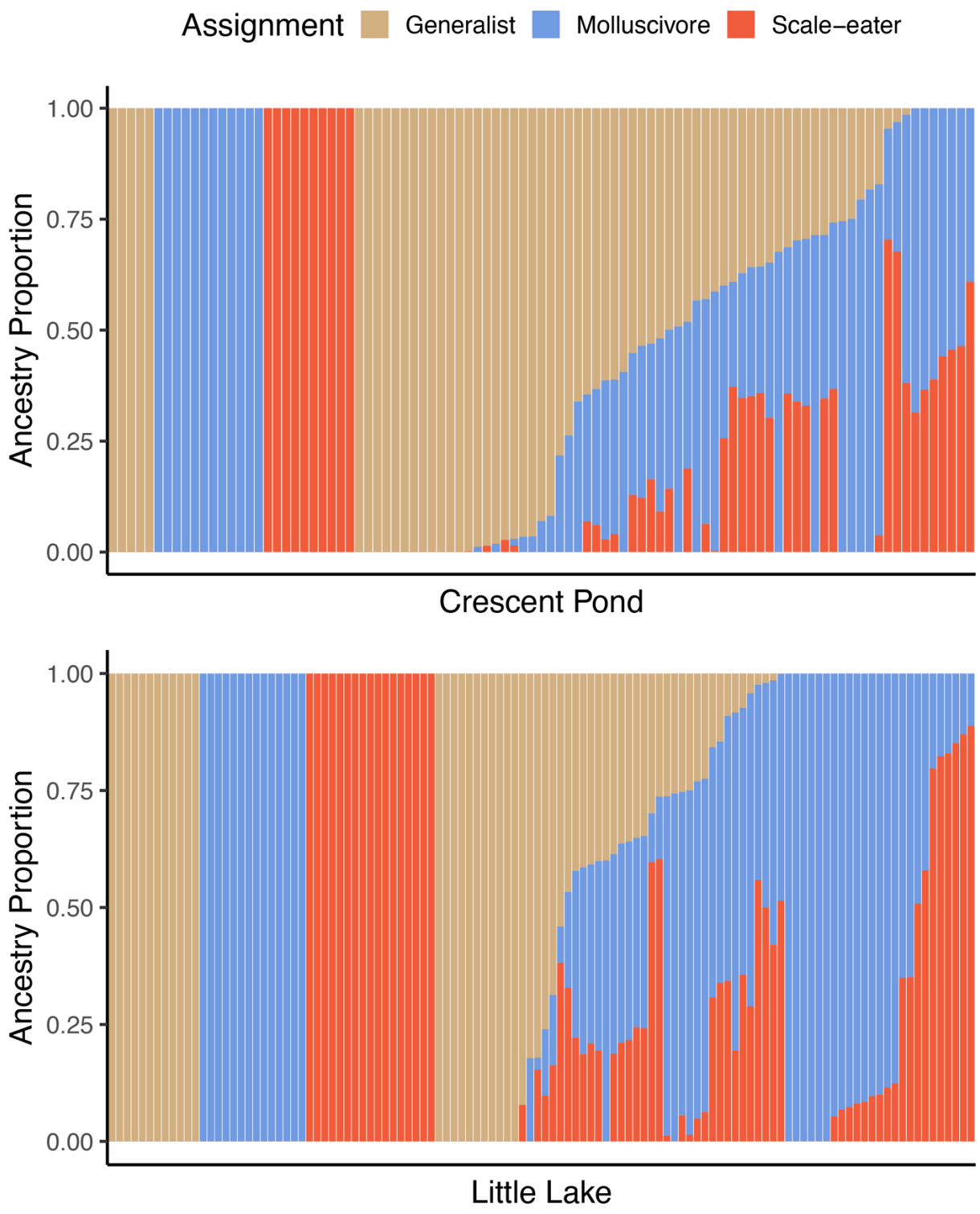

Figure 1—figure supplement 3. Supervised ADMIXTURE analyses for Crescent Pond (top) and Little Lake (bottom). Sampled individuals of each species (leftmost) individuals were assigned to one of three populations, whereas ancestry proportions were estimated for all resequenced hybrid individuals from field experiments. Colors correspond to probability of assignment to one of three assumed populations/species (K = 3) in this analysis).

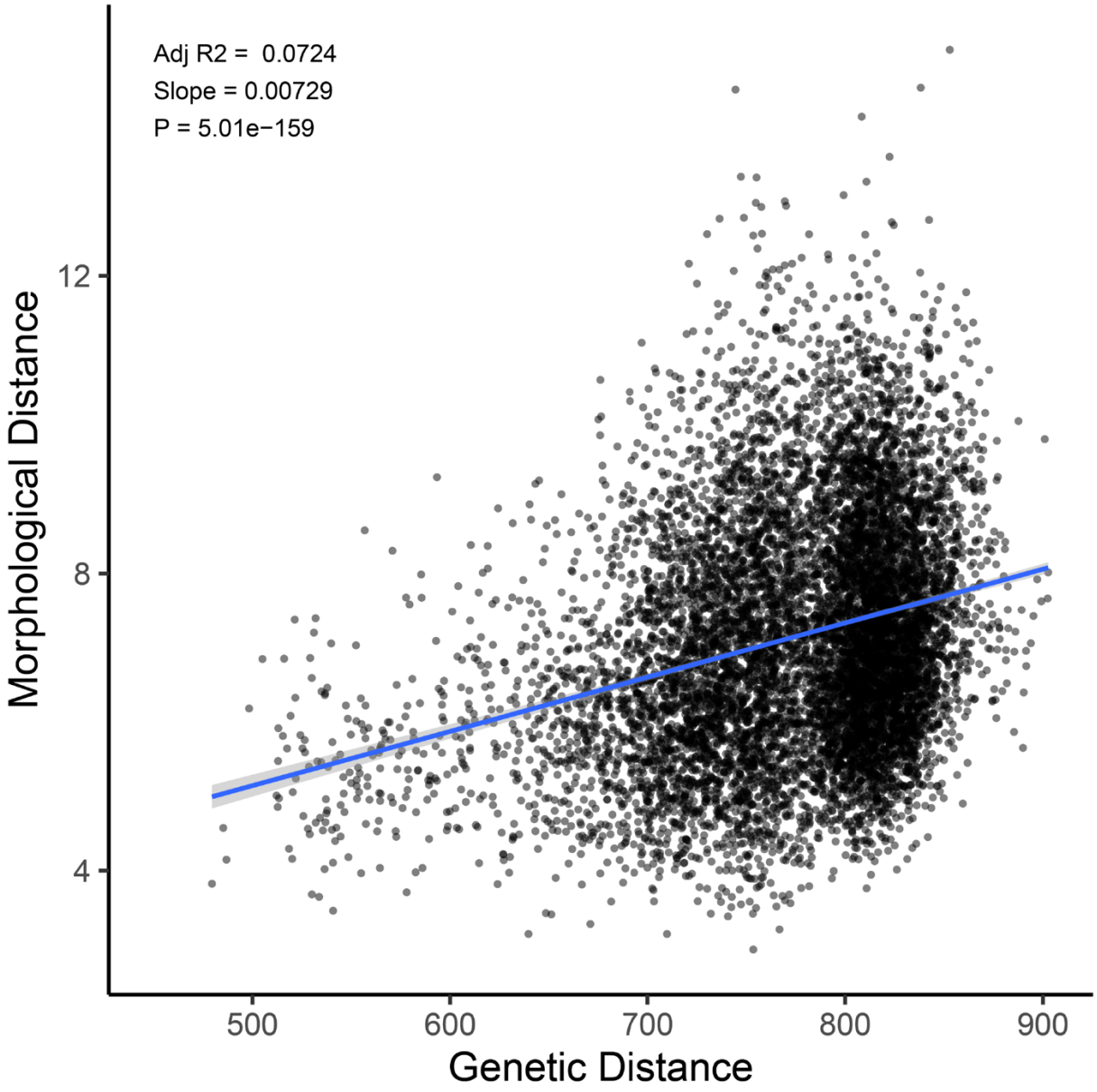

Figure 1—figure supplement 4. Genetic distance predicts morphological distance among sampled hybrids.

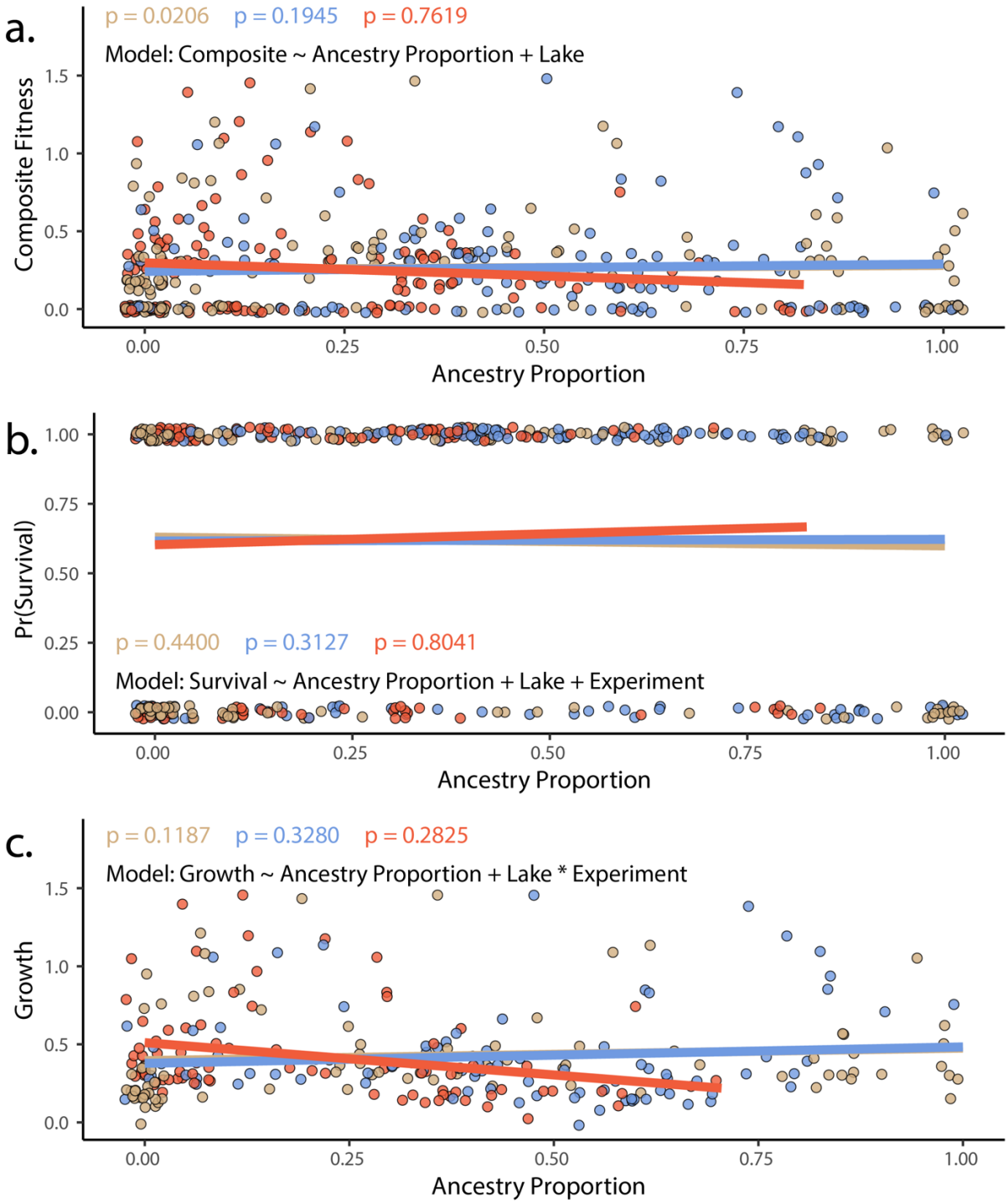

Figure 1—figure supplement 5. The proportion of generalist or specialist ancestry in hybrids did not predict in experimental hybrids using either A) composite fitness (tobit/zero-censored), B) survival (binomial) or C) growth (gaussian). Results of a generalized in which survival (modeled as a binomial) is predicted by ancestry proportion, including lake and experiment as fixed effects. Points represent individual hybrids, with each individual represented by two points, one indicating their respective scale-eater (salmon, and molluscivore (blue) ancestry proportions. *P*-values correspond to the effect of each type of ancestry (scale-eater – red, molluscivore – blue) on survival probability. Lines are predicted values and are colored according to species.

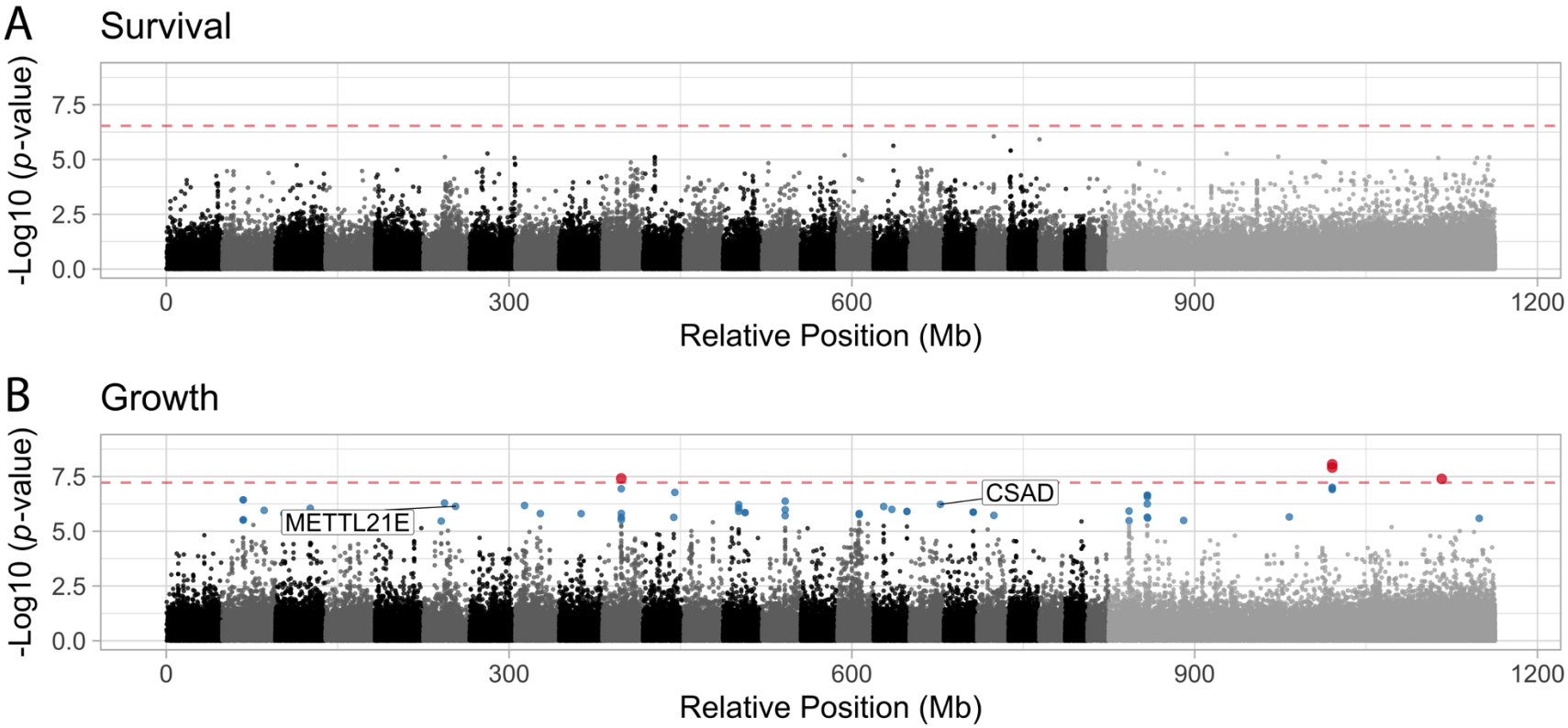

Figure 2—figure supplement 1. Manhattan plots illustrating the strength of association between individual SNPs and either Survival (A) or Growth (B) as inferred by GEMMA. Significant associations are highlighted in blue (FDR < 0.05) or red (Bonferroni correction P < 0.05). The dashed red line indicates the threshold for significance following Bonferroni p-value adjustment. METTL21E and CSAD are both highly differentiated (F_{ST} > 0.95) among specialists, differentially expressed. METTL21E is also misexpressed in F1 hybrids, meaning it exhibits gene expression that is higher or lower than observed in both parental species (88), indicating it is involved in intrinsic incompatibilities.

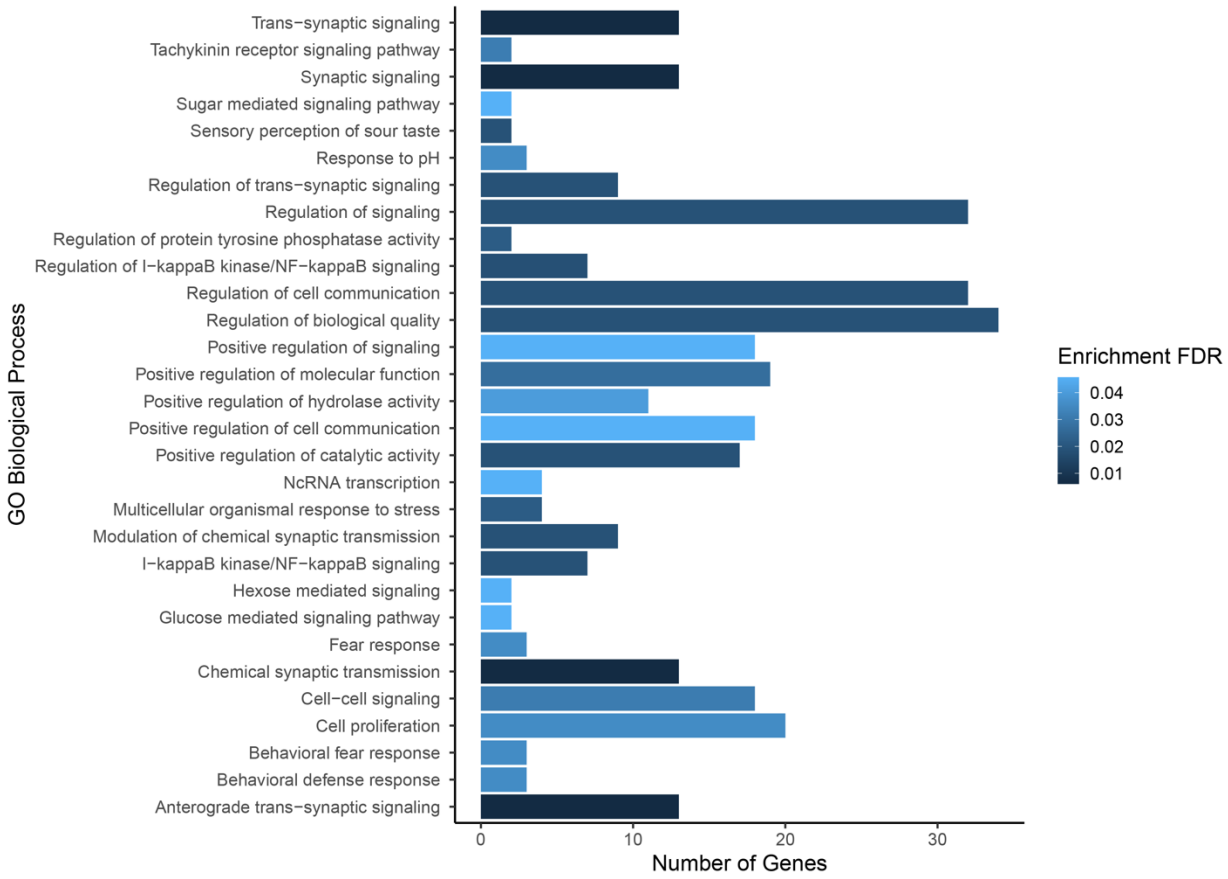

Figure 2—figure supplement 2. Gene ontology enrichment for SNPs found to be associated with composite fitness. Darker colors indicate ontologies that are more significantly enriched following FDR correction. Length of bar is proportional to the number of genes assigned to an ontology.

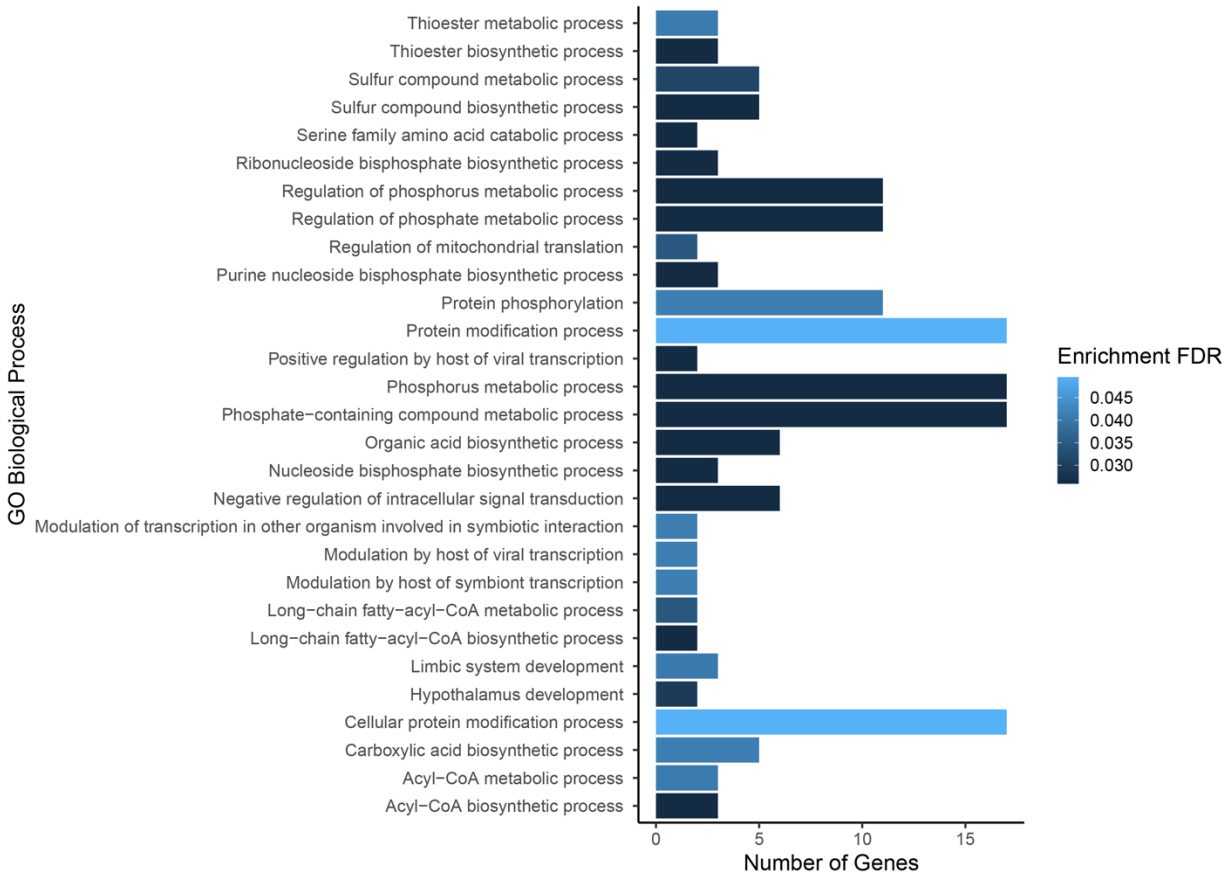

Figure 2—figure supplement 3. Gene ontology enrichment for SNPs found to be associated with growth. Darker colors indicate ontologies that are more significantly enriched following FDR correction. Length of bar is proportional to the number of genes assigned to an ontology.

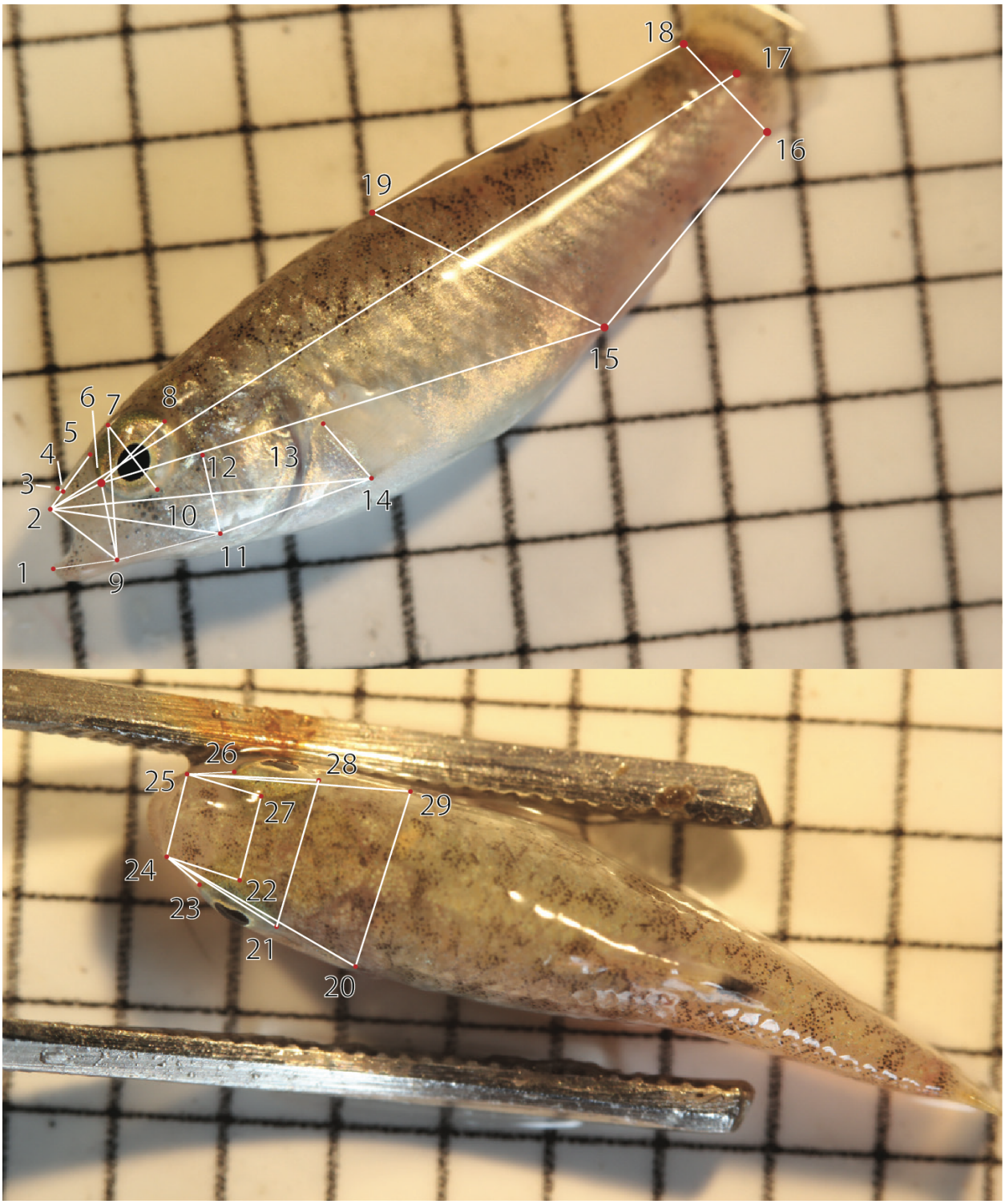

Figure 2—figure supplement 4. The 29 landmarks used to digitally measure thirty traits plus standard length using DLTDV8a (139)**.** The corresponding traits are shown in Appendix 1—table 7.

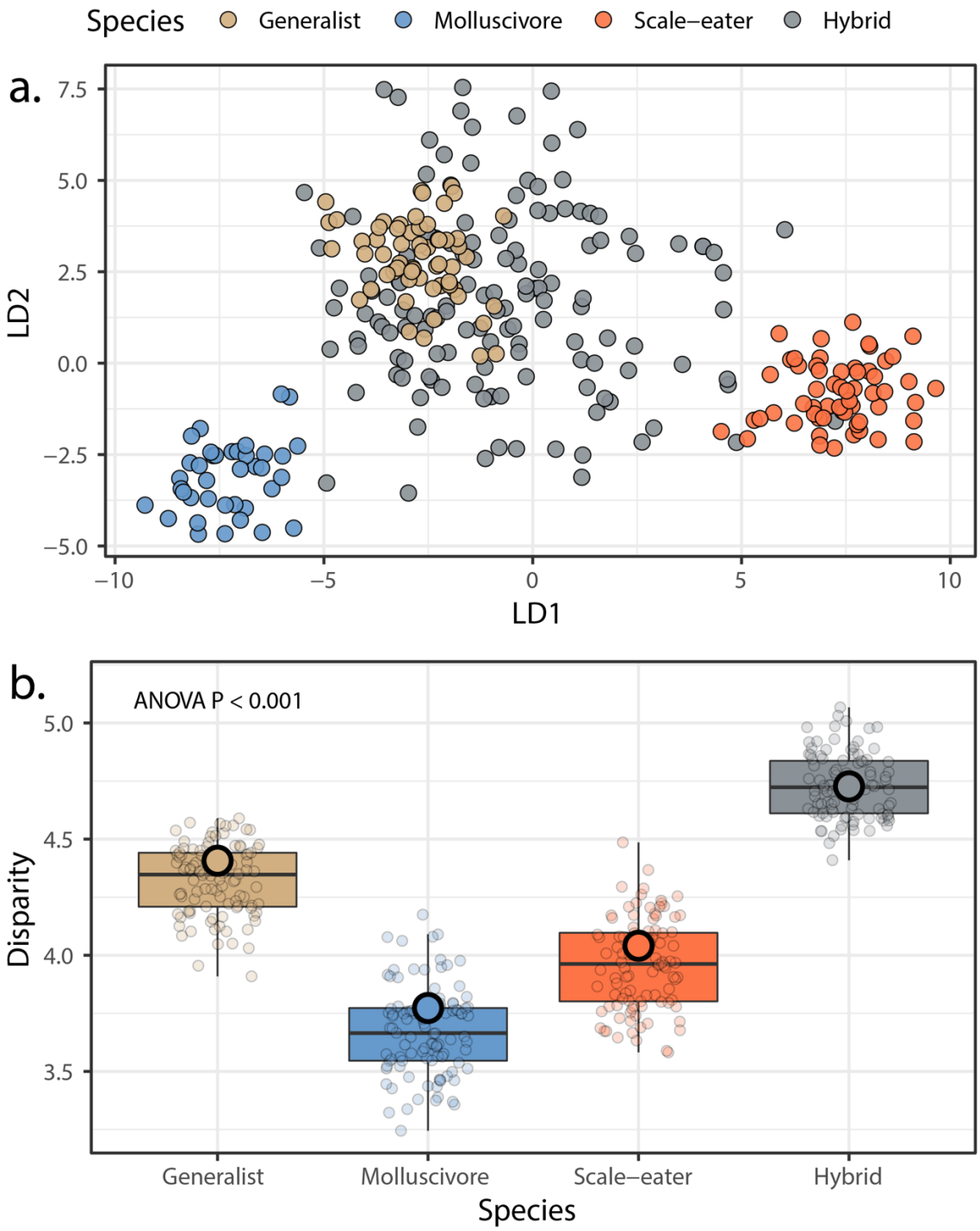

Figure 2—figure supplement 5. Morphological variation in the three San Salvador Island pupfish species and their experimentally produced hybrids. A. Linear discriminant (LD) morphospace. Parent species and hybrids are plotted using the two LD axes that together serve to distinguish species with 99.4% accuracy. **B.** Within-group disparity calculated as the median distance between each individual and the groups centroid. Small, semitransparent points are the result of 100 bootstrap replicates, and are summarized by box plots, which in turn show the median and interquartile ranges of these bootstrap replicates. Large, opaque points are the observed disparities using the full dataset per group. All pairwise comparisons using t-tests following correction for the false discovery rate were significant ($P < 0.001$).

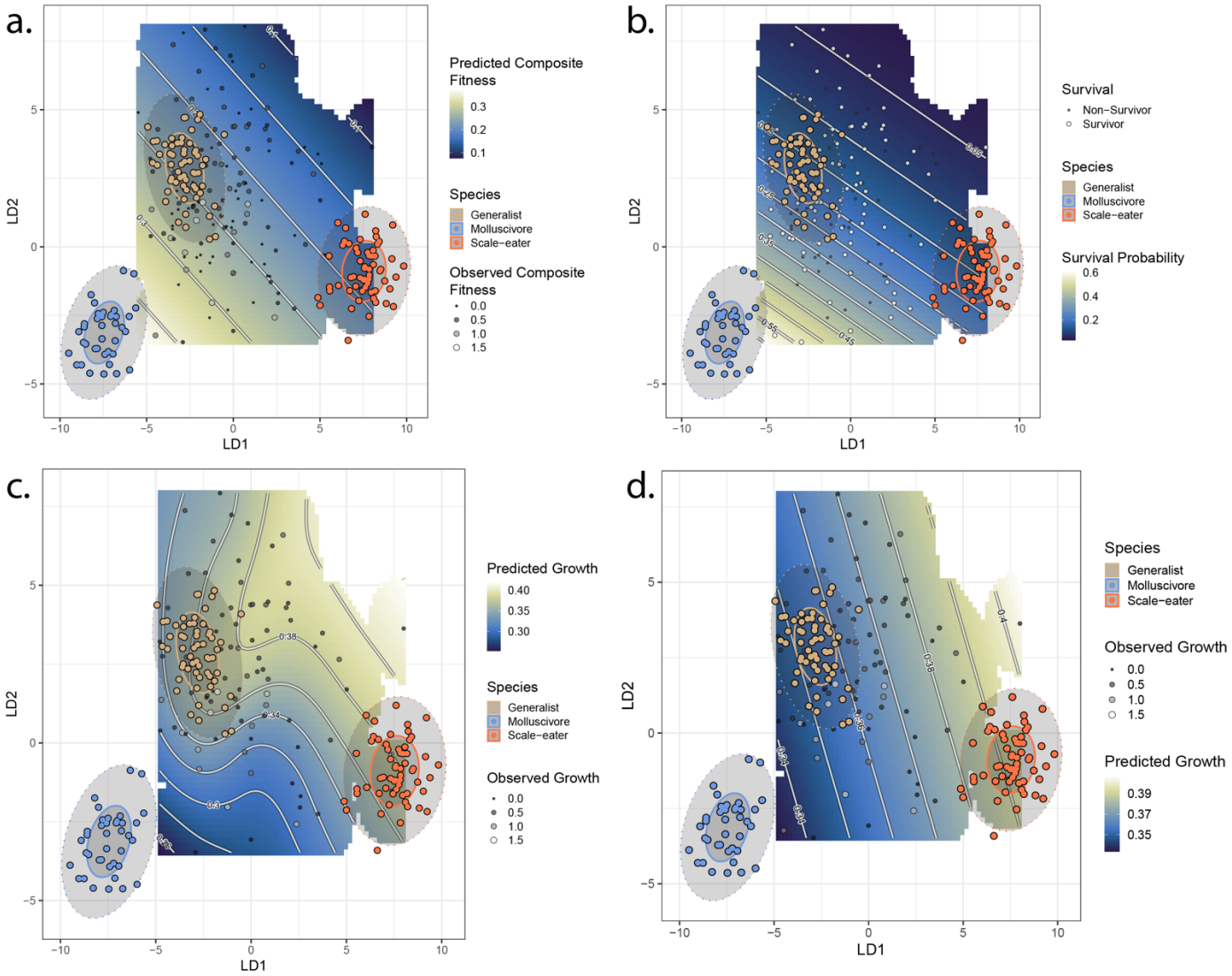

Figure 2—figure supplement 6. Best-fit fitness landscapes for composite fitness (a) survival (b), and growth without associated SNPs (c) and growth including associated SNPs (d). Colored points indicate locations of parent species in LD morphospace, and ellipses indicate their 50% (solid) and 95% (dotted) confidence intervals. Grey points indicate location of hybrid individuals, with size proportional to their fitness measure. Cooler colors on the adaptive landscape indicate lower predicted fitness.

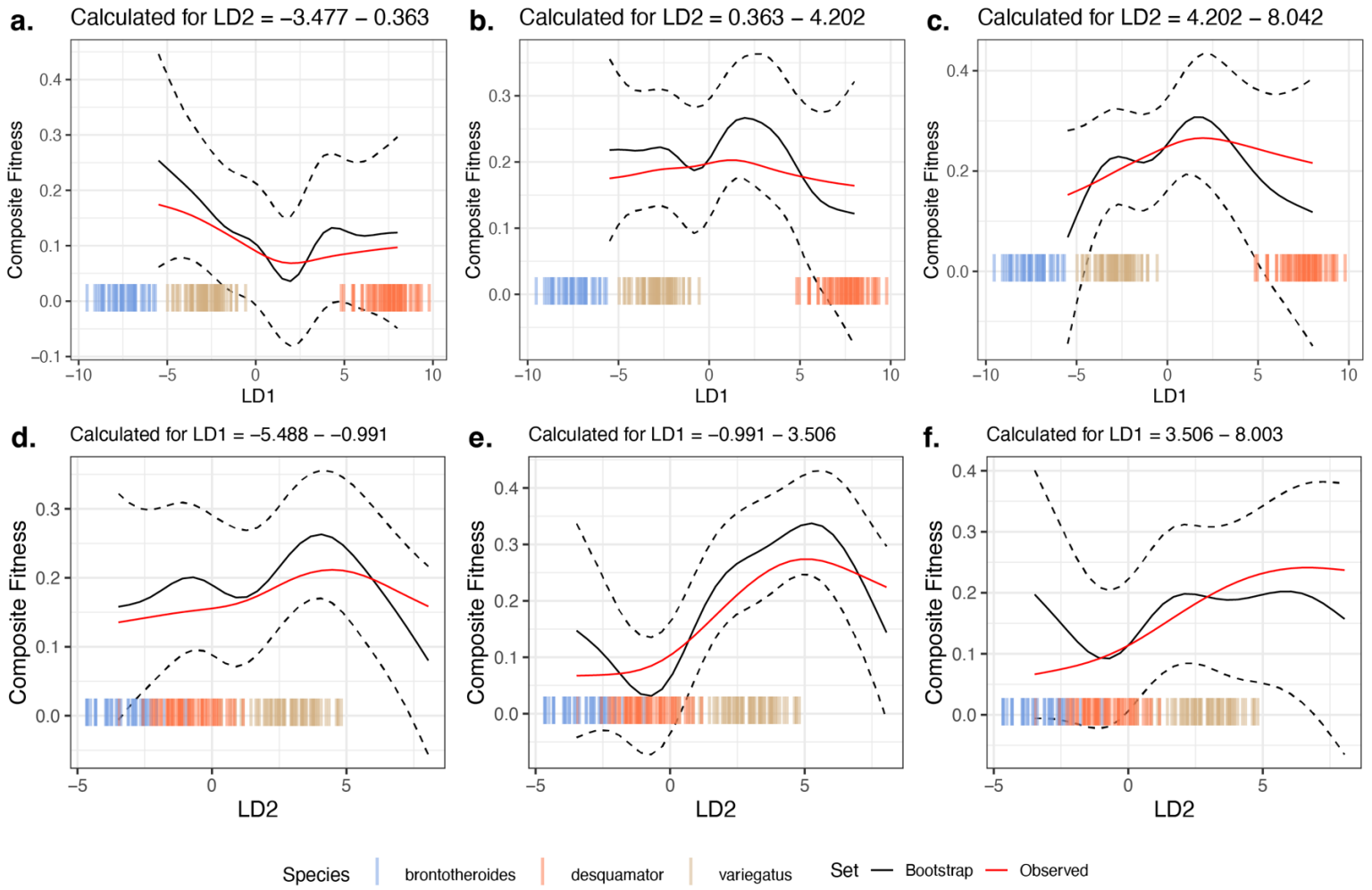

Figure 2—figure supplement 7. Comparison of 10,000 bootstrapped estimates of predicted mean composite fitness to estimations from observed data across slices of the fitness landscape. The focal fitness landscape (Figure 3c-d) was estimated using composite fitness, linear discriminant axes obtained from all morphological traits, and the most-strongly fitness associated SNPs. The mean value of predicted fitness across all bootstrap replicates is plotted as a solid black line; the dashed black line indicates ± 1 standard deviation. The observed predicted fitness is plotted as the solid red line. Observed parental morphological LD scores are plotted as colored vertical hashes: see legend at bottom. Subplots **a.**, **b.**, and **c.**, are estimates along LD1, as calculated from the bottom, middle and top third of LD2 values respectively. Subplots **d.**, **e.**, and **f.**, are estimates along LD2, as calculated from the bottom, middle and top third of LD1 values respectively.

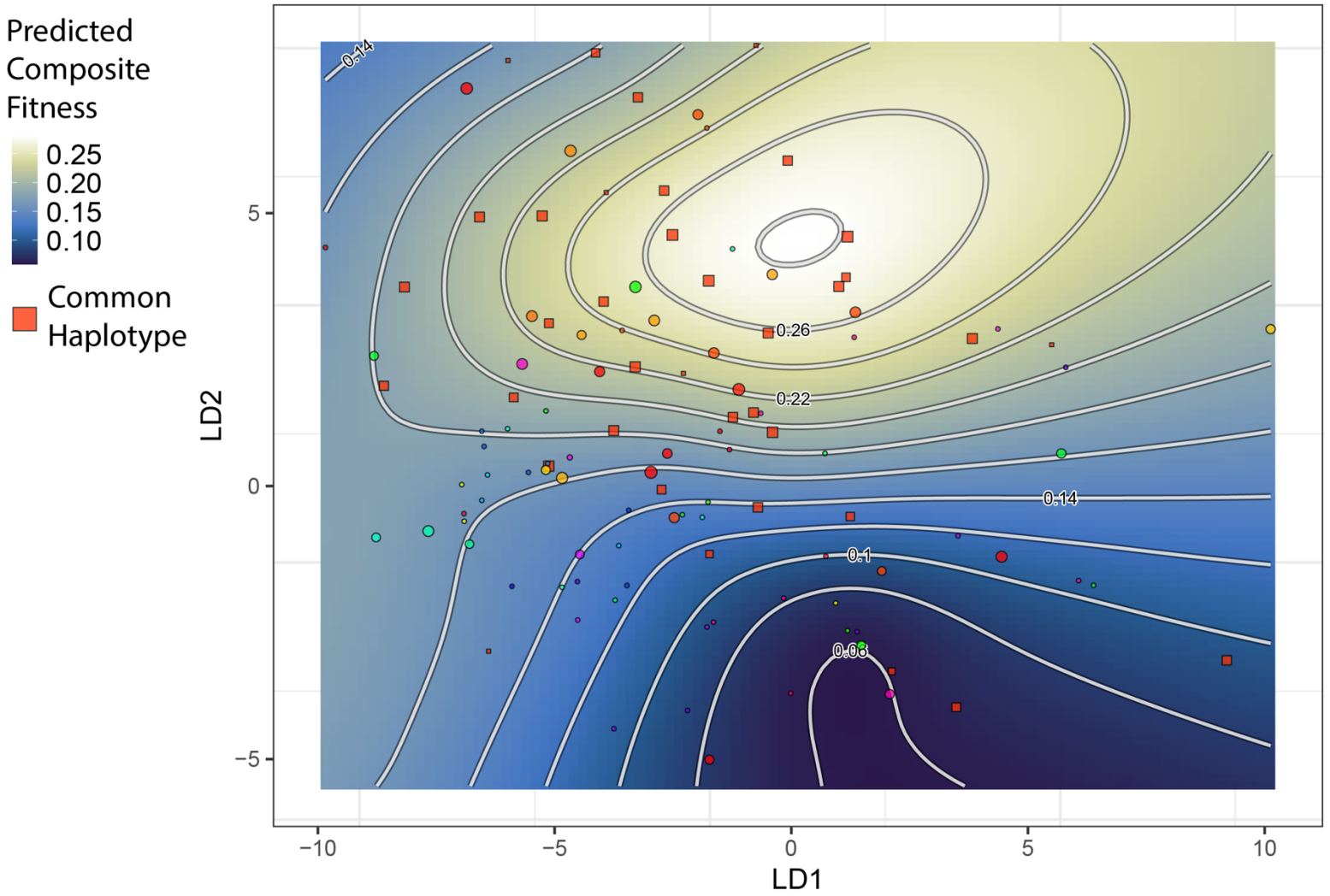

Figure 2—figure supplement 8. The topography of the composite fitness adaptive landscape is influenced by the distribution of a common SNP haplotype. Shown is the same landscape as in Figure 2, but the plotted points are unique SNP haplotypes for the thirteen most strongly fitness-associated SNPs. One haplotype is particularly frequent among hybrids; individuals with this haplotype are closer in morphospace to generalists and drive the emergence of a local fitness optimum for generalists. All other haplotypes (points) are plotted with a distinct color per haplotype.

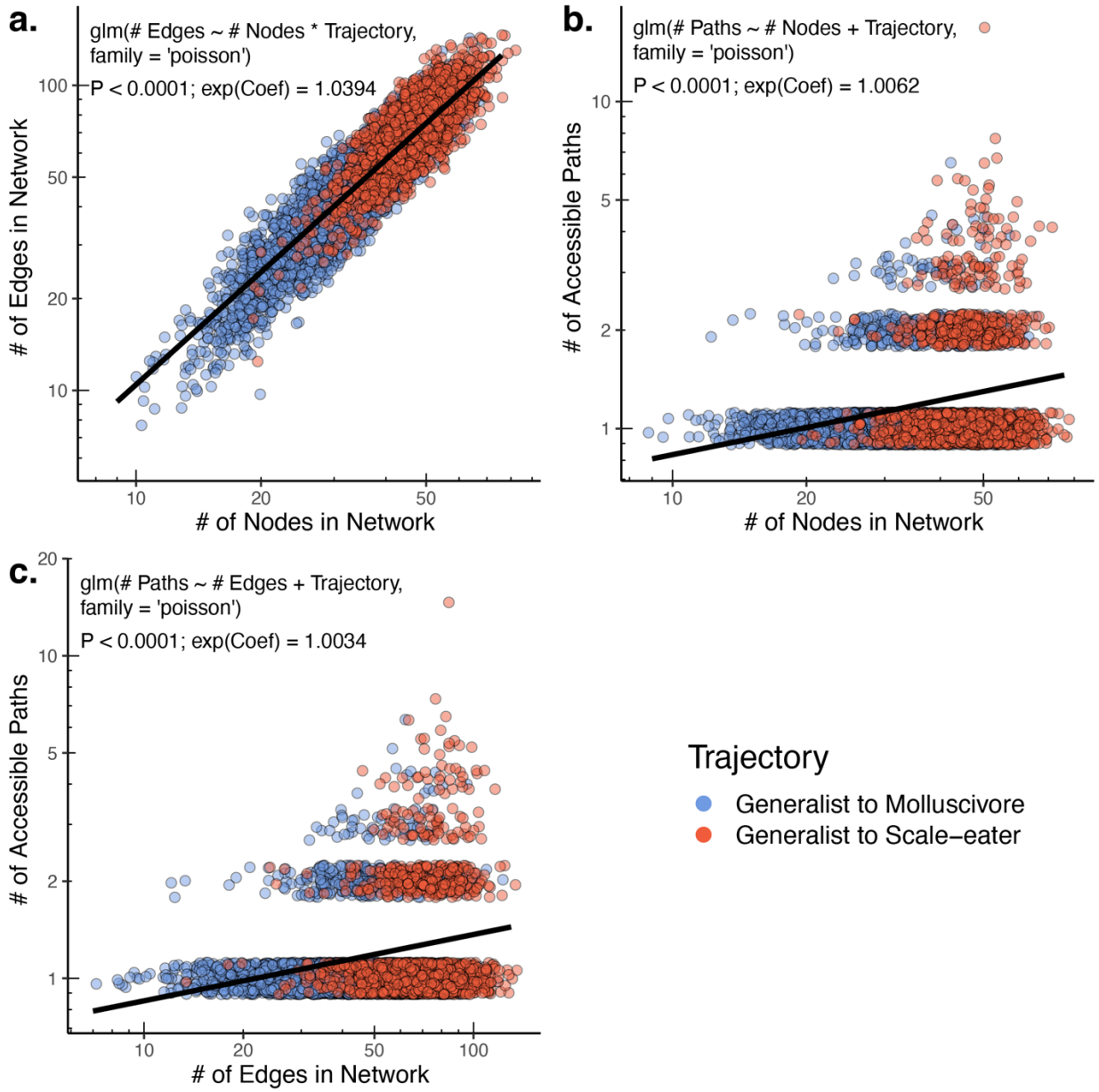

Figure 4—figure supplement 1. The raw number of accessible paths increases with network size. The number of edges (and thus number of potential paths) is strongly positively correlated with the observed number of nodes (unique SNP haplotypes) in a network (**a.**). Correspondingly, both the number of nodes (b.) and number of edges (c.) positively correlate with the number of accessible paths between generalists and specialists in a given network. Only results for composite fitness are plotted; results are consistent across fitness measures. Models correspond to those in Appendix 1—table 13. Poisson regression was chosen as each response variable correspond to count-data. Because Poisson regression models are log-linear, we report the exponentiated coefficient which corresponds to the expected multiplicative increase in the mean of Y per unit-value of X.

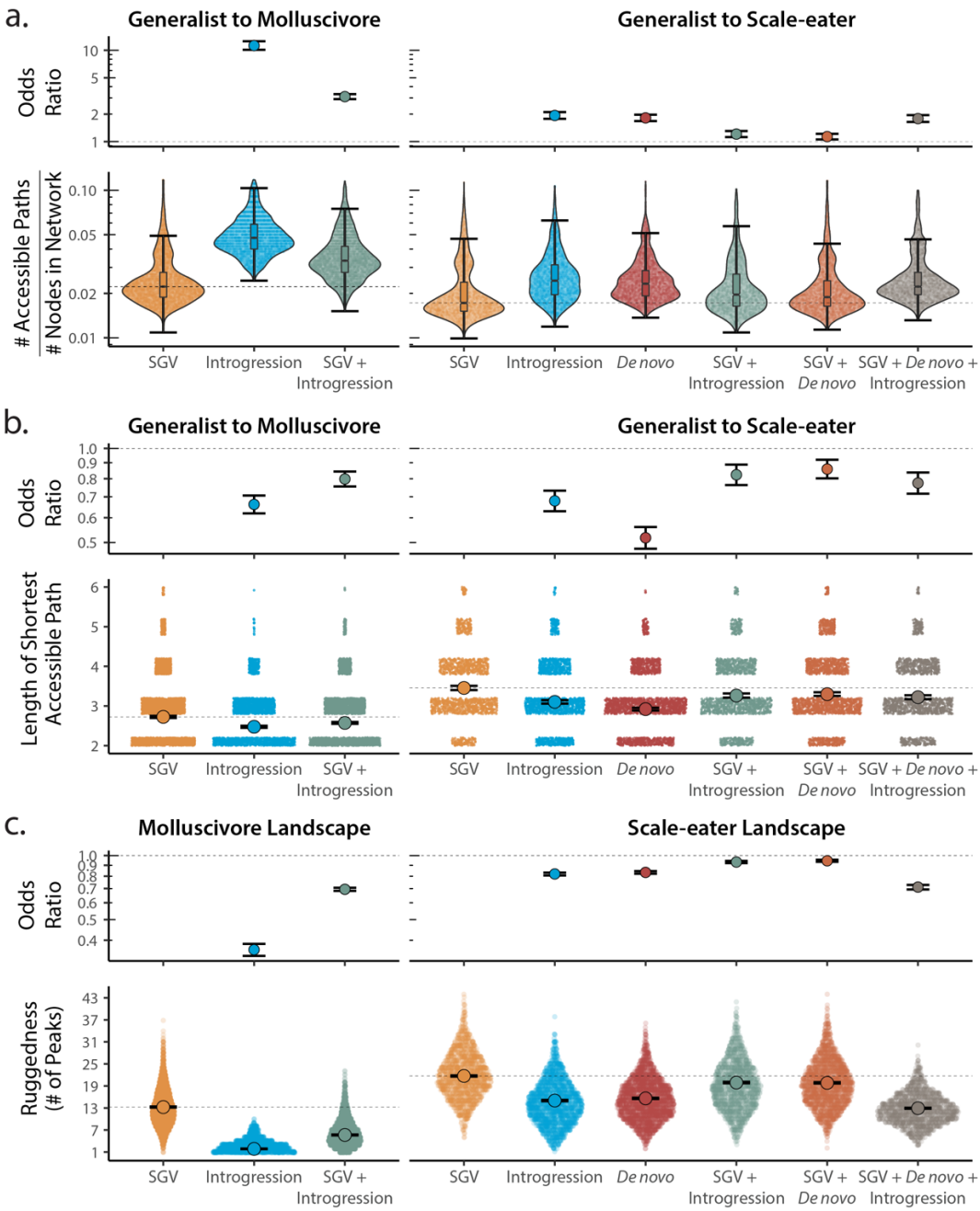

Figure 5—figure supplement 1. Adaptive loci sourced from introgression and *de novo* mutation reduce fitness landscape ruggedness and increase accessibility as compared to standing genetic variation (SGV) using survival as our proxy for fitness. Odds ratios (maximum likelihood estimate and 95% CI) indicate the effect of each source of variation on accessibility as compared to networks estimated from standing variation alone. **a.** The number of accessible (i.e. monotonically increasing in fitness) paths per network, scaled by the size of the network (# of nodes in network). Significance was assessed using a likelihood ratio test, corrected for the false discovery rate (reported in Appendix 1—table 13). Dashed lines correspond to the median estimate for standing genetic variation to aid comparison to other sources of adaptive variation. **b.** Number of mutational steps in the shortest accessible path. Means are plotted as large circles, with two standard errors shown; dashed horizontal lines correspond to the mean for standing genetic variation. **c.** Ruggedness of molluscivore and scale-eater fitness landscapes constructed from each source of genetic variation as measured by the number of peaks (genotypes with no fitter neighbors).

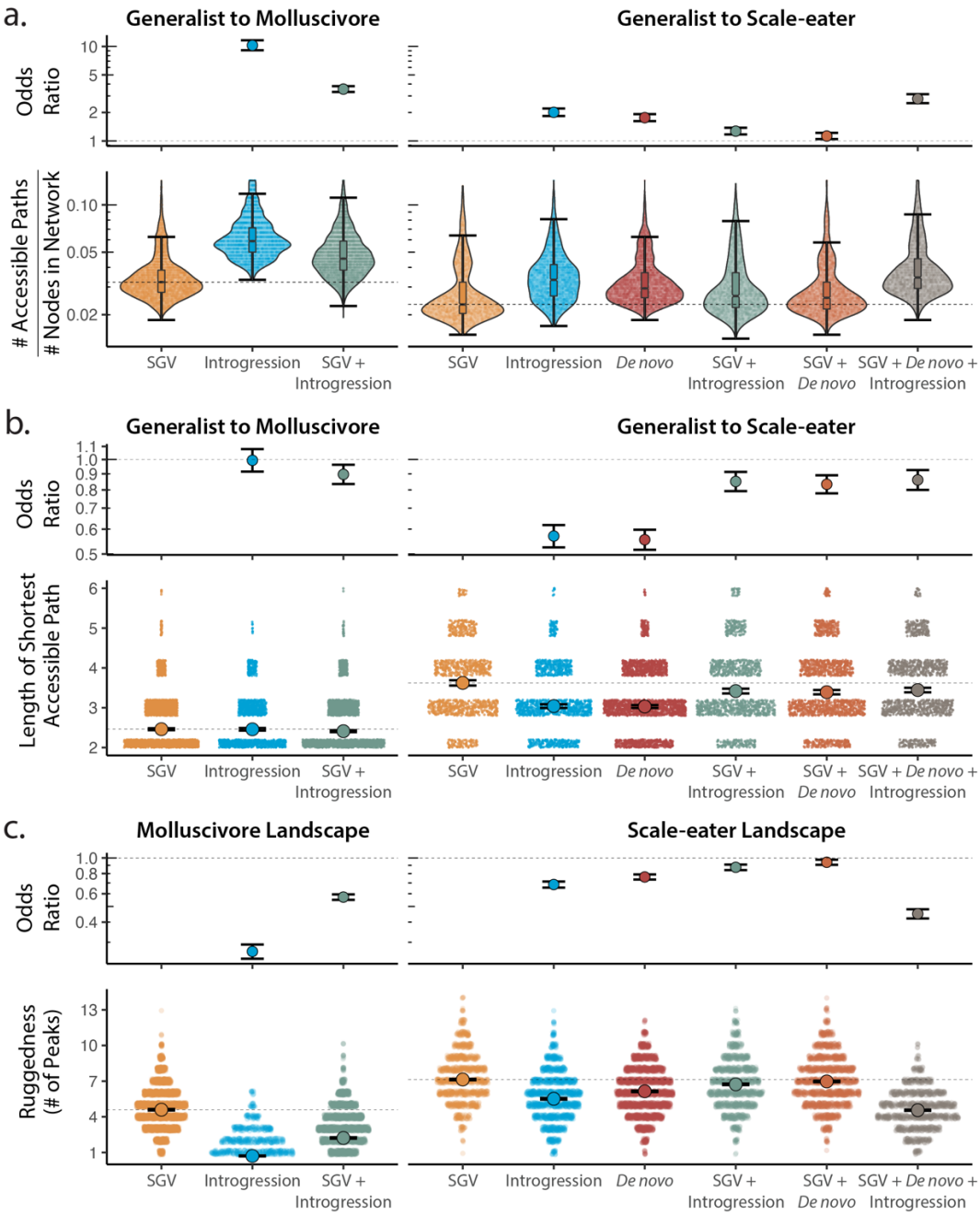

Figure 5—figure supplement 2. Adaptive loci sourced from introgression and *de novo* mutation reduce fitness landscape ruggedness and increase accessibility as compared to standing genetic variation (SGV) using growth as our proxy for fitness. Odds ratios (maximum likelihood estimate and 95% CI) indicate the effect of each source of variation on accessibility as compared to networks estimated from standing variation alone. **a.** The number of accessible (i.e. monotonically increasing in fitness) paths per network, scaled by the size of the network (# of nodes in network). Significance was assessed using a likelihood ratio test, corrected for the false discovery rate (reported in Appendix 1—table 13). Dashed lines correspond to the median estimate for standing genetic variation to aid comparison to other sources of adaptive variation. **b.** Number of mutational steps in the shortest accessible path. Means are plotted as large circles, with two standard errors shown; dashed horizontal lines correspond to the mean for standing genetic variation. **c.** Ruggedness of molluscivore and scale-eater fitness landscapes constructed from each source of genetic variation as measured by the number of peaks (genotypes with no fitter neighbors).

Appendix 1—Table 1. Samples of hybrids and parental studies used either in genomic or morphological analyses, along with associated metadata.

ID	Sequenced	Morphology	Survivorship	Experiment	Lake	Species
CP04E02	This study	Yes	Non-Survivor	Martin & Gould 2020	Crescent Pond	Hybrid
CP07F05	This study	Yes	Non-Survivor	Martin & Gould 2020	Crescent Pond	Hybrid
CP08H06	This study	Yes	Non-Survivor	Martin & Gould 2020	Crescent Pond	Hybrid
CP09C02	This study	Yes	Non-Survivor	Martin & Gould 2020	Crescent Pond	Hybrid
CP09D01	This study	Yes	Non-Survivor	Martin & Gould 2020	Crescent Pond	Hybrid
CP09F10	This study	Yes	Non-Survivor	Martin & Gould 2020	Crescent Pond	Hybrid
CP10B05	This study	Yes	Non-Survivor	Martin & Gould 2020	Crescent Pond	Hybrid
CP11C10	This study	Yes	Non-Survivor	Martin & Gould 2020	Crescent Pond	Hybrid
CP13E03	This study	Yes	Non-Survivor	Martin & Gould 2020	Crescent Pond	Hybrid
CP13F01	This study	Yes	Non-Survivor	Martin & Gould 2020	Crescent Pond	Hybrid
LL01F03	This study	Yes	Non-Survivor	Martin & Gould 2020	Little Lake	Hybrid
LL01F05	This study	Yes	Non-Survivor	Martin & Gould 2020	Little Lake	Hybrid
LL01G05	This study	Yes	Non-Survivor	Martin & Gould 2020	Little Lake	Hybrid
LL02A08	This study	Yes	Non-Survivor	Martin & Gould 2020	Little Lake	Hybrid
LL02D09	This study	Yes	Non-Survivor	Martin & Gould 2020	Little Lake	Hybrid
LL02D11	This study	Yes	Non-Survivor	Martin & Gould 2020	Little Lake	Hybrid
LL02E04	This study	Yes	Non-Survivor	Martin & Gould 2020	Little Lake	Hybrid
LL02E07	This study	Yes	Non-Survivor	Martin & Gould 2020	Little Lake	Hybrid
LL02E09	This study	Yes	Non-Survivor	Martin & Gould 2020	Little Lake	Hybrid
LL04E03	This study	Yes	Non-Survivor	Martin & Gould 2020	Little Lake	Hybrid
LL04E09	This study	Yes	Non-Survivor	Martin & Gould 2020	Little Lake	Hybrid
LL04F02	This study	Yes	Non-Survivor	Martin & Gould 2020	Little Lake	Hybrid
LL04F07	This study	Yes	Non-Survivor	Martin & Gould 2020	Little Lake	Hybrid
LL05A01	This study	Yes	Non-Survivor	Martin & Gould 2020	Little Lake	Hybrid
LL05C06	This study	Yes	Non-Survivor	Martin & Gould 2020	Little Lake	Hybrid
LL05C09	This study	Yes	Non-Survivor	Martin & Gould 2020	Little Lake	Hybrid
LL05C10	This study	Yes	Non-Survivor	Martin & Gould 2020	Little Lake	Hybrid
LL05D10	This study	Yes	Non-Survivor	Martin & Gould 2020	Little Lake	Hybrid
LL05E06	This study	Yes	Non-Survivor	Martin & Gould 2020	Little Lake	Hybrid
LL05E08	This study	Yes	Non-Survivor	Martin & Gould 2020	Little Lake	Hybrid
LL05H10	This study	Yes	Non-Survivor	Martin & Gould 2020	Little Lake	Hybrid
LL06A10	This study	Yes	Non-Survivor	Martin & Gould 2020	Little Lake	Hybrid
LL06B03	This study	Yes	Non-Survivor	Martin & Gould 2020	Little Lake	Hybrid
LL06C10	This study	Yes	Non-Survivor	Martin & Gould 2020	Little Lake	Hybrid
LL06D12	This study	Yes	Non-Survivor	Martin & Gould 2020	Little Lake	Hybrid
LL06E10	This study	Yes	Non-Survivor	Martin & Gould 2020	Little Lake	Hybrid
LL06F08	This study	Yes	Non-Survivor	Martin & Gould 2020	Little Lake	Hybrid
LL08B09	This study	Yes	Non-Survivor	Martin & Gould 2020	Little Lake	Hybrid
LL08B11	This study	Yes	Non-Survivor	Martin & Gould 2020	Little Lake	Hybrid
LL08G07	This study	Yes	Non-Survivor	Martin & Gould 2020	Little Lake	Hybrid
LL08G10	This study	Yes	Non-Survivor	Martin & Gould 2020	Little Lake	Hybrid
LL08H01	This study	Yes	Non-Survivor	Martin & Gould 2020	Little Lake	Hybrid
LL09A09	This study	Yes	Non-Survivor	Martin & Gould 2020	Little Lake	Hybrid
LL09A10	This study	Yes	Non-Survivor	Martin & Gould 2020	Little Lake	Hybrid
LL09B05	This study	Yes	Non-Survivor	Martin & Gould 2020	Little Lake	Hybrid
LL09C03	This study	Yes	Non-Survivor	Martin & Gould 2020	Little Lake	Hybrid
LL09D01	This study	Yes	Non-Survivor	Martin & Gould 2020	Little Lake	Hybrid
LL09D10	This study	Yes	Non-Survivor	Martin & Gould 2020	Little Lake	Hybrid
LL09E01	This study	Yes	Non-Survivor	Martin & Gould 2020	Little Lake	Hybrid
LL09F03	This study	Yes	Non-Survivor	Martin & Gould 2020	Little Lake	Hybrid
LL09H07	This study	Yes	Non-Survivor	Martin & Gould 2020	Little Lake	Hybrid
LL09H10	This study	Yes	Non-Survivor	Martin & Gould 2020	Little Lake	Hybrid

CP06G01	This study	Yes	Survivor	Martin & Gould 2020	Crescent Pond	Hybrid
CP06H09	This study	Yes	Survivor	Martin & Gould 2020	Crescent Pond	Hybrid
CP07E08	This study	Yes	Survivor	Martin & Gould 2020	Crescent Pond	Hybrid
CP07H01	This study	Yes	Survivor	Martin & Gould 2020	Crescent Pond	Hybrid
CP07H11	This study	Yes	Survivor	Martin & Gould 2020	Crescent Pond	Hybrid
CP08F07	This study	Yes	Survivor	Martin & Gould 2020	Crescent Pond	Hybrid
CP08G08	This study	Yes	Survivor	Martin & Gould 2020	Crescent Pond	Hybrid
CP09D02	This study	Yes	Survivor	Martin & Gould 2020	Crescent Pond	Hybrid
CP10A03	This study	Yes	Survivor	Martin & Gould 2020	Crescent Pond	Hybrid
CP10C04	This study	Yes	Survivor	Martin & Gould 2020	Crescent Pond	Hybrid
CP10C07	This study	Yes	Survivor	Martin & Gould 2020	Crescent Pond	Hybrid
CP10C12	This study	Yes	Survivor	Martin & Gould 2020	Crescent Pond	Hybrid
CP10F12	This study	Yes	Survivor	Martin & Gould 2020	Crescent Pond	Hybrid
CP10H01	This study	Yes	Survivor	Martin & Gould 2020	Crescent Pond	Hybrid
CP11B03	This study	Yes	Survivor	Martin & Gould 2020	Crescent Pond	Hybrid
CP11C08	This study	Yes	Survivor	Martin & Gould 2020	Crescent Pond	Hybrid
CP11D04	This study	Yes	Survivor	Martin & Gould 2020	Crescent Pond	Hybrid
CP11G06	This study	Yes	Survivor	Martin & Gould 2020	Crescent Pond	Hybrid
CP11G12	This study	Yes	Survivor	Martin & Gould 2020	Crescent Pond	Hybrid
CP12E05	This study	Yes	Survivor	Martin & Gould 2020	Crescent Pond	Hybrid
CP12E07	This study	Yes	Survivor	Martin & Gould 2020	Crescent Pond	Hybrid
CP12H04	This study	Yes	Survivor	Martin & Gould 2020	Crescent Pond	Hybrid
CP13B02	This study	Yes	Survivor	Martin & Gould 2020	Crescent Pond	Hybrid
CP13B08	This study	Yes	Survivor	Martin & Gould 2020	Crescent Pond	Hybrid
CP14C04	This study	Yes	Survivor	Martin & Gould 2020	Crescent Pond	Hybrid
CP15A10	This study	Yes	Survivor	Martin & Gould 2020	Crescent Pond	Hybrid
CP15B08	This study	Yes	Survivor	Martin & Gould 2020	Crescent Pond	Hybrid
CP15E01	This study	Yes	Survivor	Martin & Gould 2020	Crescent Pond	Hybrid
CP15E03	This study	Yes	Survivor	Martin & Gould 2020	Crescent Pond	Hybrid
CP17A01	This study	Yes	Survivor	Martin & Gould 2020	Crescent Pond	Hybrid
CP18B11	This study	Yes	Survivor	Martin & Gould 2020	Crescent Pond	Hybrid
CP19B02	This study	Yes	Survivor	Martin & Gould 2020	Crescent Pond	Hybrid
CP19C02	This study	Yes	Survivor	Martin & Gould 2020	Crescent Pond	Hybrid
CP19C07	This study	Yes	Survivor	Martin & Gould 2020	Crescent Pond	Hybrid
CP19F01	This study	Yes	Survivor	Martin & Gould 2020	Crescent Pond	Hybrid
CP19G03	This study	Yes	Survivor	Martin & Gould 2020	Crescent Pond	Hybrid
CPH01	This study	Yes	Survivor	Martin & Wainwright 2013	Crescent Pond	Hybrid
CPH02	This study	Yes	Survivor	Martin & Wainwright 2013	Crescent Pond	Hybrid
CPH03	This study	Yes	Survivor	Martin & Wainwright 2013	Crescent Pond	Hybrid
CPH04	This study	Yes	Survivor	Martin & Wainwright 2013	Crescent Pond	Hybrid
CPH05	This study	Yes	Survivor	Martin & Wainwright 2013	Crescent Pond	Hybrid
CPH07	This study	Yes	Survivor	Martin & Wainwright 2013	Crescent Pond	Hybrid
CPH08	This study	Yes	Survivor	Martin & Wainwright 2013	Crescent Pond	Hybrid
CPH09	This study	Yes	Survivor	Martin & Wainwright 2013	Crescent Pond	Hybrid
CPH10	This study	Yes	Survivor	Martin & Wainwright 2013	Crescent Pond	Hybrid
CPH100	This study	Yes	Survivor	Martin & Wainwright 2013	Crescent Pond	Hybrid
CPH11	This study	Yes	Survivor	Martin & Wainwright 2013	Crescent Pond	Hybrid
CPH123	This study	Yes	Survivor	Martin & Wainwright 2013	Crescent Pond	Hybrid
LL01H04	This study	Yes	Survivor	Martin & Gould 2020	Little Lake	Hybrid
LL02G09	This study	Yes	Survivor	Martin & Gould 2020	Little Lake	Hybrid
LL06B06	This study	Yes	Survivor	Martin & Gould 2020	Little Lake	Hybrid
LL06E04	This study	Yes	Survivor	Martin & Gould 2020	Little Lake	Hybrid
LL07E12	This study	Yes	Survivor	Martin & Gould 2020	Little Lake	Hybrid
LL07G04	This study	Yes	Survivor	Martin & Gould 2020	Little Lake	Hybrid
LL08A09	This study	Yes	Survivor	Martin & Gould 2020	Little Lake	Hybrid

LL175	This study	Yes	Survivor	Martin & Wainwright 2013	Little Lake	Hybrid
LL23	This study	Yes	Survivor	Martin & Wainwright 2013	Little Lake	Hybrid
LL247	This study	Yes	Survivor	Martin & Wainwright 2013	Little Lake	Hybrid
LL251	This study	Yes	Survivor	Martin & Wainwright 2013	Little Lake	Hybrid
LL271	This study	Yes	Survivor	Martin & Wainwright 2013	Little Lake	Hybrid
LLH12	This study	Yes	Survivor	Martin & Wainwright 2013	Little Lake	Hybrid
LLH34	This study	Yes	Survivor	Martin & Wainwright 2013	Little Lake	Hybrid
LLH41	This study	Yes	Survivor	Martin & Wainwright 2013	Little Lake	Hybrid
LLH51	This study	Yes	Survivor	Martin & Wainwright 2013	Little Lake	Hybrid
LLH94	This study	Yes	Survivor	Martin & Wainwright 2013	Little Lake	Hybrid
CRPA1	Richards et al. 2021	No	NA	NA	Crescent Pond	Generalist
CRPA1000	Richards et al. 2021	No	NA	NA	Crescent Pond	Generalist
CRPA1001	Richards et al. 2021	No	NA	NA	Crescent Pond	Generalist
CRPA1003	Richards et al. 2021	No	NA	NA	Crescent Pond	Generalist
CRPA3	Richards et al. 2021	No	NA	NA	Crescent Pond	Generalist
LILA1	Richards et al. 2021	No	NA	NA	Little Lake	Generalist
OSPA1	Richards et al. 2021	No	NA	NA	Osprey Pond (Little Lake)	Generalist
OSPA1000	Richards et al. 2021	No	NA	NA	Osprey Pond (Little Lake)	Generalist
OSPA1001	Richards et al. 2021	No	NA	NA	Osprey Pond (Little Lake)	Generalist
OSPA11	Richards et al. 2021	No	NA	NA	Osprey Pond (Little Lake)	Generalist
OSPA12	Richards et al. 2021	No	NA	NA	Osprey Pond (Little Lake)	Generalist
OSPA13	Richards et al. 2021	No	NA	NA	Osprey Pond (Little Lake)	Generalist
OSPA4	Richards et al. 2021	No	NA	NA	Osprey Pond (Little Lake)	Generalist
OSPA5	Richards et al. 2021	No	NA	NA	Osprey Pond (Little Lake)	Generalist
OSPA6	Richards et al. 2021	No	NA	NA	Osprey Pond (Little Lake)	Generalist
OSPA8	Richards et al. 2021	No	NA	NA	Osprey Pond (Little Lake)	Generalist
OSPA9	Richards et al. 2021	No	NA	NA	Osprey Pond (Little Lake)	Generalist
CRPM1	Richards et al. 2021	No	NA	NA	Crescent Pond	Molluscivore
CRPM10	Richards et al. 2021	No	NA	NA	Crescent Pond	Molluscivore
CRPM1000	Richards et al. 2021	No	NA	NA	Crescent Pond	Molluscivore
CRPM1001	Richards et al. 2021	No	NA	NA	Crescent Pond	Molluscivore
CRPM11	Richards et al. 2021	No	NA	NA	Crescent Pond	Molluscivore
CRPM2	Richards et al. 2021	No	NA	NA	Crescent Pond	Molluscivore
CRPM3	Richards et al. 2021	No	NA	NA	Crescent Pond	Molluscivore
CRPM5	Richards et al. 2021	No	NA	NA	Crescent Pond	Molluscivore
CRPM6	Richards et al. 2021	No	NA	NA	Crescent Pond	Molluscivore
CRPM7	Richards et al. 2021	No	NA	NA	Crescent Pond	Molluscivore
CRPM8	Richards et al. 2021	No	NA	NA	Crescent Pond	Molluscivore
CRPM9	Richards et al. 2021	No	NA	NA	Crescent Pond	Molluscivore
LILM-QTL	Richards et al. 2021	No	NA	NA	Little Lake	Molluscivore
LILM3	Richards et al. 2021	No	NA	NA	Little Lake	Molluscivore
LILM4	Richards et al. 2021	No	NA	NA	Little Lake	Molluscivore
LILM5	Richards et al. 2021	No	NA	NA	Little Lake	Molluscivore
OSPM1	Richards et al. 2021	No	NA	NA	Osprey Pond (Little Lake)	Molluscivore
OSPM1000	Richards et al. 2021	No	NA	NA	Osprey Pond (Little Lake)	Molluscivore
OSPM1001	Richards et al. 2021	No	NA	NA	Osprey Pond (Little Lake)	Molluscivore
OSPM11	Richards et al. 2021	No	NA	NA	Osprey Pond (Little Lake)	Molluscivore
OSPM2	Richards et al. 2021	No	NA	NA	Osprey Pond (Little Lake)	Molluscivore
OSPM3	Richards et al. 2021	No	NA	NA	Osprey Pond (Little Lake)	Molluscivore
OSPM4	Richards et al. 2021	No	NA	NA	Osprey Pond (Little Lake)	Molluscivore
OSPM5	Richards et al. 2021	No	NA	NA	Osprey Pond (Little Lake)	Molluscivore
OSPM7	Richards et al. 2021	No	NA	NA	Osprey Pond (Little Lake)	Molluscivore
OSPM8	Richards et al. 2021	No	NA	NA	Osprey Pond (Little Lake)	Molluscivore
OSPM9	Richards et al. 2021	No	NA	NA	Osprey Pond (Little Lake)	Molluscivore
CRPP-QTL	Richards et al. 2021	No	NA	NA	Crescent Pond	Scale-eater

LILP4	Richards et al. 2021	No	NA	NA	Little Lake	Scale-eater
LILP5	Richards et al. 2021	No	NA	NA	Little Lake	Scale-eater
OSPP1	Richards et al. 2021	No	NA	NA	Osprey Pond (Little Lake)	Scale-eater
OSPP10	Richards et al. 2021	No	NA	NA	Osprey Pond (Little Lake)	Scale-eater
OSPP1000	Richards et al. 2021	No	NA	NA	Osprey Pond (Little Lake)	Scale-eater
OSPP1001	Richards et al. 2021	No	NA	NA	Osprey Pond (Little Lake)	Scale-eater
OSPP11	Richards et al. 2021	No	NA	NA	Osprey Pond (Little Lake)	Scale-eater
OSPP2	Richards et al. 2021	No	NA	NA	Osprey Pond (Little Lake)	Scale-eater
OSPP3	Richards et al. 2021	No	NA	NA	Osprey Pond (Little Lake)	Scale-eater
OSPP4	Richards et al. 2021	No	NA	NA	Osprey Pond (Little Lake)	Scale-eater
OSPP5	Richards et al. 2021	No	NA	NA	Osprey Pond (Little Lake)	Scale-eater
OSPP7	Richards et al. 2021	No	NA	NA	Osprey Pond (Little Lake)	Scale-eater
OSPP9	Richards et al. 2021	No	NA	NA	Osprey Pond (Little Lake)	Scale-eater
CPA01	NA	Yes	Parental	NA	Crescent Pond	Generalist
CPA03	NA	Yes	Parental	NA	Crescent Pond	Generalist
CPA05	NA	Yes	Parental	NA	Crescent Pond	Generalist
CPA07	NA	Yes	Parental	NA	Crescent Pond	Generalist
CPA09	NA	Yes	Parental	NA	Crescent Pond	Generalist
CPA11	NA	Yes	Parental	NA	Crescent Pond	Generalist
CPA13	NA	Yes	Parental	NA	Crescent Pond	Generalist
CPA15	NA	Yes	Parental	NA	Crescent Pond	Generalist
CPA17	NA	Yes	Parental	NA	Crescent Pond	Generalist
CPA19	NA	Yes	Parental	NA	Crescent Pond	Generalist
CPA21	NA	Yes	Parental	NA	Crescent Pond	Generalist
CPA23	NA	Yes	Parental	NA	Crescent Pond	Generalist
CPA25	NA	Yes	Parental	NA	Crescent Pond	Generalist
CPA27	NA	Yes	Parental	NA	Crescent Pond	Generalist
CPA29	NA	Yes	Parental	NA	Crescent Pond	Generalist
CPA31	NA	Yes	Parental	NA	Crescent Pond	Generalist
CPA33	NA	Yes	Parental	NA	Crescent Pond	Generalist
CPA35	NA	Yes	Parental	NA	Crescent Pond	Generalist
CPA37	NA	Yes	Parental	NA	Crescent Pond	Generalist
CPA39	NA	Yes	Parental	NA	Crescent Pond	Generalist
CPA41	NA	Yes	Parental	NA	Crescent Pond	Generalist
CPA43	NA	Yes	Parental	NA	Crescent Pond	Generalist
CPA45	NA	Yes	Parental	NA	Crescent Pond	Generalist
CPA47	NA	Yes	Parental	NA	Crescent Pond	Generalist
CPA49	NA	Yes	Parental	NA	Crescent Pond	Generalist
CPA51	NA	Yes	Parental	NA	Crescent Pond	Generalist
CPA53	NA	Yes	Parental	NA	Crescent Pond	Generalist
CPA55	NA	Yes	Parental	NA	Crescent Pond	Generalist
CPA57	NA	Yes	Parental	NA	Crescent Pond	Generalist
CPA59	NA	Yes	Parental	NA	Crescent Pond	Generalist
LLA20	NA	Yes	Parental	NA	Little Lake	Generalist
LLA21	NA	Yes	Parental	NA	Little Lake	Generalist
LLA22	NA	Yes	Parental	NA	Little Lake	Generalist
LLA23	NA	Yes	Parental	NA	Little Lake	Generalist
LLA24	NA	Yes	Parental	NA	Little Lake	Generalist
LLA25	NA	Yes	Parental	NA	Little Lake	Generalist
LLA26	NA	Yes	Parental	NA	Little Lake	Generalist
LLA27	NA	Yes	Parental	NA	Little Lake	Generalist
LLA28	NA	Yes	Parental	NA	Little Lake	Generalist
LLA29	NA	Yes	Parental	NA	Little Lake	Generalist
LLA30	NA	Yes	Parental	NA	Little Lake	Generalist
LLA31	NA	Yes	Parental	NA	Little Lake	Generalist

LLA43	NA	Yes	Parental	NA	Little Lake	Generalist
LLA44	NA	Yes	Parental	NA	Little Lake	Generalist
LLA45	NA	Yes	Parental	NA	Little Lake	Generalist
LLA46	NA	Yes	Parental	NA	Little Lake	Generalist
LLA47	NA	Yes	Parental	NA	Little Lake	Generalist
LLA48	NA	Yes	Parental	NA	Little Lake	Generalist
LLA49	NA	Yes	Parental	NA	Little Lake	Generalist
CPM01	NA	Yes	Parental	NA	Crescent Pond	Molluscivore
CPM02	NA	Yes	Parental	NA	Crescent Pond	Molluscivore
CPM03	NA	Yes	Parental	NA	Crescent Pond	Molluscivore
CPM04	NA	Yes	Parental	NA	Crescent Pond	Molluscivore
CPM05	NA	Yes	Parental	NA	Crescent Pond	Molluscivore
CPM06	NA	Yes	Parental	NA	Crescent Pond	Molluscivore
CPM07	NA	Yes	Parental	NA	Crescent Pond	Molluscivore
CPM08	NA	Yes	Parental	NA	Crescent Pond	Molluscivore
CPM09	NA	Yes	Parental	NA	Crescent Pond	Molluscivore
CPM10	NA	Yes	Parental	NA	Crescent Pond	Molluscivore
CPM11	NA	Yes	Parental	NA	Crescent Pond	Molluscivore
CPM12	NA	Yes	Parental	NA	Crescent Pond	Molluscivore
CPM13	NA	Yes	Parental	NA	Crescent Pond	Molluscivore
CPM14	NA	Yes	Parental	NA	Crescent Pond	Molluscivore
CPM15	NA	Yes	Parental	NA	Crescent Pond	Molluscivore
CPM16	NA	Yes	Parental	NA	Crescent Pond	Molluscivore
CPM17	NA	Yes	Parental	NA	Crescent Pond	Molluscivore
CPM18	NA	Yes	Parental	NA	Crescent Pond	Molluscivore
CPM19	NA	Yes	Parental	NA	Crescent Pond	Molluscivore
CPM20	NA	Yes	Parental	NA	Crescent Pond	Molluscivore
LLM01	NA	Yes	Parental	NA	Little Lake	Molluscivore
LLM02	NA	Yes	Parental	NA	Little Lake	Molluscivore
LLM03	NA	Yes	Parental	NA	Little Lake	Molluscivore
LLM04	NA	Yes	Parental	NA	Little Lake	Molluscivore
LLM05	NA	Yes	Parental	NA	Little Lake	Molluscivore
LLM06	NA	Yes	Parental	NA	Little Lake	Molluscivore
LLM07	NA	Yes	Parental	NA	Little Lake	Molluscivore
LLM08	NA	Yes	Parental	NA	Little Lake	Molluscivore
LLM09	NA	Yes	Parental	NA	Little Lake	Molluscivore
LLM10	NA	Yes	Parental	NA	Little Lake	Molluscivore
LLM11	NA	Yes	Parental	NA	Little Lake	Molluscivore
LLM12	NA	Yes	Parental	NA	Little Lake	Molluscivore
LLM13	NA	Yes	Parental	NA	Little Lake	Molluscivore
LLM14	NA	Yes	Parental	NA	Little Lake	Molluscivore
LLM15	NA	Yes	Parental	NA	Little Lake	Molluscivore
LLM16	NA	Yes	Parental	NA	Little Lake	Molluscivore
LLM17	NA	Yes	Parental	NA	Little Lake	Molluscivore
LLM18	NA	Yes	Parental	NA	Little Lake	Molluscivore
CPP01	NA	Yes	Parental	NA	Crescent Pond	Scale-eater
CPP02	NA	Yes	Parental	NA	Crescent Pond	Scale-eater
CPP03	NA	Yes	Parental	NA	Crescent Pond	Scale-eater
CPP04	NA	Yes	Parental	NA	Crescent Pond	Scale-eater
CPP05	NA	Yes	Parental	NA	Crescent Pond	Scale-eater
CPP06	NA	Yes	Parental	NA	Crescent Pond	Scale-eater
CPP07	NA	Yes	Parental	NA	Crescent Pond	Scale-eater
CPP08	NA	Yes	Parental	NA	Crescent Pond	Scale-eater
CPP09	NA	Yes	Parental	NA	Crescent Pond	Scale-eater
CPP10	NA	Yes	Parental	NA	Crescent Pond	Scale-eater

CPP22	NA	Yes	Parental	NA	Crescent Pond	Scale-eater
CPP23	NA	Yes	Parental	NA	Crescent Pond	Scale-eater
CPP24	NA	Yes	Parental	NA	Crescent Pond	Scale-eater
CPP25	NA	Yes	Parental	NA	Crescent Pond	Scale-eater
CPP26	NA	Yes	Parental	NA	Crescent Pond	Scale-eater
CPP27	NA	Yes	Parental	NA	Crescent Pond	Scale-eater
CPP28	NA	Yes	Parental	NA	Crescent Pond	Scale-eater
CPP29	NA	Yes	Parental	NA	Crescent Pond	Scale-eater
CPP30	NA	Yes	Parental	NA	Crescent Pond	Scale-eater
LLP01	NA	Yes	Parental	NA	Little Lake	Scale-eater
LLP02	NA	Yes	Parental	NA	Little Lake	Scale-eater
LLP03	NA	Yes	Parental	NA	Little Lake	Scale-eater
LLP04	NA	Yes	Parental	NA	Little Lake	Scale-eater
LLP05	NA	Yes	Parental	NA	Little Lake	Scale-eater
LLP06	NA	Yes	Parental	NA	Little Lake	Scale-eater
LLP07	NA	Yes	Parental	NA	Little Lake	Scale-eater
LLP08	NA	Yes	Parental	NA	Little Lake	Scale-eater
LLP09	NA	Yes	Parental	NA	Little Lake	Scale-eater
LLP10	NA	Yes	Parental	NA	Little Lake	Scale-eater
LLP11	NA	Yes	Parental	NA	Little Lake	Scale-eater
LLP12	NA	Yes	Parental	NA	Little Lake	Scale-eater
LLP13	NA	Yes	Parental	NA	Little Lake	Scale-eater
LLP14	NA	Yes	Parental	NA	Little Lake	Scale-eater
LLP15	NA	Yes	Parental	NA	Little Lake	Scale-eater
LLP16	NA	Yes	Parental	NA	Little Lake	Scale-eater
LLP17	NA	Yes	Parental	NA	Little Lake	Scale-eater
LLP18	NA	Yes	Parental	NA	Little Lake	Scale-eater
LLP19	NA	Yes	Parental	NA	Little Lake	Scale-eater
LLP20	NA	Yes	Parental	NA	Little Lake	Scale-eater
LLP21	NA	Yes	Parental	NA	Little Lake	Scale-eater
LLP22	NA	Yes	Parental	NA	Little Lake	Scale-eater
LLP23	NA	Yes	Parental	NA	Little Lake	Scale-eater
LLP24	NA	Yes	Parental	NA	Little Lake	Scale-eater
LLP25	NA	Yes	Parental	NA	Little Lake	Scale-eater
LLP26	NA	Yes	Parental	NA	Little Lake	Scale-eater
LLP27	NA	Yes	Parental	NA	Little Lake	Scale-eater
LLP28	NA	Yes	Parental	NA	Little Lake	Scale-eater
LLP29	NA	Yes	Parental	NA	Little Lake	Scale-eater
LLP30	NA	Yes	Parental	NA	Little Lake	Scale-eater

Appendix 1—Table 2. Models tested to assess the extent to which specialist ancestry predicts measures of fitness and their respective fits using all samples and an unsupervised admixture analysis. Best-fit models are bolded.

Fitness Measure	Model Family	Species	Model	AIC	Ancestry Coefficient	Ancestry *P*-value
Composite	Tobit	Generalist	Composite ~ AncestryProp	202.40	0.02	0.8525
			Composite ~ AncestryProp + Lake	**196.02**	**-0.11**	**0.3847**
			Composite ~ AncestryProp + Experiment	203.38	0.08	0.5223
			Composite ~ AncestryProp + Lake + Experiment	197.56	-0.06	0.6610
			Composite ~ AncestryProp + Lake * Experiment	197.77	-0.10	0.5071
		Molluscivore	Composite ~ AncestryProp	202.26	0.06	0.6745
			Composite ~ AncestryProp + Lake	**195.08**	**0.20**	**0.1945**
			Composite ~ AncestryProp + Experiment	203.74	0.03	0.8131
			Composite ~ AncestryProp + Lake + Experiment	196.54	0.17	0.2700
			Composite ~ AncestryProp + Lake * Experiment	196.66	0.20	0.2129
		Scale-eater	Composite ~ AncestryProp	201.64	-0.17	0.3725
			Composite ~ AncestryProp + Lake	196.69	-0.06	0.7619
			Composite ~ AncestryProp + Experiment	201.62	-0.33	0.1463
			Composite ~ AncestryProp + Lake + Experiment	196.90	-0.22	0.3595
			Composite ~ AncestryProp + Lake * Experiment	**197.61**	**-0.19**	**0.4393**
Growth	Gaussian	Generalist	Growth ~ AncestryProp	42.47	0.08	0.4084
			Growth ~ AncestryProp + Lake	18.85	0.32	0.0010
			Growth ~ AncestryProp + Experiment	13.43	-0.32	0.0032
			Growth ~ AncestryProp + Lake + Experiment	-23.42	-0.07	0.4413
			Growth ~ AncestryProp + Lake * Experiment	**-89.90**	**0.10**	**0.1187**
		Molluscivore	Growth ~ AncestryProp	42.52	0.11	0.4231
			Growth ~ AncestryProp + Lake	29.24	-0.13	0.3383
			Growth ~ AncestryProp + Experiment	13.91	0.35	0.0041
			Growth ~ AncestryProp + Lake + Experiment	-23.57	0.09	0.3932
			Growth ~ AncestryProp + Lake * Experiment	**-88.32**	**-0.07**	**0.3280**
		Scale-eater	Growth ~ AncestryProp	36.71	-0.41	0.0122
			Growth ~ AncestryProp + Lake	12.25	-0.64	0.0000
			Growth ~ AncestryProp + Experiment	21.98	0.14	0.4870
			Growth ~ AncestryProp + Lake + Experiment	-22.80	0.00	0.9950
			Growth ~ AncestryProp + Lake * Experiment	**-88.53**	**-0.11**	**0.2825**
Survival	Binomial	Generalist	Survival ~ AncestryProp	188.70	-0.13	0.7769
			Survival ~ AncestryProp + Lake	151.13	-1.59	0.0144
			Survival ~ AncestryProp + Experiment	159.06	0.92	0.0793
			Survival ~ AncestryProp + Lake + Experiment	**123.49**	**-0.54**	**0.4400**
			Survival ~ AncestryProp + Lake * Experiment	125.49	-0.54	0.4400
		Molluscivore	Survival ~ AncestryProp	188.78	0.03	0.9643
			Survival ~ AncestryProp + Lake	155.11	1.13	0.0936
			Survival ~ AncestryProp + Experiment	161.41	-0.53	0.3709
			Survival ~ AncestryProp + Lake + Experiment	**123.06**	**0.76**	**0.3127**
			Survival ~ AncestryProp + Lake * Experiment	125.06	0.76	0.3127
		Scale-eater	Survival ~ AncestryProp	188.61	0.34	0.6756
			Survival ~ AncestryProp + Lake	154.93	1.60	0.0852
			Survival ~ AncestryProp + Experiment	158.99	-1.69	0.0828
			Survival ~ AncestryProp + Lake + Experiment	**124.04**	**-0.28**	**0.8041**
			Survival ~ AncestryProp + Lake * Experiment	126.04	-0.28	0.8041

Appendix 1—Table 3. Models tested to assess the extent to which specialist ancestry predicts measures of fitness and their respective fits using all samples and a supervised admixture analysis. Best-fit models are bolded.

Fitness Measure	Model Family	Species	Model	AIC	Ancestry Coefficient	Ancestry *P*-value
Composite	Tobit	Generalist	Composite ~ AncestryProp	201.70	0.09	0.3883
			Composite ~ AncestryProp + Lake	**196.79**	**0.00**	**0.9774**
			Composite ~ AncestryProp + Experiment	201.56	0.19	0.1375
			Composite ~ AncestryProp + Lake + Experiment	197.39	0.08	0.5475
			Composite ~ AncestryProp + Lake * Experiment	198.06	0.06	0.6961
		Molluscivore	Composite ~ AncestryProp	202.39	-0.03	0.8382
			Composite ~ AncestryProp + Lake	**196.49**	**0.08**	**0.5870**
			Composite ~ AncestryProp + Experiment	203.59	-0.06	0.6576
			Composite ~ AncestryProp + Lake + Experiment	197.68	0.04	0.7787
			Composite ~ AncestryProp + Lake * Experiment	198.03	0.07	0.6638
		Scale-eater	Composite ~ AncestryProp	201.06	-0.22	0.2395
			Composite ~ AncestryProp + Lake	196.33	-0.13	0.4993
			Composite ~ AncestryProp + Experiment	200.40	-0.41	0.0717
			Composite ~ AncestryProp + Lake + Experiment	**195.82**	**-0.32**	**0.1705**
			Composite ~ AncestryProp + Lake * Experiment	196.60	-0.29	0.2091
Growth	Gaussian	Generalist	Growth ~ AncestryProp	39.30	0.17	0.0525
			Growth ~ AncestryProp + Lake	11.24	0.37	0.0000
			Growth ~ AncestryProp + Experiment	19.52	-0.18	0.0915
			Growth ~ AncestryProp + Lake + Experiment	-22.80	0.01	0.9525
			Growth ~ AncestryProp + Lake * Experiment	**-93.03**	**0.14**	**0.0206**
		Molluscivore	Growth ~ AncestryProp	43.11	-0.03	0.8005
			Growth ~ AncestryProp + Lake	26.45	-0.23	0.0581
			Growth ~ AncestryProp + Experiment	18.62	0.23	0.0541
			Growth ~ AncestryProp + Lake + Experiment	-22.89	0.03	0.7653
			Growth ~ AncestryProp + Lake * Experiment	**-89.91**	**-0.10**	**0.1177**
		Scale-eater	Growth ~ AncestryProp	32.80	-0.50	0.0015
			Growth ~ AncestryProp + Lake	6.53	-0.69	0.0000
			Growth ~ AncestryProp + Experiment	22.48	-0.02	0.9330
			Growth ~ AncestryProp + Lake + Experiment	-23.14	-0.09	0.5710
			Growth ~ AncestryProp + Lake * Experiment	**-89.59**	**-0.15**	**0.1427**
Survival	Binomial	Generalist	Survival ~ AncestryProp	188.75	-0.09	0.8445
			Survival ~ AncestryProp + Lake	152.86	-1.30	0.0292
			Survival ~ AncestryProp + Experiment	157.53	1.13	0.0334
			Survival ~ AncestryProp + Lake + Experiment	**124.09**	**-0.08**	**0.9038**
			Survival ~ AncestryProp + Lake * Experiment	126.09	-0.08	0.9038
		Molluscivore	Survival ~ AncestryProp	188.78	-0.05	0.9246
			Survival ~ AncestryProp + Lake	156.09	0.89	0.1683
			Survival ~ AncestryProp + Experiment	160.74	-0.70	0.2264
			Survival ~ AncestryProp + Lake + Experiment	**123.85**	**0.36**	**0.6142**
			Survival ~ AncestryProp + Lake * Experiment	125.85	0.36	0.6142
		Scale-eater	Survival ~ AncestryProp	188.58	0.35	0.6522
			Survival ~ AncestryProp + Lake	155.46	1.36	0.1160
			Survival ~ AncestryProp + Experiment	158.78	-1.70	0.0770
			Survival ~ AncestryProp + Lake + Experiment	**123.77**	**-0.64**	**0.5753**
			Survival ~ AncestryProp + Lake * Experiment	125.77	-0.64	0.5753

Appendix 1—Table 4. Models tested to assess the extent to which specialist ancestry predicts measures of fitness and their respective fits using only samples from the second field experiment (Martin and Gould 2020) and an unsupervised admixture analysis. Best-fit models are bolded.

Fitness Measure	Model Family	Species	Model	AIC	Ancestry Coefficient	Ancestry *P*-value
Composite	Tobit	Generalist	Composite ~ AncestryProp	187.62	0.11	0.5151
			Composite ~ AncestryProp + Lake	**179.83**	**-0.13**	**0.5004**
			Composite ~ AncestryProp * Lake	181.65	-0.04	0.8924
		Molluscivore	Composite ~ AncestryProp	188.04	0.02	0.9170
			Composite ~ AncestryProp + Lake	**178.97**	**0.24**	**0.2536**
			Composite ~ AncestryProp * Lake	179.95	-0.04	0.9036
		Scale-eater	Composite ~ AncestryProp	186.12	-0.43	0.1743
			Composite ~ AncestryProp + Lake	**179.90**	**-0.20**	**0.5361**
			Composite ~ AncestryProp * Lake	180.85	0.28	0.6288
Growth	Gaussian	Generalist	Growth ~ AncestryProp	27.50	-0.34	0.0070
			Growth ~ AncestryProp + Lake	-51.14	0.08	0.2452
			Growth ~ AncestryProp * Lake	**-53.47**	**0.01**	**0.9339**
		Molluscivore	Growth ~ AncestryProp	28.21	0.38	0.0103
			Growth ~ AncestryProp + Lake	**-50.78**	**-0.08**	**0.3149**
			Growth ~ AncestryProp * Lake	-49.16	-0.05	0.6565
		Scale-eater	Growth ~ AncestryProp	34.00	0.29	0.3072
			Growth ~ AncestryProp + Lake	-50.03	-0.08	0.5823
			Growth ~ AncestryProp * Lake	**-52.24**	**0.09**	**0.5772**
Survival	Binomial	Generalist	Survival ~ AncestryProp	157.06	0.92	0.0793
			Survival ~ AncestryProp + Lake	**121.49**	**-0.54**	**0.4400**
			Survival ~ AncestryProp * Lake	123.46	-0.36	0.7660
		Molluscivore	Survival ~ AncestryProp	159.41	-0.53	0.3709
			Survival ~ AncestryProp + Lake	**121.06**	**0.76**	**0.3127**
			Survival ~ AncestryProp * Lake	122.70	-0.04	0.9788
		Scale-eater	Survival ~ AncestryProp	156.99	-1.69	0.0828
			Survival ~ AncestryProp + Lake	**122.04**	**-0.28**	**0.8041**
			Survival ~ AncestryProp * Lake	123.24	2.00	1.0000

Appendix 1—Table 5. Models tested to assess the extent to which genome-wide variation (PC1/PC2) predicts measures of fitness and their respective fits using all samples and an unsupervised admixture analysis. Best-fit models are bolded.

Fitness Measure	Model Family	Principle Component	Model	AIC	Ancestry Coefficient	Ancestry *P*-value
Composite	Tobit	PC1	**Composite ~ PC1**	**193.80**	**1.67**	**0.0043**
			Composite ~ PC1 + Lake	195.52	3.07	0.2586
			Composite ~ PC1 + Experiment	194.27	1.80	0.0030
			Composite ~ PC1 + Lake + Experiment	195.36	4.52	0.1233
			Composite ~ PC1 + Lake * Experiment	197.07	3.62	0.2831
		PC2	Composite ~ PC2	202.44	-0.01	0.9907
			Composite ~ PC2 + Lake	195.45	1.20	0.2456
			Composite ~ PC2 + Experiment	203.75	0.21	0.8294
			Composite ~ PC2 + Lake + Experiment	**195.21**	**1.79**	**0.1130**
			Composite ~ PC2 + Lake * Experiment	196.35	1.57	0.1738
Growth	Gaussian	PC1	Growth ~ PC1	30.97	-1.62	0.0006
			Growth ~ PC1 + Lake	29.37	1.57	0.3723
			Growth ~ PC1 + Experiment	-32.37	-2.92	0.0000
			Growth ~ PC1 + Lake + Experiment	-30.92	-3.87	0.0055
			Growth ~ PC1 + Lake * Experiment	**-87.40**	**0.33**	**0.7638**
		PC2	Growth ~ PC2	23.61	2.88	0.0002
			Growth ~ PC2 + Lake	23.61	2.00	0.0119
			Growth ~ PC2 + Experiment	14.04	2.04	0.0044
			Growth ~ PC2 + Lake + Experiment	-23.65	-0.61	0.3677
			Growth ~ PC2 + Lake * Experiment	**-87.49**	**0.20**	**0.6724**
Survival	Binomial	PC1	Survival ~ PC1	156.24	15.09	0.0000
			Survival ~ PC1 + Lake	157.87	6.04	0.6943
			Survival ~ PC1 + Experiment	**121.52**	**17.78**	**0.0000**
			Survival ~ PC1 + Lake + Experiment	123.51	15.92	0.4386
			Survival ~ PC1 + Lake * Experiment	125.51	15.92	0.4386
		PC2	Survival ~ PC2	157.96	-9.44	0.0268
			Survival ~ PC2 + Lake	157.96	-1.21	0.7988
			Survival ~ PC2 + Experiment	160.72	-5.63	0.2248
			Survival ~ PC2 + Lake + Experiment	**123.39**	**4.89**	**0.4047**
			Survival ~ PC2 + Lake * Experiment	125.39	4.89	0.4047

Appendix 1—Table 6. SNPs found to be strongly associated with composite fitness using SnpEff (136)**.** SNPs that were identified as being strongly associated with both growth and composite fitness are italicized, and those that remain significant after a Bonferroni correction are bolded.

Scaffold	Position	Significance	REF	ALT	Variant Type	Gene Identifier	Gene Card
HiC_scaffold_1	32071263	FDR	A	C	intergenic	CBRO_00000660-CBRO_00000661	Znf250-Ptgdr2
HiC_scaffold_1	**43866598**	**Bonferroni**	**G**	**A**	**intergenic**	**CBRO_00000910-CBRO_00000911**	**PPM1K-OVCH2**
HiC_scaffold_1	43867614	FDR	C	T	intergenic	CBRO_00000910-CBRO_00000911	PPM1K-OVCH2
HiC_scaffold_3	2658774	FDR	T	A	intergenic	CBRO_00017856-CBRO_00017857	KMT2E-Magi2
HiC_scaffold_3	2658775	FDR	T	C	intergenic	CBRO_00017856-CBRO_00017857	KMT2E-Magi2
HiC_scaffold_3	2658793	FDR	C	A	intergenic	CBRO_00017856-CBRO_00017857	KMT2E-Magi2
HiC_scaffold_4	18899496	FDR	T	C	intergenic	CBRO_00012427-CBRO_00012428	UNKNOWN-edc4
HiC_scaffold_5	18306419	FDR	C	G	upstream; intergenic	CBRO_00001232; CBRO_00001231-CBRO_00001232	xlrs1; PPEF2-xlrs1
HiC_scaffold_5	18306428	FDR	A	T	upstream; intergenic	CBRO_00001232; CBRO_00001231-CBRO_00001232	xlrs1; PPEF2-xlrs1
HiC_scaffold_5	18307019	FDR	G	T	intronic	CBRO_00001232	xlrs1
HiC_scaffold_5	18307030	FDR	G	A	intronic	CBRO_00001232	xlrs1
HiC_scaffold_5	18311696	FDR	C	T	intronic	CBRO_00001232	xlrs1
HiC_scaffold_5	40475116	FDR	T	A	intergenic	CBRO_00001627-CBRO_00001628	SLC25A44-UBE2Q2
HiC_scaffold_7	10290141	FDR	T	C	downstream; intergenic	CBRO_00009717; CBRO_00009716-CBRO_00009717	Nfkbie; SLC35B2-Nfkbie
HiC_scaffold_7	10290142	FDR	G	C	downstream; intergenic	CBRO_00009717; CBRO_00009716-CBRO_00009717	Nfkbie; SLC35B2-Nfkbie
HiC_scaffold_7	10290165	FDR	A	G	downstream; intergenic	CBRO_00009717; CBRO_00009716-CBRO_00009717	Nfkbie; SLC35B2-Nfkbie
HiC_scaffold_7	10290166	FDR	T	C	downstream; intergenic	CBRO_00009717; CBRO_00009716-CBRO_00009717	Nfkbie; SLC35B2-Nfkbie
HiC_scaffold_7	10290168	FDR	T	C	downstream; intergenic	CBRO_00009717; CBRO_00009716-CBRO_00009717	Nfkbie; SLC35B2-Nfkbie
HiC_scaffold_7	13815058	FDR	A	G	synonymous; downstream	CBRO_00009805; CBRO_00009804	Aloxe3; UNKNOWN
HiC_scaffold_7	13815326	FDR	C	T	intronic	CBRO_00009805	Aloxe3
HiC_scaffold_7	15349830	FDR	C	A	intergenic	CBRO_00009834-CBRO_00009835	Adcy8-efr3b

HiC_scaffold_7	18378061	FDR	T	A	intergenic	CBRO_00009902-CBRO_00009903	Fam84a-DDX1
HiC_scaffold_8	**20263964**	**Bonferroni**	**G**	**A**	**upstream; intergenic**	**CBRO_00010647; CBRO_00010647-CBRO_00010648**	**Srcin1; Srcin1-Srcin1**
HiC_scaffold_8	31539262	FDR	G	A	upstream; intergenic	CBRO_00010835; CBRO_00010834-CBRO_00010835	Gjd3; Gjd3-Gjd3
HiC_scaffold_11	3106766	FDR	T	A	intronic	CBRO_00013361	prkdc
HiC_scaffold_11	3138733	FDR	G	A	intergenic	CBRO_00013361-CBRO_00013362	prkdc-arhgap29
HiC_scaffold_11	5658921	FDR	A	G	intronic	CBRO_00013404	KAZN
HiC_scaffold_14	17556007	FDR	C	T	intergenic	CBRO_00014134-CBRO_00014135	UNKNOWN-Abr
HiC_scaffold_14	17556026	FDR	C	A	intergenic	CBRO_00014134-CBRO_00014135	UNKNOWN-Abr
HiC_scaffold_16	32837191	FDR	T	C	intronic	CBRO_00003226	KIF1B
HiC_scaffold_16	35727503	FDR	G	C	intergenic	CBRO_00003289-CBRO_00003290	Pip5k1c-Polr2e
HiC_scaffold_16	40215889	FDR	G	A	intergenic	CBRO_00003383-CBRO_00003384	chst10-UNKNOWN
HiC_scaffold_16	40300592	FDR	C	A	intergenic	CBRO_00003384-CBRO_00003385	UNKNOWN-Carmil3
HiC_scaffold_18	26969972	FDR	T	G	intronic	CBRO_00013239	CSAD
HiC_scaffold_18	26970123	FDR	C	T	synonymous	CBRO_00013239	CSAD
HiC_scaffold_18	26970601	FDR	T	A	intronic	CBRO_00013239	CSAD
HiC_scaffold_18	26978410	FDR	G	A	intronic	CBRO_00013240	Znf740
HiC_scaffold_20	332642	FDR	G	A	missense	CBRO_00016084	GTF3C4
HiC_scaffold_20	332689	FDR	A	G	missense	CBRO_00016084	GTF3C4
HiC_scaffold_20	14820437	FDR	A	T	intronic	CBRO_00016304	MALT1
HiC_scaffold_20	14820448	FDR	T	C	intronic	CBRO_00016304	MALT1
HiC_scaffold_24	1469530	FDR	G	T	intergenic	CBRO_00014375-CBRO_00014376	UNKNOWN-UNKNOWN
HiC_scaffold_24	3223583	FDR	T	A	intergenic	CBRO_00014421-CBRO_00014422	Gal3st3-RIN2
HiC_scaffold_24	11618442	FDR	T	G	intronic	CBRO_00014601	ABCA4
HiC_scaffold_24	**15964553**	**Bonferroni**	**C**	**T**	**intergenic**	**CBRO_00014635-CBRO_00014636**	**Lrfn2-SNX15**
HiC_scaffold_27	1898180	FDR	G	A	downstream; intergenic	CBRO_00005887; CBRO_00005886-CBRO_00005887	UNKNOWN; hoxb13a-UNKNOWN
HiC_scaffold_27	8137335	FDR	G	T	intronic	CBRO_00005998	SMARCA4
HiC_scaffold_27	9065056	FDR	C	A	intergenic	CBRO_00006026-CBRO_00006027	ANKFN1-ccdc134
HiC_scaffold_27	12370585	FDR	C	T	intergenic	CBRO_00006131-CBRO_00006132	SHISA9-Desi1

HiC_scaffold_27	32078665	FDR	C	G	intergenic	CBRO_00006685-CBRO_00006686	med25-Lrrc4b
HiC_scaffold_27	34904388	FDR	A	C	intergenic	CBRO_00006756-CBRO_00006757	Grin2c-nog3
HiC_scaffold_27	35431570	FDR	G	C	intergenic	CBRO_00006756-CBRO_00006757	Grin2c-nog3
HiC_scaffold_27	35431578	FDR	C	T	intergenic	CBRO_00006756-CBRO_00006757	Grin2c-nog3
HiC_scaffold_27	35431585	FDR	A	G	intergenic	CBRO_00006756-CBRO_00006757	Grin2c-nog3
HiC_scaffold_34	16654675	FDR	G	C	intergenic	CBRO_00001997-CBRO_00001998	MDFIC2-foxp1b
HiC_scaffold_34	19393244	FDR	A	T	upstream; intergenic	CBRO_00002027; CBRO_00002027-CBRO_00002028	SUOX; SUOX-SUOX
HiC_scaffold_34	22010499	FDR	C	T	intronic	CBRO_00002117	GNAI2
HiC_scaffold_34	31220916	FDR	T	A	upstream; intergenic	CBRO_00002389; CBRO_00002388-CBRO_00002389	CTTNBP2NL; Kcnd3-CTTNBP2NL
HiC_scaffold_34	37769304	FDR	A	C	intergenic	CBRO_00002519-CBRO_00002520	ASIC2-asic1
HiC_scaffold_37	5963405	FDR	T	C	intergenic	CBRO_00011020-CBRO_00011021	C14orf93-pim2
HiC_scaffold_37	11017168	FDR	G	A	intergenic	CBRO_00011155-CBRO_00011156	GALNT12-elp2
HiC_scaffold_37	13822135	FDR	A	G	upstream; intergenic	CBRO_00011221; CBRO_00011220-CBRO_00011221	SATB1; KCNH8-SATB1
HiC_scaffold_37	13823678	FDR	G	A	upstream; intergenic	CBRO_00011221; CBRO_00011220-CBRO_00011221	SATB1; KCNH8-SATB1
HiC_scaffold_37	13832007	FDR	T	A	missense	CBRO_00011221	SATB1
HiC_scaffold_37	16920863	FDR	T	C	intergenic	CBRO_00011259-CBRO_00011260	CSMD1-UNKNOWN
HiC_scaffold_37	**18591438**	**Bonferroni**	**G**	**A**	**intergenic**	**CBRO_00011301-CBRO_00011302**	**cck-trim71**
HiC_scaffold_37	18591463	FDR	C	T	intergenic	CBRO_00011301-CBRO_00011302	cck-trim71
HiC_scaffold_37	18596716	FDR	A	T	intergenic	CBRO_00011301-CBRO_00011302	cck-trim71
HiC_scaffold_40	5885291	FDR	G	T	downstream; intergenic	CBRO_00016614; CBRO_00016613-CBRO_00016614	C14orf93 homolog; HTR2A-C14orf93 homolog
HiC_scaffold_43	2568535	FDR	A	G	intergenic	CBRO_00008246-CBRO_00008247	UNKNOWN-Gpr68
HiC_scaffold_44	25886134	FDR	A	C	intergenic	CBRO_00007276-CBRO_00007277	RAPGEF2-QDPR
HiC_scaffold_45	885834	FDR	A	C	upstream; intergenic	CBRO_00018766; CBRO_00018766-CBRO_00018767	Mog; Mog-EPHB4
HiC_scaffold_45	2213441	FDR	G	T	intronic	CBRO_00018814	Nlrp12
HiC_scaffold_46	856248	FDR	A	G	intergenic	CBRO_00007439-CBRO_00007440	UNKNOWN-NLRP12
HiC_scaffold_46	1232350	FDR	G	A	intronic	CBRO_00007448	NEB

HiC_scaffold_46	30183758	FDR	C	G	intergenic	CBRO_00008059-CBRO_00008060	TFRC-Rgs11
HiC_scaffold_46	32048848	FDR	A	C	intronic	CBRO_00008105	Hsd17b7
HiC_scaffold_46	32050109	FDR	G	T	synonymous	CBRO_00008105	Hsd17b7
HiC_scaffold_46	**35151009**	**Bonferroni**	**T**	**C**	**downstream; intergenic**	**CBRO_00008165; CBRO_00008165-CBRO_00008166**	**Klf9; Klf9-Tsen15**
HiC_scaffold_46	35163681	FDR	T	C	downstream; intergenic	CBRO_00008166; CBRO_00008167; CBRO_00008166-CBRO_00008167	Tsen15; UNKNOWN; Tsen15-UNKNOWN
HiC_scaffold_46	35164267	FDR	A	G	downstream; intergenic	CBRO_00008166; CBRO_00008167; CBRO_00008166-CBRO_00008167	Tsen15; UNKNOWN; Tsen15-UNKNOWN
HiC_scaffold_47	787141	FDR	T	G	upstream; intergenic	CBRO_00008838; CBRO_00008837-CBRO_00008838	Nlrc3; NLRC3-Nlrc3
HiC_scaffold_47	4300295	FDR	G	A	downstream; intergenic	CBRO_00008933; CBRO_00008933-CBRO_00008934	NEK6; NEK6-Psmb7
HiC_scaffold_47	6767766	FDR	T	C	intergenic	CBRO_00008991-CBRO_00008992	TACR1-Grk5
HiC_scaffold_52	20791197	FDR	T	A	upstream; intronic	CBRO_00011892; CBRO_00011891	rabl3; GTF2E1
HiC_scaffold_52	22551701	FDR	G	C	intergenic	CBRO_00011922-CBRO_00011923	ALS2-Serp2
HiC_scaffold_52	31021517	FDR	C	T	intergenic	CBRO_00012051-CBRO_00012052	Tmeff2-slc39a10
HiC_scaffold_53	**11317840**	**Bonferroni**	**A**	**G**	**intergenic**	**CBRO_00005178-CBRO_00005179**	**Fucolectin-1-Fucolectin-5**
HiC_scaffold_53	11326035	FDR	C	T	intergenic	CBRO_00005178-CBRO_00005179	Fucolectin-1-Fucolectin-5
HiC_scaffold_53	11326410	FDR	G	A	intergenic	CBRO_00005178-CBRO_00005179	Fucolectin-1-Fucolectin-5
HiC_scaffold_53	11331079	FDR	A	G	intergenic	CBRO_00005178-CBRO_00005179	Fucolectin-1-Fucolectin-5
HiC_scaffold_53	15966447	FDR	G	A	upstream; downstream; intergenic	CBRO_00005235; CBRO_00005234; CBRO_00005234-CBRO_00005235	Tmem222; WDTC1; WDTC1-Tmem222
HiC_scaffold_53	17413090	FDR	A	G	missense	CBRO_00005274	Mag
HiC_scaffold_53	20715576	FDR	C	A	intergenic	CBRO_00005380-CBRO_00005381	Scrt2-Ino80c
HiC_scaffold_53	20715623	FDR	G	A	intergenic	CBRO_00005380-CBRO_00005381	Scrt2-Ino80c
HiC_scaffold_53	20715851	FDR	A	G	intergenic	CBRO_00005380-CBRO_00005381	Scrt2-Ino80c
HiC_scaffold_53	27386094	FDR	G	T	intronic	CBRO_00005625	Arhgef1
HiC_scaffold_53	27396961	FDR	T	A	intronic	CBRO_00005625	Arhgef1
HiC_scaffold_53	27398605	FDR	T	G	downstream; intergenic	CBRO_00005625; CBRO_00005625-CBRO_00005626	Arhgef1; Arhgef1-CD79A
HiC_scaffold_53	33282501	FDR	A	G	intergenic	CBRO_00005732-CBRO_00005733	mios-GLCCI1

HiC_scaffold_53	39228193	FDR	T	C	intergenic	CBRO_00005830-CBRO_00005831	UNKNOWN-GnRHR2
HiC_scaffold_53	**39228264**	**Bonferroni**	**C**	**T**	**intergenic**	**CBRO_00005830-CBRO_00005831**	**UNKNOWN-GnRHR2**
HiC_scaffold_53	39228942	FDR	A	T	intergenic	CBRO_00005830-CBRO_00005831	UNKNOWN-GnRHR2
HiC_scaffold_53	39279263	FDR	G	T	intronic	CBRO_00005832	IGDCC3
HiC_scaffold_53	39770914	FDR	A	T	intronic	CBRO_00005849	Cpne4
HiC_scaffold_611	5621	FDR	A	T	intergenic	CHR_START-CBRO_00020243	CHR_START-fzdz-a
HiC_scaffold_611	5625	FDR	G	T	intergenic	CHR_START-CBRO_00020243	CHR_START-fzdz-a
HiC_scaffold_611	5634	FDR	T	A	intergenic	CHR_START-CBRO_00020243	CHR_START-fzdz-a
HiC_scaffold_1053	3494	FDR	A	G	downstream; intergenic	CBRO_00020503; CHR_START-CBRO_00020503	UBE2G2; CHR_START-UBE2G2
HiC_scaffold_1133	9946	FDR	A	G	intergenic	.	.
HiC_scaffold_1371	7318	FDR	C	T	upstream; intergenic	CBRO_00021026; CHR_START-CBRO_00021026	UNKNOWN; CHR_START-UNKNOWN
HiC_scaffold_1848	**40119**	**Bonferroni**	**C**	**A**	**intergenic**	**.**	**.**
HiC_scaffold_1848	**40465**	**Bonferroni**	**T**	**A**	**intergenic**	**.**	**.**
HiC_scaffold_1848	**40590**	**Bonferroni**	**T**	**C**	**intergenic**	**.**	**.**
HiC_scaffold_1848	40877	FDR	T	C	intergenic	.	.
HiC_scaffold_1848	41351	FDR	T	C	intergenic	.	.
HiC_scaffold_2220	10128	FDR	G	T	intergenic	.	.
HiC_scaffold_4461	**12939**	**Bonferroni**	**T**	**A**	**intergenic**	**.**	**.**
HiC_scaffold_4665	13941	FDR	C	T	intergenic	.	.
HiC_scaffold_6275	6000	FDR	C	A	intergenic	.	.
HiC_scaffold_6337	5745	FDR	T	G	intronic	CBRO_00021217	PKP3
HiC_scaffold_6769	2796	FDR	G	A	intergenic	.	.
HiC_scaffold_6963	5970	FDR	C	A	intergenic	.	.
HiC_scaffold_6963	6101	FDR	A	G	intergenic	.	.
HiC_scaffold_9280	3448	FDR	G	A	intergenic	.	.
HiC_scaffold_9949	52	FDR	C	T	intergenic	.	.
HiC_scaffold_10928	3575	FDR	G	A	downstream; intergenic	CBRO_00021896; CHR_START-CBRO_00021896	CYP2A10; CHR_START-CYP2A10
HiC_scaffold_11921	5560	FDR	A	T	intergenic	.	.
HiC_scaffold_12068	2929	FDR	G	T	intergenic	.	.

HiC_scaffold_12778	**1456**	**Bonferroni**	**T**	**A**	**missense**	**CBRO_00022026**	**COL8A1**
HiC_scaffold_17578	180	FDR	T	G	intergenic	.	.
HiC_scaffold_18999	**1084**	**Bonferroni**	**A**	**G**	**intergenic**	**.**	**.**

Appendix 1—Table 7. Gene ontology term enrichment for genes associated with composite fitness.

Functional Category	Enrichment FDR	Genes in list	Total genes	Genes
Anterograde trans-synaptic signaling	0.0060	13	746	GRIN2C, SHISA9, ALS2, KIF1B, ASIC1, GNAI2, TACR1, ADCY8, LRFN2, ABR, RAPGEF2, ASIC2, PIP5K1C
Synaptic signaling	0.0060	13	762	GRIN2C, SHISA9, ALS2, KIF1B, ASIC1, GNAI2, TACR1, ADCY8, LRFN2, ABR, RAPGEF2, ASIC2, PIP5K1C
Trans-synaptic signaling	0.0060	13	756	GRIN2C, SHISA9, ALS2, KIF1B, ASIC1, GNAI2, TACR1, ADCY8, LRFN2, ABR, RAPGEF2, ASIC2, PIP5K1C
Chemical synaptic transmission	0.0060	13	746	GRIN2C, SHISA9, ALS2, KIF1B, ASIC1, GNAI2, TACR1, ADCY8, LRFN2, ABR, RAPGEF2, ASIC2, PIP5K1C
Regulation of I-kappaB kinase/NF-kappaB signaling	0.0179	7	241	NEK6, SLC35B2, MALT1, NLRP12, NLRC3, DDX1, PIM2
Regulation of trans-synaptic signaling	0.0185	9	468	GRIN2C, SHISA9, ASIC1, GNAI2, TACR1, ADCY8, LRFN2, ABR, RAPGEF2
Regulation of cell communication	0.0185	32	3903	NEK6, SLC35B2, MALT1, NLRP12, PPEF2, GRIN2C, NLRC3, SLC39A10, SHISA9, ALS2, RAPGEF2, SMARCA4, MAGI2, RGS11, ARHGEF1, DDX1, PIM2, ASIC1, GNAI2, TACR1, ADCY8, LRFN2, ABR, PTGDR2, CCK, GPR68, MIOS, SCRT2, PSMB7, ARHGAP29, PIP5K1C, GRK5
Regulation of signaling	0.0185	32	3952	NEK6, SLC35B2, MALT1, NLRP12, PPEF2, GRIN2C, NLRC3, SLC39A10, SHISA9, ALS2, RAPGEF2, SMARCA4, MAGI2, RGS11, ARHGEF1, DDX1, PIM2, ASIC1, GNAI2, TACR1, ADCY8, LRFN2, ABR, PTGDR2, CCK, GPR68, MIOS, SCRT2, PSMB7, ARHGAP29, PIP5K1C, GRK5
Modulation of chemical synaptic transmission	0.0185	9	467	GRIN2C, SHISA9, ASIC1, GNAI2, TACR1, ADCY8, LRFN2, ABR, RAPGEF2
Sensory perception of sour taste	0.0185	2	5	ASIC2, ASIC1
Regulation of biological quality	0.0185	34	4319	GRIN2C, KCNH8, SLC39A10, SHISA9, PRKDC, TACR1, SMARCA4, KCND3, ABCA4, TRIM71, KMT2E, TFRC, PIM2, MAG, ASIC2, ASIC1, GNAI2, LRRC4B, HSD17B7, WDTC1, ADCY8, LRFN2, ABR, ALOXE3, CSMD1, CCK, SRCIN1, ALS2, GPR68, RAPGEF2, NEB, PSMB7, NFKBIE, PIP5K1C
I-kappaB kinase/NF-kappaB signaling	0.0185	7	280	NEK6, SLC35B2, MALT1, NLRP12, NLRC3, DDX1, PIM2
Positive regulation of catalytic activity	0.0185	17	1514	PPM1K, ALS2, RAPGEF2, MAGI2, SRCIN1, RGS11, ARHGEF1, GNAI2, GTF3C4, RIN2, ARHGAP29, ABR, CCK, SLC39A10, MALT1, ADCY8, NLRP12
Regulation of protein tyrosine phosphatase activity	0.0216	2	6	GNAI2, SLC39A10
Multicellular organismal response to stress	0.0216	4	74	ALS2, ASIC1, TACR1, CCK
Positive regulation of molecular function	0.0270	19	1901	PPM1K, MALT1, ALS2, RAPGEF2, SMARCA4, MAGI2, SRCIN1, RGS11, ARHGEF1, GNAI2, GTF3C4, RIN2, ARHGAP29, ADCY8, ABR, CCK, SLC39A10, MED25, NLRP12
Cell-cell signaling	0.0311	18	1774	GRIN2C, SHISA9, ALS2, KIF1B, ASIC1, GNAI2, TACR1, ADCY8, LRFN2, ABR, GRK5, GPR68, SMARCA4, RAPGEF2, MAGI2, ASIC2, PSMB7, PIP5K1C
Tachykinin receptor signaling pathway	0.0314	2	8	TACR1, GRK5
Cell proliferation	0.0355	20	2165	TFRC, PIM2, RAPGEF2, CD79A, GNAI2, TACR1, COL8A1, MALT1, SATB1, PTGDR2, CCK, SLC39A10, TRIM71, PRKDC, MED25, KLF9, GRK5, NLRC3, MAGI2, ARHGEF1
Behavioral fear response	0.0355	3	39	ALS2, ASIC1, CCK
Response to pH	0.0355	3	41	ASIC1, ASIC2, GPR68
Behavioral defense response	0.0355	3	40	ALS2, ASIC1, CCK
Fear response	0.0355	3	41	ALS2, ASIC1, CCK
Positive regulation of hydrolase activity	0.0401	11	833	ALS2, RAPGEF2, MAGI2, RGS11, ARHGEF1, RIN2, ARHGAP29, ABR, CCK, SLC39A10, NLRP12
NcRNA transcription	0.0457	4	110	GTF3C4, SMARCA4, POLR2E, GTF2E1
Hexose mediated signaling	0.0457	2	13	SMARCA4, ADCY8
Sugar mediated signaling pathway	0.0457	2	13	SMARCA4, ADCY8
Glucose mediated signaling pathway	0.0457	2	13	SMARCA4, ADCY8
Positive regulation of cell communication	0.0457	18	1937	NEK6, SLC35B2, MALT1, GRIN2C, SLC39A10, ALS2, RAPGEF2, SMARCA4, NLRP12, DDX1, PIM2, GNAI2, TACR1, ADCY8, PTGDR2, GPR68, MIOS, PSMB7
Positive regulation of signaling	0.0457	18	1945	NEK6, SLC35B2, MALT1, GRIN2C, SLC39A10, ALS2, RAPGEF2, SMARCA4, NLRP12, DDX1, PIM2, GNAI2, TACR1, ADCY8, PTGDR2, GPR68, MIOS, PSMB7

Appendix 1—Table 8. SNPs found to be strongly associated with growth SnpEff (136)**.** SNPs that were identified as being strongly associated with both growth and composite fitness are italicized, and those that remain significant after a Bonferroni correction are bolded.

Scaffold	Position	Significance	REF	ALT	Variant Type	Gene Identifier	Gene Card
HiC_scaffold_4	8897671	FDR	A	T	intergenic	CBRO_00012254-CBRO_00012255	Megf10-UNKNOWN
HiC_scaffold_4	16057698	FDR	C	A	intergenic	CBRO_00012386-CBRO_00012387	CCND2-Mlycd
HiC_scaffold_4	29273446	FDR	T	C	synonymous	CBRO_00012620	CKAP5
HiC_scaffold_4	29273458	FDR	C	T	synonymous	CBRO_00012620	CKAP5
HiC_scaffold_5	18259775	FDR	C	A	upstream; intergenic	CBRO_00001229; CBRO_00001229-CBRO_00001230	AP1S2; AP1S2-phka2
HiC_scaffold_5	*18306419*	*FDR*	*C*	*G*	*upstream; intergenic*	*CBRO_00001232; CBRO_00001231-CBRO_00001232*	*xlrs1; PPEF2-xlrs1*
HiC_scaffold_5	*18306428*	*FDR*	*A*	*T*	*upstream; intergenic*	*CBRO_00001232; CBRO_00001231-CBRO_00001232*	*xlrs1; PPEF2-xlrs1*
HiC_scaffold_5	*18307019*	*FDR*	*G*	*T*	*intronic*	*CBRO_00001232*	*xlrs1*
HiC_scaffold_5	*18307030*	*FDR*	*G*	*A*	*intronic*	*CBRO_00001232*	*xlrs1*
HiC_scaffold_5	36619253	FDR	T	C	intergenic	CBRO_00001583-CBRO_00001584	Chst12-ZDHHC13
HiC_scaffold_7	*13815058*	*FDR*	*A*	*G*	*synonymous; downstream*	*CBRO_00009805; CBRO_00009804*	*Aloxe3; UNKNOWN*
HiC_scaffold_7	13823565	FDR	T	C	intronic	CBRO_00009806	Fbxo30
HiC_scaffold_7	13824467	FDR	A	G	missense	CBRO_00009806	Fbxo30
HiC_scaffold_7	19371997	FDR	C	T	upstream; intergenic	CBRO_00009922; CBRO_00009921-CBRO_00009922	ELOVL4; TENT5A-ELOVL4
HiC_scaffold_7	19372002	FDR	T	G	upstream; intergenic	CBRO_00009922; CBRO_00009921-CBRO_00009922	ELOVL4; TENT5A-ELOVL4
HiC_scaffold_8	20265076	FDR	T	C	upstream; intergenic	CBRO_00010647; CBRO_00010647-CBRO_00010648	Srcin1; Srcin1-Srcin1
HiC_scaffold_8	20265098	FDR	G	C	upstream; intergenic	CBRO_00010647; CBRO_00010647-CBRO_00010648	Srcin1; Srcin1-Srcin1
HiC_scaffold_8	20278571	FDR	G	A	intergenic	CBRO_00010647-CBRO_00010648	Srcin1-Srcin1
HiC_scaffold_9	15585466	FDR	C	G	missense	CBRO_00004552	Tmem260
HiC_scaffold_9	18453213	FDR	A	G	intergenic	CBRO_00004639-CBRO_00004640	Bub1b-PAK6
HiC_scaffold_9	28127377	FDR	C	T	intergenic	CBRO_00004857-CBRO_00004858	METTL21E-RASA3
HiC_scaffold_10	193812	FDR	C	G	intergenic	CBRO_00018931-CBRO_00018932	Spsb4-UNKNOWN

HiC_scaffold_11	25632195	FDR	C	T	intergenic	CBRO_00013717-CBRO_00013718	CDH10-Cdh6
HiC_scaffold_11	25632258	FDR	C	T	intergenic	CBRO_00013717-CBRO_00013718	CDH10-Cdh6
HiC_scaffold_11	25632641	FDR	A	G	intergenic	CBRO_00013717-CBRO_00013718	CDH10-Cdh6
HiC_scaffold_14	14624430	FDR	T	C	intergenic	CBRO_00014084-CBRO_00014085	KDM6B-FGF11
HiC_scaffold_18	26970449	FDR	C	T	intronic	CBRO_00013239	CSAD
HiC_scaffold_27	*8137335*	*FDR*	*G*	*T*	*intronic*	*CBRO_00005998*	*SMARCA4*
HiC_scaffold_27	21919164	FDR	G	T	synonymous	CBRO_00006396	SSTR2
HiC_scaffold_29	2136546	FDR	A	T	upstream; intergenic	CBRO_00016347; CBRO_00016347-CBRO_00016348	RAPGEF6; RAPGEF6-ACSL6
HiC_scaffold_29	2147361	FDR	C	T	intergenic	CBRO_00016347-CBRO_00016348	RAPGEF6-ACSL6
HiC_scaffold_31	6226140	FDR	A	C	intronic	CBRO_00017224	ranbp9
HiC_scaffold_34	7439419	FDR	G	T	intergenic	CBRO_00001828-CBRO_00001829	rnf152-CAMTA1
HiC_scaffold_34	30571660	FDR	C	A	intronic	CBRO_00002374	SHMT2
HiC_scaffold_40	4693917	FDR	G	A	intronic	CBRO_00016589	SLC37A1
HiC_scaffold_40	4694015	FDR	T	C	synonymous	CBRO_00016589	SLC37A1
HiC_scaffold_40	4723358	FDR	A	G	intronic	CBRO_00016591	UBXN4
HiC_scaffold_40	4732538	FDR	T	C	intronic	CBRO_00016591	UBXN4
HiC_scaffold_40	4734825	FDR	G	T	intronic	CBRO_00016591	UBXN4
HiC_scaffold_40	4780518	FDR	G	C	intronic	CBRO_00016592	ITGB2
HiC_scaffold_40	5016538	FDR	C	A	upstream; intergenic	CBRO_00016599; CBRO_00016599-CBRO_00016600	RRP1B; RRP1B-ITGB2
HiC_scaffold_43	26869231	FDR	C	G	synonymous	CBRO_00008677	lrpprc
HiC_scaffold_43	27800569	FDR	C	T	downstream; intergenic	CBRO_00008685; CBRO_00008685-CBRO_00008686	timp3; timp3-ETV6
HiC_scaffold_44	19344526	FDR	C	T	intergenic	CBRO_00007178-CBRO_00007179	ATP11C-sox3
HiC_scaffold_46	16495639	FDR	G	A	intronic	CBRO_00007743	PHLPP1
HiC_scaffold_46	16510323	FDR	G	A	intronic	CBRO_00007743	PHLPP1
HiC_scaffold_46	16512668	FDR	T	A	intronic	CBRO_00007743	PHLPP1
HiC_scaffold_46	**16512886**	**Bonferroni**	**T**	**A**	**intronic**	**CBRO_00007743**	**PHLPP1**
HiC_scaffold_46	16513809	FDR	T	C	synonymous	CBRO_00007743	PHLPP1
HiC_scaffold_52	19031083	FDR	T	A	intergenic	CBRO_00011872-CBRO_00011873	NRP2-MREG

HiC_scaffold_52	19031216	FDR	A	T	intergenic	CBRO_00011872-CBRO_00011873	NRP2-MREG
HiC_scaffold_1848	***40119***	***Bonferroni***	***C***	***A***	***intergenic***	**.**	**.**
HiC_scaffold_1848	***40465***	***Bonferroni***	***T***	***A***	***intergenic***	**.**	**.**
HiC_scaffold_1848	*40590*	*FDR*	*T*	*C*	*intergenic*	.	.
HiC_scaffold_1848	*40877*	*FDR*	*T*	*C*	*intergenic*	.	.
HiC_scaffold_1848	*41351*	*FDR*	*T*	*C*	*intergenic*	.	.
HiC_scaffold_7644	**5971**	**Bonferroni**	**T**	**G**	**intergenic**	**.**	**.**
HiC_scaffold_12681	4019	FDR	T	C	upstream; intergenic	CBRO_00022068; CBRO_00022068-CHR_END	UNKNOWN; UNKNOWN-CHR_END

Appendix 1—Table 9. Gene ontology term enrichment for genes associated with growth.

Functional Category	Enrichment FDR	Genes in list	Total genes	Genes
Negative regulation of intracellular signal transduction	0.0259	6	537	PPEF2, RNF152, RASA3, RANBP9, PHLPP1, TIMP3
Phosphorus metabolic process	0.0259	17	3597	PHLPP1, CCND2, PAK6, PPEF2, SHMT2, MLYCD, RRP1B, ITGB2, SRCIN1, PHKA2, ELOVL4, BUB1B, RANBP9, TIMP3, CAMTA1, ACSL6, RASA3
Phosphate-containing compound metabolic process	0.0259	17	3570	PHLPP1, CCND2, PAK6, PPEF2, SHMT2, MLYCD, RRP1B, ITGB2, SRCIN1, PHKA2, ELOVL4, BUB1B, RANBP9, TIMP3, CAMTA1, ACSL6, RASA3
Serine family amino acid catabolic process	0.0259	2	17	SHMT2, CSAD
Organic acid biosynthetic process	0.0259	6	466	ELOVL4, SHMT2, MLYCD, CHST12, ALOXE3, CSAD
Regulation of phosphate metabolic process	0.0259	11	1870	PHLPP1, CCND2, PAK6, PPEF2, SHMT2, RRP1B, ITGB2, SRCIN1, RANBP9, TIMP3, CAMTA1
Nucleoside bisphosphate biosynthetic process	0.0259	3	82	MLYCD, ELOVL4, ACSL6
Ribonucleoside bisphosphate biosynthetic process	0.0259	3	82	MLYCD, ELOVL4, ACSL6
Purine nucleoside bisphosphate biosynthetic process	0.0259	3	82	MLYCD, ELOVL4, ACSL6
Long-chain fatty-acyl-CoA biosynthetic process	0.0259	2	19	ELOVL4, ACSL6
Thioester biosynthetic process	0.0259	3	66	MLYCD, ELOVL4, ACSL6
Positive regulation by host of viral transcription	0.0259	2	18	SMARCA4, RRP1B
Sulfur compound biosynthetic process	0.0259	5	207	MLYCD, CHST12, ELOVL4, CSAD, ACSL6
Regulation of phosphorus metabolic process	0.0259	11	1872	PHLPP1, CCND2, PAK6, PPEF2, SHMT2, RRP1B, ITGB2, SRCIN1, RANBP9, TIMP3, CAMTA1
Acyl-CoA biosynthetic process	0.0259	3	66	MLYCD, ELOVL4, ACSL6
Hypothalamus development	0.0291	2	22	NRP2, SOX3
Sulfur compound metabolic process	0.0312	5	393	MLYCD, CHST12, ELOVL4, CSAD, ACSL6
Long-chain fatty-acyl-CoA metabolic process	0.0343	2	26	ELOVL4, ACSL6
Regulation of mitochondrial translation	0.0343	2	26	LRPPRC, SHMT2
Limbic system development	0.0405	3	115	NRP2, KDM6B, SOX3
Acyl-CoA metabolic process	0.0406	3	119	MLYCD, ELOVL4, ACSL6
Thioester metabolic process	0.0406	3	119	MLYCD, ELOVL4, ACSL6
Protein phosphorylation	0.0412	11	2093	PHLPP1, CCND2, PAK6, PPEF2, ITGB2, SRCIN1, PHKA2, BUB1B, RANBP9, TIMP3, RASA3
Modulation by host of viral transcription	0.0412	2	33	SMARCA4, RRP1B
Carboxylic acid biosynthetic process	0.0412	5	465	ELOVL4, SHMT2, MLYCD, CHST12, ALOXE3
Modulation of transcription in other organism involved in symbiotic interaction	0.0412	2	34	SMARCA4, RRP1B
Modulation by host of symbiont transcription	0.0412	2	33	SMARCA4, RRP1B
Cellular protein modification process	0.0495	17	4434	PHLPP1, CCND2, PAK6, PPEF2, RNF152, ITGB2, SPSB4, SRCIN1, PHKA2, FBXO30, KDM6B, BUB1B, RANBP9, TIMP3, CAMTA1, SHMT2, RASA3
Protein modification process	0.0495	17	4434	PHLPP1, CCND2, PAK6, PPEF2, RNF152, ITGB2, SPSB4, SRCIN1, PHKA2, FBXO30, KDM6B, BUB1B, RANBP9, TIMP3, CAMTA1, SHMT2, RASA3

Appendix 1—Table 10. List of the 31 morphological traits measured for this study, and standard length; corresponding landmark ID's match those shown in Figure 2—figure supplement 3.

Trait Index	Trait Description	Trait Shorthand	Points
1	Nasal protrusion	nose	3-4
2	Nasal length	foresnout	2-5
3	Orbit to anal fin insertion	bellylen	6-15
4	Lateral facial length	snoutlen	2-6
5	Upper jaw to pectoral girdle	jaw2pect	2-14
6	Lateral skull length	pmx2add	2-11
7	Premaxilla length	pmxlen	2-9
8	Lower mandible length	jawlen	1-9
9	Jaw joint to orbit	foreeyewidth	6-9
10	Horizontal orbit diameter	eyewidth	6-8
11	Vertical orbit diameter	eyeht	7-10
12	Head height	headht	7-9
13	Suspensorium length	suspensorium	9-11
14	Adductor height	adductorht	11-12
15	Subopercle to pectoral girdle	ad2pect	11-14
16	Pectoral fin insertion width	pectinsertion	13-14
17	Anal to caudal distance	analtocaudal	15-16
18	Caudal peduncle height	caudalpedht	16-18
19	Dorsal to caudal distance	dorsaltocaudal	18-19
20	Body depth	bodydepth	15-19
21	Nasal protrusion angle	nasalangle	7-5-3
22	Premaxilla to orbit angle	topeyeangle	7-2-10
23	Premaxilla to adductor angle	lowereyeangle	7-2-11
24	Dorsal facial length	dorsalsnoutlen	23-24, 25-26
25	Adductor to premaxilla	eyetosnout	21-24, 25-28
26	Neurocranium to premaxilla	headlen	24-20, 25-29
27	Orbit to premaxilla	innereyetosnout	22-24, 25-27
28	Interorbital width	cranialwidth	22-27
29	Orbital neurocranium width	hindeyewidth	21-28
30	Max. neurocranium width	headwidth	20-29
31	Standard length (SL)	SL	2-17

Appendix 1—Table 11. Generalized additive models fitted to composite fitness. Model fit was assessed using AICc, and Akaike Weights represent proportional model support. A thin plate spline for the two linear discriminant axes s(LD1, LD2) is always included, as is a fixed effect of either experiment (i.e. Martin & Wainwright 2013, Martin and Gould 2020) or Lake (Crescent Pond/Little Lake) or an interaction between the two. In the last two models, Experiment and Lake are included as splines, modeled using a factor smooth (bs = "fs"). The best fit model had 5 estimated degrees of freedom.

Model	AICc	ΔAICc	Akaike Weights
Composite ~ s(LD1, LD2) + Experiment + Lake	*99.114*	*0.000*	*0.825*
Composite ~ s(LD1, LD2) + Experiment * Lake	102.210	3.096	0.175
Composite ~ s(LD1, LD2) + s(LD1) + s(LD2) + Experiment + Lake	131.456	32.342	< 0.001
Composite ~ s(LD1, LD2) + s(LD1) + s(LD2) + Experiment * Lake	135.894	36.781	< 0.001
Composite ~ s(LD1, LD2) + s(LD1, Experiment, bs = "fs") + s(LD2, Experiment, bs = "fs") + Lake	230.428	131.314	< 0.001
Composite ~ s(LD1, LD2) + s(LD1, Lake, bs = "fs") + s(LD2, Lake, bs = "fs") + Experiment	230.868	131.754	< 0.001

Appendix 1—Table 12.

Generalized additive models fitted to growth. Model fit was assessed using AICc, and Akaike Weights represent proportional model support. A thin plate spline for the two linear discriminant axes s(LD1, LD2) is always included, as is a fixed effect of either experiment (i.e. Martin & Wainwright 2013, Martin and Gould 2020) or Lake (Crescent Pond/Little Lake) or an interaction between the two. In the last two models, Experiment and Lake are included as splines, modeled using a factor smooth (bs = "fs"). The best fit model had 8.93 estimated degrees of freedom.

Model	AICc	ΔAICc	Akaike Weights
*Growth ~ s(LD1, LD2) + Experiment * Lake*	*-44.658*	*0.000*	*1*
Growth ~ s(LD1, LD2) + Experiment + Lake	3.904	48.562	< 0.001
Growth ~ s(LD1, LD2) + s(LD1) + s(LD2) + Experiment * Lake	46.249	90.907	< 0.001
Growth ~ s(LD1, LD2) + s(LD1) + s(LD2) + Experiment + Lake	89.121	133.779	< 0.001
Growth ~ s(LD1, LD2) + s(LD1, Lake, bs = "fs") + s(LD2, Lake, bs = "fs") + Experiment	690.379	735.038	< 0.001
Growth ~ s(LD1, LD2) + s(LD1, Experiment, bs = "fs") + s(LD2, Experiment, bs = "fs") + Lake	693.748	738.406	< 0.001

Appendix 1—Table 13. Generalized additive models fitted to survival. Model fit was assessed using AICc, and Akaike Weights represent proportional model support. A thin plate spline for the two linear discriminant axes s(LD1, LD2) is always included, as is a fixed effect of either experiment (i.e. Martin & Wainwright 2013, Martin and Gould 2020) or Lake (Crescent Pond/Little Lake) or an interaction between the two. In the last two models, Experiment and Lake are included as splines, modeled using a factor smooth (bs = "fs"). The best fit model had 5 estimated degrees of freedom.

Model	**AICc**	**ΔAICc**	**Akaike Weights**
Survival ~ s(LD1, LD2) + Experiment + Lake	*141.057*	*0.000*	*0.849*
Survival ~ s(LD1, LD2) + Experiment * Lake	144.504	3.447	0.151
Survival ~ s(LD1, LD2) + s(LD1) + s(LD2) + Experiment + Lake	173.399	32.342	< 0.001
Survival ~ s(LD1, LD2) + s(LD1) + s(LD2) + Experiment * Lake	178.189	37.132	< 0.001
Survival ~ s(LD1, LD2) + s(LD1, Experiment, bs = "fs") + s(LD2, Experiment, bs = "fs") + Lake	273.547	132.490	< 0.001
Survival ~ s(LD1, LD2) + s(LD1, Lake, bs = "fs") + s(LD2, Lake, bs = "fs") + Experiment	273.694	132.637	< 0.001

Appendix 1—Table 14. Generalized additive models fitted to growth including SNPs most strongly associated with composite fitness. Model fit was assessed using AICc, and Akaike Weights represent proportional model support. The best fit model for composite fitness using morphology alone (see Table 8) was used as the base model. The SNPs that were most strongly associated with composite fitness (following a Bonferroni correction) were included as fixed effects, modeled as splines using a factor smooth, treating genotype as an ordered factor. Note that three SNPs were excluded due to their close proximity to other SNPs that were more strongly associated. All SNPs were considered individually, as well as all SNPs together. We were unable to assess all possible combinations of SNPs due to the vast number of potential models given the number of SNPs under consideration; rather, we fit one final model that only included SNPs found to be significant in the full model. In turn this model led to a substantial improvement in AICc. The best fit model had 20.29 estimated degrees of freedom.

Model	AICc	ΔAICc	Akaike Weights
Composite Fitness ~ s(LD1, LD2) + Experiment + Lake + s(Site1) + s(Site2) + s(Site6) + s(Site7) + s(Site8) + s(Site9) + s(Site10)	*4.586*	*0.000*	*0.999*
Composite Fitness ~ s(LD1, LD2) + Experiment + Lake + s(Site1) + s(Site2) + s(Site3) + s(Site4) + s(Site5) + s(Site6) + s(Site7) + s(Site8) + s(Site9) + s(Site10)	40.876	36.290	< 0.001
Composite Fitness ~ s(LD1, LD2) + Experiment + Lake + s(Site3)	55.588	51.001	< 0.001
Composite Fitness ~ s(LD1, LD2) + Experiment + Lake + s(Site7)	58.386	53.800	< 0.001
Composite Fitness ~ s(LD1, LD2) + Experiment + Lake + s(Site4)	65.453	60.867	< 0.001
Composite Fitness ~ s(LD1, LD2) + Experiment + Lake + s(Site2)	71.245	66.658	< 0.001
Composite Fitness ~ s(LD1, LD2) + Experiment + Lake + s(Site5)	72.329	67.743	< 0.001
Composite Fitness ~ s(LD1, LD2) + Experiment + Lake + s(Site1)	73.671	69.085	< 0.001
Composite Fitness ~ s(LD1, LD2) + Experiment + Lake + s(Site8)	74.413	69.827	< 0.001
Composite Fitness ~ s(LD1, LD2) + Experiment + Lake + s(Site9)	74.680	70.094	< 0.001
Composite Fitness ~ s(LD1, LD2) + Experiment + Lake + s(Site10)	88.977	84.391	< 0.001
Composite Fitness ~ s(LD1, LD2) + Experiment + Lake + s(Site6)	90.427	85.841	< 0.001
Composite Fitness ~ s(LD1, LD2) + Experiment + Lake	99.114	94.527	< 0.001

Note: Site1 = HiC_Scaffold_1:43866598, Site2 = HiC_Scaffold_53:11317840, Site3 = HiC_Scaffold_46:35151009, Site4 = HiC_Scaffold_8:20263964, Site5 = 37:18591438, Site5 = HiC_Scaffold_37:18591438, Site6 = HiC_Scaffold_24:15964553, Site7 = HiC_Scaffold_1848:40590, Site8 = HiC_Scaffold_4461:12939, Site9 = HiC_Scaffold_12778:1456, Site10 = HiC_Scaffold_18999:1084.

Appendix 1—Table 15. Generalized additive models fitted to growth including SNPs most strongly associated with growth. Model fit was assessed using AICc, and Akaike Weights represent proportional model support. The best fit model for growth using morphology alone (see Table 9) was used as the base model. Each of the four SNPs that were most strongly associated with growth (following a Bonferroni correction) were included as fixed effects, modeled as splines using a factor smooth, treating genotype as an ordered factor. All SNPs were considered individually, as well as all possible combinations. This was only feasible due to the small number of SNPs assessed (four). The best fit model had 7.97 estimated degrees of freedom.

Model	AICc	ΔAICc	Akaike Weights
Growth ~ s(LD1, LD2) + Experiment * Lake + s(Site3) + s(Site4)	-67.649	0.000	0.490
Growth ~ s(LD1, LD2) + Experiment * Lake + s(Site3)	-65.634	2.015	0.179
Growth ~ s(LD1, LD2) + Experiment * Lake + s(Site1)	-64.161	3.488	0.086
Growth ~ s(LD1, LD2) + Experiment * Lake + s(Site1) + s(Site3)	-63.926	3.723	0.076
Growth ~ s(LD1, LD2) + Experiment * Lake + s(Site1) + s(Site2)	-63.861	3.788	0.074
Growth ~ s(LD1, LD2) + Experiment * Lake + s(Site2) + s(Site4)	-63.503	4.146	0.062
Growth ~ s(LD1, LD2) + Experiment * Lake + s(Site2)	-61.849	5.800	0.027
Growth ~ s(LD1, LD2) + Experiment * Lake + s(Site1) + s(Site4)	-58.044	9.604	0.004
Growth ~ s(LD1, LD2) + Experiment * Lake + s(Site4)	-56.068	11.581	0.001
Growth ~ s(LD1, LD2) + Experiment * Lake + s(Site1) + s(Site3) + s(Site4)	-54.878	12.770	< 0.001
Growth ~ s(LD1, LD2) + Experiment * Lake + s(Site1) + s(Site2) + s(Site4)	-54.509	13.140	< 0.001
Growth ~ s(LD1, LD2) + Experiment * Lake + s(Site2) + s(Site3)	-47.602	20.047	< 0.001
Growth ~ s(LD1, LD2) + Experiment * Lake	-44.658	22.990	< 0.001
Growth ~ s(LD1, LD2) + Experiment * Lake + s(Site1) + s(Site2) + s(Site3)	-41.689	25.960	< 0.001
Growth ~ s(LD1, LD2) + Experiment * Lake + s(Site1) + s(Site2) + s(Site3) + s(Site4)	-29.801	37.847	< 0.001

Note: Site1 = HiC_Scaffold_46:16512886, Site2 = HiC_Scaffold_1848:40119, Site3 = HiC_Scaffold_1848:40465, Site4 = HiC_Scaffold_7644:5971

Appendix 1—Table 16. General linear models fitted to examine the relationship between aspects of network size (i.e. number of nodes, number of edges linking neighboring nodes) and the number of accessible paths between generalists and specialists. Models were fitted using each of the three different fitness measures; bolded lines correspond to the best-fit model for each response variable, within each measure of fitness. Poisson regression was chosen as each response variable correspond to count-data. Because Poisson regression models are log-linear, we report both the estimated coefficient, as well as it's exponentiated value which corresponds to the expected multiplicative increase in the mean of Y per unit-value of X.

Fitness Measure	Model	Family	AIC	Coefficient	exp(Coefficient)	P-value
	# Edges in Network ~ # Nodes in Network	Poisson	34260.63	0.0342	1.0348	< 0.0001
	# Edges in Network ~ # Nodes in Network + Trajectory	Poisson	34260.93	0.0344	1.0350	< 0.0001
	# Edges in Network ~ # Nodes in Network * Trajectory	**Poisson**	**33599.17**	**0.0386**	**1.0394**	**< 0.0001**
	# Accessible Paths ~ # Nodes In Network	Poisson	12207.29	0.0082	1.0083	< 0.0001
Composite	**# Accessible Paths ~ # Nodes In Network + Trajectory**	**Poisson**	**12203.83**	**0.0061**	**1.0062**	**< 0.0001**
	# Accessible Paths ~ # Nodes In Network * Trajectory	Poisson	12204.89	0.0071	1.0071	< 0.0001
	# Accessible Paths ~ # Edges In Network	Poisson	12203.07	0.0044	1.0044	< 0.0001
	# Accessible Paths ~ # Edges In Network + Trajectory	**Poisson**	**12200.31**	**0.0034**	**1.0034**	**< 0.0001**
	# Accessible Paths ~ # Edges In Network * Trajectory	Poisson	12201.69	0.0039	1.0039	< 0.0001
	# Edges in Network ~ # Nodes in Network	Poisson	26739.96	0.0478	1.0489	< 0.0001
	# Edges in Network ~ # Nodes in Network + Trajectory	Poisson	26711.02	0.0489	1.0501	< 0.0001
	# Edges in Network ~ # Nodes in Network * Trajectory	**Poisson**	**26507.72**	**0.0532**	**1.0546**	**< 0.0001**
	# Accessible Paths ~ # Nodes In Network	Poisson	10162.51	0.0106	1.0107	< 0.0001
Growth	**# Accessible Paths ~ # Nodes In Network + Trajectory**	**Poisson**	**10160.39**	**0.0083**	**1.0083**	**0.0002**
	# Accessible Paths ~ # Nodes In Network * Trajectory	Poisson	10162.28	0.0088	1.0089	0.0011
	# Accessible Paths ~ # Edges In Network	Poisson	10159.39	0.0062	1.0062	< 0.0001
	# Accessible Paths ~ # Edges In Network + Trajectory	**Poisson**	**10157.09**	**0.0050**	**1.0050**	**< 0.0001**
	# Accessible Paths ~ # Edges In Network * Trajectory	Poisson	10159.09	0.0050	1.0050	0.0010
	# Edges in Network ~ # Nodes in Network	Poisson	32986.67	0.0346	1.0352	< 0.0001
	# Edges in Network ~ # Nodes in Network + Trajectory	Poisson	32978.31	0.0350	1.0356	< 0.0001
	# Edges in Network ~ # Nodes in Network * Trajectory	**Poisson**	**32437.55**	**0.0384**	**1.0392**	**< 0.0001**
	# Accessible Paths ~ # Nodes In Network	**Poisson**	**11725.19**	**0.0058**	**1.0058**	**< 0.0001**
Survival	# Accessible Paths ~ # Nodes In Network + Trajectory	Poisson	11727.13	0.0056	1.0056	0.0001
	# Accessible Paths ~ # Nodes In Network * Trajectory	Poisson	11727.11	0.0068	1.0068	< 0.0001
	# Accessible Paths ~ # Edges In Network	**Poisson**	**11722.24**	**0.0032**	**1.0032**	**< 0.0001**
	# Accessible Paths ~ # Edges In Network + Trajectory	Poisson	11724.23	0.0031	1.0031	< 0.0001
	# Accessible Paths ~ # Edges In Network * Trajectory	Poisson	11725.27	0.0036	1.0036	< 0.0001

Appendix 1—Table 17. Accessibility of specialists to generalists and the ruggedness of their respective fitness landscapes. Odds ratios were obtained by modelling the association between each summary statistic and the species from which adaptive loci were used to construct the fitness network. Scale-eaters were treated as the baseline of comparison in the comparison of odds ratios; thus, positive odds ratios imply that summary statistics for molluscivore fitness networks are greater than those constructed from scale-eater adaptive loci and vice versa. For generalist to specialist comparisons, accessible paths were identified between one randomly sampled generalist node and one randomly sampled specialist node. For comparison of the peaks in networks, these summary statistics were calculated from either molluscivore or scale-eater fitness networks, identifying the number of peaks (nodes with no fitter neighbors – see Methods), and the scaled (total divided by number of nodes in the network) number of accessible paths separating all focal specialist nodes and all peaks in the network.

Comparison	**Summary Statistic**	**Mean / SE** *Molluscivore Network*	**Mean / SE** *Scale-Eater Network*	**Odds Ratio: (95% CI)** *Molluscivore / Scale Eater*	**LRT *P*-value**
Generalist to Specialist	*Number of nodes in network*	22.994 / 0.106	31.000 / 0.177	0.818: (0.807, 0.829)	< 0.0001
	Number of accessible paths	1.105 / 0.007	1.268 / 0.018	0.515: (0.449, 0.588)	< 0.0001
	Scaled number of accessible paths	0.051 / 0.001	0.042 / 0.001	2.095: (1.934, 2.274)	< 0.0001
	Length of shortest accessible path	2.410 / 0.012	3.444 / 0.029	0.253: (0.231, 0.277)	< 0.0001
Peaks in Network	*Number of peaks*	3.274 / 0.035	4.637 / 0.046	0.604: (0.575, 0.634)	< 0.0001
	Scaled number of accessible paths to peaks	0.095 / 0.001	0.087 / 0.001	1.514: (1.404, 1.635)	< 0.0001
	Length of shortest accessible path to nearest peak	0.823 / 0.022	1.482 / 0.029	0.539: (0.500, 0.579)	< 0.0001

Appendix 1—Table 18. Influence of different sources of adaptive genetic variation on accessibility of fitness paths separating either generalists from molluscivores, or generalists and scale-eaters using all samples. Results for networks using all three measures of fitness (composite fitness, survival, and growth) are reported. Networks were constructed from random draws of five SNPs from either Standing genetic variation (SGV), introgression, or *de novo* mutations, as well as their combinations. Odds ratios were obtained by modelling the association between each accessibility measure and the source of genetic variation used to construct the fitness network, relative to networks constructed from standing variation. Thus, positive odds ratios imply that networks from standing variation have measures of accessibility that are smaller as compared to the alternative (e.g. introgression, *de novo* mutations, etc).

Trajectory	Source	Accessibility	Composite Fitness			Growth			Survival		
			Mean / SE	LRT P-value	Odds Ratio: (95% CI)	Mean / SE	LRT P-value	Odds Ratio: (95% CI)	Mean / SE	LRT P-value	Odds Ratio: (95% CI)
Generalist to Molluscivore	*Introgression*	# Nodes in network	22.095 / 0.118	< 0.0001	0.627: (0.606, 0.646)	17.630 / 0.098	< 0.0001	0.556: (0.535, 0.577)	21.845 / 0.108	< 0.0001	0.628: (0.608, 0.646)
		# Accessible paths	1.071 / 0.005	< 0.0001	0.442: (0.378, 0.515)	1.099 / 0.007	< 0.0001	0.721: (0.613, 0.842)	1.039 / 0.004	< 0.0001	0.214: (0.174, 0.259)
		# Accessible paths / # nodes in network	0.052 / 0.0004	< 0.0001	17.131: (15.076, 19.556)	0.066 / 0.0006	< 0.0001	10.272: (9.105, 11.636)	0.051 / 0.0003	< 0.0001	11.256: (10.121, 12.560)
		Length of shortest accessible path	2.480 / 0.013	< 0.0001	0.768: (0.717, 0.823)	2.457 / 0.016	0.8826	0.994: (0.915, 1.079)	2.475 / 0.012	< 0.0001	0.662: (0.619, 0.707)
		Ruggedness (# of peaks)	1.444 / 0.025	< 0.0001	0.250: (0.234, 0.268)	0.706 / 0.018	< 0.0001	0.252: (0.233, 0.271)	1.863 / 0.033	< 0.0001	0.397: (0.378, 0.416)
	SGV + Introgression	# Nodes in network	32.167 / 0.146	< 0.0001	0.820: (0.813, 0.827)	22.994 / 0.106	< 0.0001	0.777: (0.768, 0.786)	32.386 / 0.144	< 0.0001	0.826: (0.819, 0.833)
		# Accessible paths	1.117 / 0.007	< 0.0001	0.694: (0.624, 0.771)	1.105 / 0.006	< 0.0001	0.773: (0.684, 0.873)	1.140 / 0.007	< 0.0001	0.666: (0.608, 0.728)
		# Accessible paths / # nodes in network	0.037 / 0.0002	< 0.0001	3.974: (3.707, 4.266)	0.051 / 0.0003	< 0.0001	3.538: (3.297, 3.802)	0.038 / 0.0003	< 0.0001	3.108: (2.922, 3.309)
		Length of shortest accessible path	2.524 / 0.012	< 0.0001	0.843: (0.793, 0.894)	2.410 / 0.011	0.0050	0.897: (0.835, 0.962)	2.573 / 0.012	< 0.0001	0.798: (0.755, 0.843)
		Ruggedness (# of peaks)	3.906 / 0.034	< 0.0001	0.523: (0.509, 0.537)	2.218 / 0.028	< 0.0001	0.556: (0.539, 0.574)	5.651 / 0.056	< 0.0001	0.690: (0.680, 0.700)
Generalist to Scale-eater	*Introgression*	# Nodes in network	45.783 / 0.261	< 0.0001	0.866: (0.858, 0.874)	33.569 / 0.232	< 0.0001	0.838: (0.827, 0.849)	45.423 / 0.270	< 0.0001	0.870: (0.862, 0.879)
		# Accessible paths	1.190 / 0.012	< 0.0001	0.632: (0.564, 0.706)	1.178 / 0.013	< 0.0001	0.637: (0.556, 0.728)	1.191 / 0.012	< 0.0001	0.668: (0.593, 0.751)
		# Accessible paths / # nodes in network	0.027 / 0.0003	< 0.0001	1.790: (1.658, 1.936)	0.037 / 0.0004	< 0.0001	2.011: (1.837, 2.206)	0.028 / 0.0003	< 0.0001	1.931: (1.778, 2.101)
		Length of shortest accessible path	3.033 / 0.021	< 0.0001	0.552: (0.513, 0.593)	3.040 / 0.023	< 0.0001	0.570: (0.525, 0.618)	3.103 / 0.021	< 0.0001	0.679: (0.629, 0.733)
		Ruggedness (# of peaks)	7.879 / 0.036	< 0.0001	0.752: (0.739, 0.766)	5.516 / 0.033	< 0.0001	0.724: (0.709, 0.740)	15.020 / 0.088	< 0.0001	0.838: (0.831, 0.845)
	De novo	# Nodes in network	46.292 / 0.177	< 0.0001	0.835: (0.826, 0.844)	35.650 / 0.129	< 0.0001	0.796: (0.783, 0.808)	46.251 / 0.199	< 0.0001	0.844: (0.835, 0.854)
		# Accessible paths	1.234 / 0.012	< 0.0001	0.736: (0.673, 0.803)	1.196 / 0.011	< 0.0001	0.686: (0.612, 0.766)	1.172 / 0.011	< 0.0001	0.628: (0.559, 0.703)
		# Accessible paths / # nodes in network	0.027 / 0.0002	< 0.0001	1.908: (1.770, 2.061)	0.034 / 0.0003	< 0.0001	1.764: (1.622, 1.922)	0.026 / 0.0002	< 0.0001	1.818: (1.678, 1.972)
		Length of shortest accessible path	3.088 / 0.018	< 0.0001	0.589: (0.553, 0.628)	3.029 / 0.018	< 0.0001	0.555: (0.515, 0.597)	2.920 / 0.017	< 0.0001	0.518: (0.477, 0.560)
		Ruggedness (# of peaks)	8.381 / 0.034	< 0.0001	0.806: (0.792, 0.819)	6.145 / 0.031	< 0.0001	0.809: (0.792, 0.825)	15.615 / 0.079	< 0.0001	0.836: (0.829, 0.843)
	SGV + Introgression	# Nodes in network	56.559 / 0.272	< 0.0001	0.952: (0.945, 0.959)	40.858 / 0.238	< 0.0001	0.925: (0.915, 0.935)	55.717 / 0.302	< 0.0001	0.950: (0.943, 0.957)
		# Accessible paths	1.331 / 0.019	0.0199	0.904: (0.831, 0.981)	1.304 / 0.021	0.1646	0.928: (0.835, 1.031)	1.312 / 0.022	0.1469	0.932: (0.850, 1.018)
		# Accessible paths / # nodes in network	0.024 / 0.0003	< 0.0001	1.167: (1.089, 1.252)	0.033 / 0.0005	< 0.0001	1.270: (1.172, 1.379)	0.024 / 0.0004	< 0.0001	1.209: (1.121, 1.304)
		Length of shortest accessible path	3.415 / 0.026	< 0.0001	0.828: (0.777, 0.882)	3.419 / 0.031	< 0.0001	0.851: (0.793, 0.913)	3.263 / 0.026	< 0.0001	0.823: (0.763, 0.887)
		Ruggedness (# of peaks)	9.319 / 0.036	< 0.0001	0.943: (0.928, 0.957)	6.731 / 0.030	< 0.0001	0.912: (0.895, 0.930)	19.924 / 0.089	< 0.0001	0.954: (0.948, 0.960)
	SGV + De novo	# Nodes in network	56.723 / 0.214	< 0.0001	0.947: (0.941, 0.954)	42.261 / 0.177	< 0.0001	0.936: (0.926, 0.946)	56.488 / 0.230	< 0.0001	0.951: (0.943, 0.958)
		# Accessible paths	1.344 / 0.019	0.0522	0.931: (0.865, 1.001)	1.287 / 0.018	0.0473	0.901: (0.816, 0.994)	1.315 / 0.023	0.1632	0.949: (0.879, 1.021)
		# Accessible paths / # nodes in network	0.024 / 0.0003	< 0.0001	1.155: (1.081, 1.235)	0.031 / 0.0004	0.0017	1.128: (1.046, 1.218)	0.024 / 0.0004	0.0004	1.134: (1.057, 1.218)
		Length of shortest accessible path	3.431 / 0.024	< 0.0001	0.842: (0.794, 0.892)	3.391 / 0.027	< 0.0001	0.834: (0.780, 0.891)	3.299 / 0.023	< 0.0001	0.859: (0.802, 0.920)
		Ruggedness (# of peaks)	9.525 / 0.035	0.0006	0.973: (0.958, 0.988)	6.975 / 0.029	0.0006	0.967: (0.949, 0.986)	19.849 / 0.085	< 0.0001	0.950: (0.944, 0.956)
	SGV + De novo + Introgression	# Nodes in network	46.882 / 0.200	< 0.0001	0.826: (0.816, 0.837)	31.000 / 0.177	< 0.0001	0.722: (0.703, 0.739)	46.875 / 0.222	< 0.0001	0.835: (0.823, 0.845)
		# Accessible paths	1.322 / 0.019	0.0125	0.896: (0.824, 0.971)	1.268 / 0.018	0.0102	0.855: (0.762, 0.956)	1.247 / 0.018	0.0001	0.811: (0.726, 0.900)
		# Accessible paths / # nodes in network	0.029 / 0.0004	< 0.0001	1.879: (1.734, 2.041)	0.042 / 0.0006	< 0.0001	2.798: (2.511, 3.128)	0.027 / 0.0004	< 0.0001	1.785: (1.640, 1.948)
		Length of shortest accessible path	3.484 / 0.026	< 0.0001	0.876: (0.823, 0.932)	3.444 / 0.029	< 0.0001	0.861: (0.800, 0.925)	3.221 / 0.024	< 0.0001	0.775: (0.716, 0.838)
		Ruggedness (# of peaks)	7.440 / 0.029	< 0.0001	0.650: (0.637, 0.664)	4.555 / 0.025	< 0.0001	0.485: (0.471, 0.500)	12.933 / 0.062	< 0.0001	0.725: (0.716, 0.734)

Appendix 1—Table 19. Influence of different sources of adaptive genetic variation on accessibility of fitness paths separating either generalists from molluscivores, or generalists and scale-eaters using only samples from the second field experiment (Martin & Gould 2021). Results for networks using all three measures of fitness (composite fitness, survival, and growth) are reported. Networks were constructed from random draws of five SNPs from either Standing genetic variation (SGV), introgression, or *de novo* mutations, as well as their combinations. Odds ratios were obtained by modelling the association between each accessibility measure and the source of genetic variation used to construct the fitness network, relative to networks constructed from standing variation. Thus, positive odds ratios imply that networks from standing variation have measures of accessibility that are smaller as compared to the alternative (e.g. introgression, *de novo* mutations, etc).

Trajectory	Source	Accessibility	Composite Fitness			Growth			Survival		
			Mean / SE	LRT P-value	Odds Ratio: (95% CI)	Mean / SE	LRT P-value	Odds Ratio: (95% CI)	Mean / SE	LRT P-value	Odds Ratio: (95% CI)
Generalist to Molluscivore	*Introgression*	# Nodes in network	22.062 / 0.118	< 0.0001	0.628: (0.608, 0.648)	17.632 / 0.099	< 0.0001	0.556: (0.535, 0.577)	21.836 / 0.107	< 0.0001	0.617: (0.596, 0.637)
		# Accessible paths	1.067 / 0.005	< 0.0001	0.402: (0.341, 0.471)	1.107 / 0.008	< 0.0001	0.721: (0.618, 0.836)	1.039 / 0.004	< 0.0001	0.205: (0.167, 0.248)
		# Accessible paths / # nodes in network	0.052 / 0.0004	< 0.0001	16.263: (14.350, 18.515)	0.066 / 0.0006	< 0.0001	9.411: (8.375, 10.617)	0.051 / 0.0003	< 0.0001	10.698: (9.642, 11.907)
		Length of shortest accessible path	2.483 / 0.013	< 0.0001	0.751: (0.700, 0.804)	2.465 / 0.016	0.7601	0.987: (0.908, 1.073)	2.473 / 0.013	< 0.0001	0.652: (0.610, 0.695)
		Ruggedness (# of peaks)	1.437 / 0.025	< 0.0001	0.247: (0.230, 0.264)	0.702 / 0.018	< 0.0001	0.257: (0.238, 0.276)	1.853 / 0.033	< 0.0001	0.405: (0.386, 0.425)
	SGV + Introgression	# Nodes in network	32.301 / 0.146	< 0.0001	0.824: (0.818, 0.831)	23.042 / 0.103	< 0.0001	0.769: (0.760, 0.779)	32.488 / 0.144	< 0.0001	0.826: (0.819, 0.832)
		# Accessible paths	1.134 / 0.007	< 0.0001	0.753: (0.681, 0.832)	1.115 / 0.007	< 0.0001	0.778: (0.693, 0.871)	1.146 / 0.008	< 0.0001	0.664: (0.609, 0.723)
		# Accessible paths / # nodes in network	0.037 / 0.0002	< 0.0001	3.929: (3.671, 4.210)	0.051 / 0.0003	< 0.0001	3.505: (3.267, 3.765)	0.037 / 0.0002	< 0.0001	3.053: (2.874, 3.245)
		Length of shortest accessible path	2.538 / 0.012	< 0.0001	0.842: (0.793, 0.893)	2.426 / 0.011	0.0136	0.907: (0.846, 0.974)	2.597 / 0.013	< 0.0001	0.819: (0.777, 0.863)
		Ruggedness (# of peaks)	3.954 / 0.034	< 0.0001	0.518: (0.504, 0.532)	2.243 / 0.028	< 0.0001	0.560: (0.542, 0.577)	5.742 / 0.056	< 0.0001	0.690: (0.680, 0.700)
Generalist to Scale-eater	*Introgression*	# Nodes in network	45.775 / 0.254	< 0.0001	0.864: (0.855, 0.872)	33.658 / 0.219	< 0.0001	0.837: (0.826, 0.849)	45.306 / 0.264	< 0.0001	0.862: (0.853, 0.870)
		# Accessible paths	1.202 / 0.013	< 0.0001	0.723: (0.647, 0.803)	1.180 / 0.013	< 0.0001	0.733: (0.639, 0.835)	1.208 / 0.013	< 0.0001	0.743: (0.661, 0.830)
		# Accessible paths / # nodes in network	0.027 / 0.0003	< 0.0001	1.959: (1.809, 2.125)	0.037 / 0.0004	< 0.0001	2.243: (2.038, 2.476)	0.028 / 0.0003	< 0.0001	2.087: (1.916, 2.279)
		Length of shortest accessible path	3.108 / 0.022	< 0.0001	0.605: (0.564, 0.648)	3.063 / 0.022	< 0.0001	0.568: (0.523, 0.615)	3.132 / 0.022	< 0.0001	0.713: (0.662, 0.768)
		Ruggedness (# of peaks)	7.928 / 0.036	< 0.0001	0.760: (0.747, 0.773)	5.572 / 0.033	< 0.0001	0.727: (0.712, 0.743)	15.072 / 0.087	< 0.0001	0.838: (0.831, 0.845)
	De novo	# Nodes in network	46.510 / 0.177	< 0.0001	0.843: (0.834, 0.851)	35.882 / 0.129	< 0.0001	0.808: (0.796, 0.820)	46.454 / 0.196	< 0.0001	0.843: (0.833, 0.852)
		# Accessible paths	1.223 / 0.011	< 0.0001	0.775: (0.708, 0.846)	1.202 / 0.011	0.0002	0.806: (0.723, 0.896)	1.168 / 0.010	< 0.0001	0.639: (0.566, 0.717)
		# Accessible paths / # nodes in network	0.027 / 0.0002	< 0.0001	2.010: (1.861, 2.176)	0.034 / 0.0003	< 0.0001	1.934: (1.768, 2.121)	0.026 / 0.0002	< 0.0001	1.874: (1.730, 2.034)
		Length of shortest accessible path	3.100 / 0.018	< 0.0001	0.602: (0.566, 0.640)	3.049 / 0.018	< 0.0001	0.564: (0.524, 0.605)	2.935 / 0.017	< 0.0001	0.553: (0.512, 0.596)
		Ruggedness (# of peaks)	8.336 / 0.034	< 0.0001	0.798: (0.784, 0.812)	6.147 / 0.030	< 0.0001	0.803: (0.787, 0.820)	15.630 / 0.079	< 0.0001	0.837: (0.830, 0.844)
	SGV + Introgression	# Nodes in network	56.208 / 0.268	< 0.0001	0.952: (0.946, 0.959)	41.204 / 0.243	< 0.0001	0.937: (0.928, 0.947)	55.697 / 0.277	< 0.0001	0.948: (0.940, 0.955)
		# Accessible paths	1.339 / 0.021	0.6195	0.980: (0.907, 1.060)	1.285 / 0.020	0.922	0.985: (0.885, 1.097)	1.307 / 0.020	0.256	0.946: (0.866, 1.031)
		# Accessible paths / # nodes in network	0.024 / 0.0004	< 0.0001	1.234: (1.151, 1.325)	0.032 / 0.0005	< 0.0001	1.299: (1.196, 1.413)	0.024 / 0.0004	< 0.0001	1.231: (1.144, 1.327)
		Length of shortest accessible path	3.465 / 0.026	< 0.0001	0.860: (0.809, 0.914)	3.460 / 0.030	< 0.0001	0.860: (0.802, 0.922)	3.306 / 0.025	0.0001	0.867: (0.807, 0.932)
		Ruggedness (# of peaks)	9.231 / 0.036	< 0.0001	0.930: (0.915, 0.944)	6.666 / 0.030	< 0.0001	0.902: (0.885, 0.920)	19.815 / 0.090	< 0.0001	0.951: (0.945, 0.957)
	SGV + De novo	# Nodes in network	56.259 / 0.212	< 0.0001	0.947: (0.940, 0.953)	41.991 / 0.173	< 0.0001	0.936: (0.925, 0.946)	56.339 / 0.224	< 0.0001	0.949: (0.942, 0.956)
		# Accessible paths	1.329 / 0.017	0.4575	0.966: (0.895, 1.042)	1.290 / 0.020	0.922	0.995: (0.905, 1.097)	1.329 / 0.018	0.5596	0.976: (0.900, 1.059)
		# Accessible paths / # nodes in network	0.024 / 0.0003	< 0.0001	1.233: (1.153, 1.319)	0.031 / 0.0004	< 0.0001	1.225: (1.133, 1.326)	0.024 / 0.0003	< 0.0001	1.243: (1.158, 1.335)
		Length of shortest accessible path	3.452 / 0.023	< 0.0001	0.851: (0.803, 0.902)	3.379 / 0.025	< 0.0001	0.800: (0.748, 0.856)	3.288 / 0.022	< 0.0001	0.852: (0.797, 0.912)
		Ruggedness (# of peaks)	9.406 / 0.035	< 0.0001	0.953: (0.938, 0.968)	6.898 / 0.029	< 0.0001	0.948: (0.930, 0.966)	19.782 / 0.084	< 0.0001	0.947: (0.941, 0.953)
	SGV + De novo + Introgression	# Nodes in network	47.220 / 0.207	< 0.0001	0.841: (0.831, 0.851)	31.051 / 0.183	< 0.0001	0.740: (0.723, 0.757)	47.117 / 0.224	< 0.0001	0.840: (0.829, 0.850)
		# Accessible paths	1.298 / 0.018	0.074	0.918: (0.842, 0.998)	1.289 / 0.022	0.922	0.994: (0.894, 1.104)	1.221 / 0.016	< 0.0001	0.790: (0.705, 0.879)
		# Accessible paths / # nodes in network	0.028 / 0.0004	< 0.0001	1.945: (1.792, 2.116)	0.043 / 0.0007	< 0.0001	3.307: (2.936, 3.741)	0.027 / 0.0004	< 0.0001	1.784: (1.639, 1.946)
		Length of shortest accessible path	3.497 / 0.025	< 0.0001	0.879: (0.827, 0.935)	3.479 / 0.030	0.0001	0.869: (0.809, 0.933)	3.269 / 0.024	< 0.0001	0.826: (0.766, 0.891)
		Ruggedness (# of peaks)	7.361 / 0.031	< 0.0001	0.650: (0.637, 0.664)	4.530 / 0.026	< 0.0001	0.490: (0.475, 0.504)	12.869 / 0.062	< 0.0001	0.725: (0.716, 0.734)